631777
134p.

FINAL REPORT

FOR THE

AEROASSISTED ORBITAL TRANSFER VEHICLE CONTROL TECHNOLOGY

CONTRACT NO. NAS 8-37358

AUGUST 26, 1988

PREPARED FOR:
George C. Marshall Space Flight Center
National Aeronautics and Space Administration,
Marshall Space Flight Center, AL. 35812

W.W. CIMINO
CONRTOL ANALYST

M.A. LANGEHOUGH
PRINCIPAL INVESTIGATOR

I. A. HIRSCH
PROGRAM MANAGER

BOEING AEROSPACE

P. O. BOX 3999

SEATTLE, WASHINGTON 98124-2499

TABLE OF CONTENTS

TABLE OF CONTENTS (cont'd)

LIST OF FIGURES

LIST OF FIGURES (cont'd)

LIST OF FIGURES (cont'd)

LIST OF TABLES

1.0 SUMMARY

This is the final report for the Control Technology Aeroassisted Orbital Transfer Vehicle study contract (NAS8-37358).

The long range goal of the Aeroassisted Orbital Transfer Vehicle (AOTV) program is to furnish NASA with a reusable orbital transfer vehicle with a larger payload capability, achieved by replacing a propulsive orbit transfer maneuver with an aeroassisted maneuver. The focus of this contract has been to develop the control technology required to identify the sophistication required for the AOTV control system. Our primary control objective has been to develop control techniques which minimize the exit condition errors while minimizing the control effector energy usage. The control technology also promotes low cost, high reliability, serviceability, refueling, recalibration, autonomy, and space-basing.

The primary design challenge for the AOTV mission is to minimize the fuel used for atmospheric maneuvering and orbit establishment following the aerobraking maneuver. (Fuel used for orbit establishment is estimated by assuming impulsive velocity changes, referred to as ΔV burns.) This can be accomplished with a combination of effective guidance and control algorithms. The HYPAS algorithm used in this study made it necessary to use large thrusters to give the vehicle a response fast enough to follow the quickly changing large angle guidance commands.

An angle-of-attack and bank angle command control technique has been developed consistent with the AOTV guidance approach. Both on-off thrusters and proportional thruster systems have been analyzed for the control effectors. For the proportional thrusters, a classical linear control design was synthesized. For the conventional on-off thrusters, a phase-plane control algorithm was developed. Both designs furnish adequate control with the proportional thruster technique using less energy. An angle-of-attack adaptive controller was used to minimize the RCS fuel usage due to payload center of gravity uncertainties. A semi-adaptive gain computer was developed to minimize the mission data load.

The control techniques were verified using a detailed 6DOF simulation. The effect of parameter uncertainty on mission performance and guidance/control performance was examined. Uncertainties in the entry state, mass properties, atmosphere, aerodynamics, and sensor data were evaluated.

The vehicle performed well for most parameter variations, being the most sensitive to entry state errors and least sensitive to sensor and aerodynamic errors, suggesting that the system is very sensitive to the guidance and not as sensitive to uncertainties in the dynamics. This turned out to be the case as the primary difficulty in controlling the AOTV in this study was getting enough control authority to effectively follow the HYPAS guidance

commands.

Several advanced control concepts are presented in the report. Advanced technology for the AOTV includes semi-adaptive and fully adaptive control techniques, as well as control designs which minimize cost and increase reliability.

A nonlinear six-degree-of-freedom (6DOF) simulation was used to evaluate the attitude control techniques. The simulation included the Hybrid Predictive Aerobraking Scheme (HYPAS) guidance algorithm, Global Reference Atmosphere Model (GRAM) atmosphere models, and full nonlinear equations of motion including orbital effects.

A three-degree-of-freedom (3DOF) simulation was used for comparison purposes. The 3DOF simulation included the same guidance algorithm but only point-mass dynamics and no control system. Outputs of the two simulations were compared to validate correct implementation of the guidance algorithm and equations of motion.

2.0 CONTROL CONCEPT

The control concept for the AOTV was developed based on the mission requirements, the dynamic properties of the shaped-brake vehicle, and the operation of the guidance algorithm. The following sections describe each of these elements and the resulting attitude control system.

2.1 Mission

Several AOTV concepts, including a ballute-type vehicle, a lifting-brake vehicle, and a shaped-brake vehicle, have been considered in recent studies, see Figure 2.1-1. The shaped-brake vehicle was used in this study.

The vehicles are used to transfer payloads between geosynchronous (GEO) and low earth orbit (LEO). A pass through the Earth's atmosphere, referred to as the "aeropass," is used to "brake" the vehicle for insertion into the low earth orbit. The aeropass reduces the amount of fuel required to slow the vehicle. Figure 2.1-2 shows a transfer from GEO to LEO. Following the aeropass, three propulsive burns are used to establish the correct low earth orbit. These burns are also shown on Figure 2.1-2. A typical altitude versus velocity profile is shown in Figure 2.1-3. Notice that the vehicle exits the atmosphere (roughly 400,000 feet) 9500 feet per second slower than the entrance velocity. Figures 2.1-4 and 2.1-5 show the dynamic pressure and the bank angle versus time

angle versus time profiles for the nominal mission, respectively.

2.2 AOTV Shaped-Brake Characteristics

The shaped-brake concept has the property that the lift vector can be directed by rolling the vehicle around the velocity vector. Thus, the vehicle can be used to pull into or out of the orbital plane as well as up or down, see Figure 2.2-1. The shaped-brake vehicle typically flies at large angles of attack (70° - 80°), meaning that the rolling motion about the velocity vector is principally a yawing motion in the body axes. The shaped-brake vehicle and the aerodynamic and control coordinate systems are shown in Figure 2.2-1. The aerodynamic characteristics of the shaped-brake are shown in Figure 2.2-2. For the vehicle used in this study, the L/D ratio was 0.2.

2.3 AOTV Performance Corridor

The shaped-brake AOTV has a lifting characteristic that can be used to control the vehicle trajectory and obtain a desirable exit velocity and inclination. The L/D ratio defines a region of successful mission operation, referred to as the control corridor, as illustrated in Figure 2.3-1. The name control corridor comes from the fact that within this region, the AOTV can be successfully controlled and guided to the exit window by directing the lift vector. Bigger L/D ratios correspond to wider corridors. If the trajectory carries the vehicle outside of the corridor, the

AOTV will not achieve the desired exit window. The upper corridor boundary is characterized by a continuous downward pointing lift vector, which is used to pull the vehicle into the atmosphere in order to decelerate to an acceptable exit speed. Conversely, the lower corridor boundary is characterized by a continuous upward pointing lift vector, used to avoid excessive speed depletion. Figure 2.3-2 shows the relationship between the total orbit insertion ΔV burn and the control corridor. Inside the corridor, a minimum ΔV burn can be achieved rotating the lift vector such that the desired trajectory is obtained.

The control corridor width is closely related to the lift characteristic of the vehicle; with a high L/D ratio, the AOTV has more control authority and is more capable of pulling in and out of the atmosphere. Conversely, at a low L/D ratio, the corridor width is reduced. Figure 2.3-3 shows a plot of the control corridor width versus the L/D ratio. This figure represents the maximum corridor width available with a perfect navigation and guidance/control system, and with no orbital inclination change.

The minimum control corridor width required, resulting from navigation (entry state) error and aerodynamic uncertainties, is summarized in Figure 2.3-4. The detailed analysis for each of the variables can be found in the sensitivity study (Sections 5.2 and 5.5). Combining the effect from the listed errors and uncertainties yields a minimum corridor width of 4.99 nautical miles. A 35% margin results in a control corridor width

requirement of 6.75 nautical miles.

Figure 2.3-5 shows the impact of the L/D ratio on the maximum plane change capability. It indicates that the higher the lift the more turning capability is available. However, an orbit plane change reduces the available control corridor width because the vehicle must spend time to correct direction as well as speed. The effect of the plane change can be seen in Figure 2.3-6.

2.4 Guidance System (HYPAS)

The HYPAS (Hybrid Predictive Aerobraking Scheme) guidance algorithm was obtained from MSFC and implemented in the 6DOF and 3DOF simulations. The scheme consists of two coupled algorithms for aeroassisted orbit maneuvers. One algorithm operates to control the out-of-plane motion in order to achieve the desired orbit plane. The second algorithm operates in the vertical plane by targeting the exit conditions to achieve the desired orbit apogee. The vertical plane algorithm has two phases. The first phase is an equlibrium glide phase in which the guidance parameters can be adjusted to control the minimum altitude, maximum g-load, and heating rates. The exit phase (second phase) guides to the desired apogee altitude and attempts to minimize the ΔV required for insertion into the final low earth orbit (LEO).

The algorithm output is a bank angle command. The angle-of-attack for the lifting brake is constant and the bank angle is used to

control the direction of the lift vector. A negative bank angle command will pull the vehicle to the left and a positive bank angle command will pull the vehicle to the right (velocity axes). If the magnitude of the command is less than 90 degrees, the lift vector will pull the vehicle away from the Earth. If the magnitude of the command is greater than 90 degrees the vehicle will be pulled toward the Earth. The four quadrants are shown in Figure 2.4-1.

2.5 Control Technique

A reaction control system was developed to manuever the vehicle in response to the guidance commands. A block diagram of the AOTV classical control system and attitude control blocks is shown in Figure 2.5-1. The reaction control systems reside in the pitch, yaw, and roll blocks. The inputs to the RCS are the attitude errors and the outputs are torques about the corresponding axes. The following two sections describe the choice of the control effector and the operation of the control system.

2.5.1 Control Effectors

Two types of control effectors were considered for the AOTV, 1) reaction control jets (thrusters), and 2) aerodynamic trim surfaces. Thrusters are required for control in the space environment, while the aerodynamic trim tab could be used in the aeropass. The added complexity of the trim tab (control surface,

actuator, power source) and the lack of a requirement for precise angle-of-attack control reduced the need for the trim surface. The guidance algorithm does not require control of the angle-of-attack because it assumes that the vehicle is stable and operating at the aerodynamically trimmed angle-of-attack. It is not feasible to trim the vehicle a different angle-of-attack with the reaction control jets in the atmosphere due to excessive fuel use.

The thrusters were located such that they do not impinge upon the vehicle structure and are shielded from the heating wake. The locations are at 15.7 feet fore and aft of the center of gravity, and 5.0 feet on each side of the centerline. Figure 2.5.1-1 shows the vehicle and the thruster locations. Only the yaw thrusters create a pure moment on the vehicle; the pitch and roll thrusters also produce a force along the positive body Z axis. At the trimmed angle-of-attack, this produces a small ΔV effect.

2.5.2 Control System

Two RCS control techniques were developed for the AOTV. Both methods were designed to accommodate bank and angle-of-attack commands from the guidance algorithm. The first control design uses classical linear control theory with proportional thrusters. Recent advances in thruster technology have made the use of throttleable thrusters feasible. The control system uses attitude and derived rate feedback in a proportional/derivative

control architecture. The gains for each axis were chosen to give a 0.2 Hz response and a damping ratio of 0.8.

The second design uses conventional on-off thrusters in a phase-plane control algorithm. The phase-plane uses parabolic switching curves derived from the maximum acceleration capability and a rectangular dead zone to mimimize minimum-bit limit cycling. The parabolic switching curves give minimum time respone to an error signal and no chattering along the switching line. Figure 2.5.2-1 is a block diagram of the two control system layouts. The pitch, yaw, and roll control law blocks in Figure 2.5-1 can be either of the above mentioned control techniques. Figure 2.5.2-2 lists the parameters for each axis for both control techniques.

ENGINEERING TECHNOLOGY

AOTV Concepts

Boeing Aerospace Company

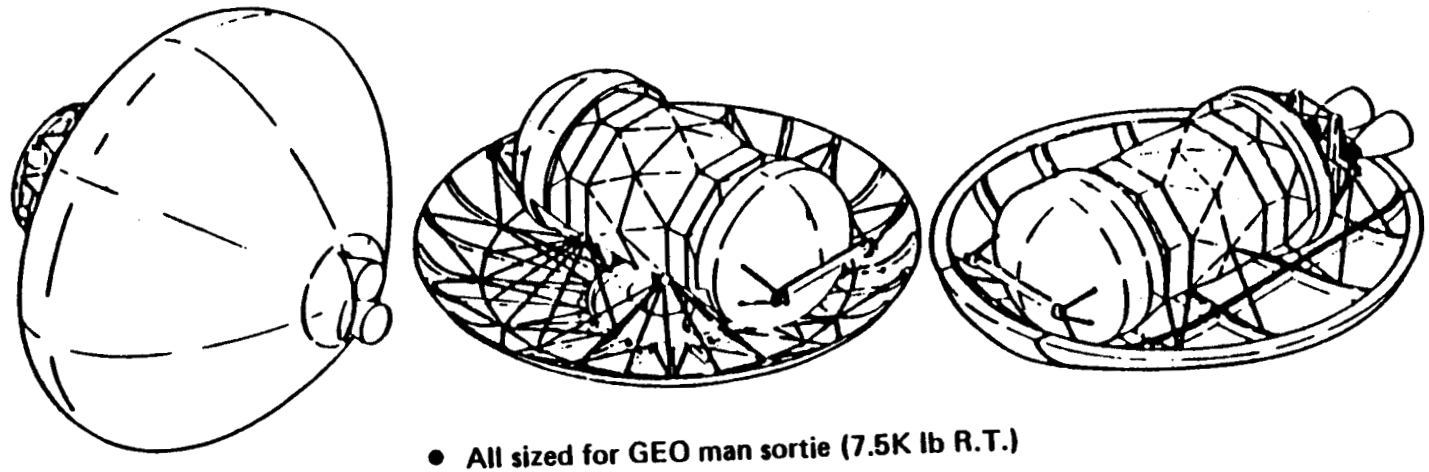

- All sized for GEO man sortie (7.5K lb R.T.)

	Ballute brake	Lifting brake	Shaped brake
• Aeromaneuver features	T/D = 1.5 B/W = 1500°F	L/D = .117	L/D = .234
• Vehicle size (ft)	14.5 x 35.7 Ballute 50-ft dia.	42 dia.	44 x 36
• Dry weight (lb) (brake wt.)	9189 (2712)	9947 (3276)	10314 (3608)

Figure 2.1-1

ENGINEERING TECHNOLOGY

AOTV Mission Profile

Boeing Aerospace Company

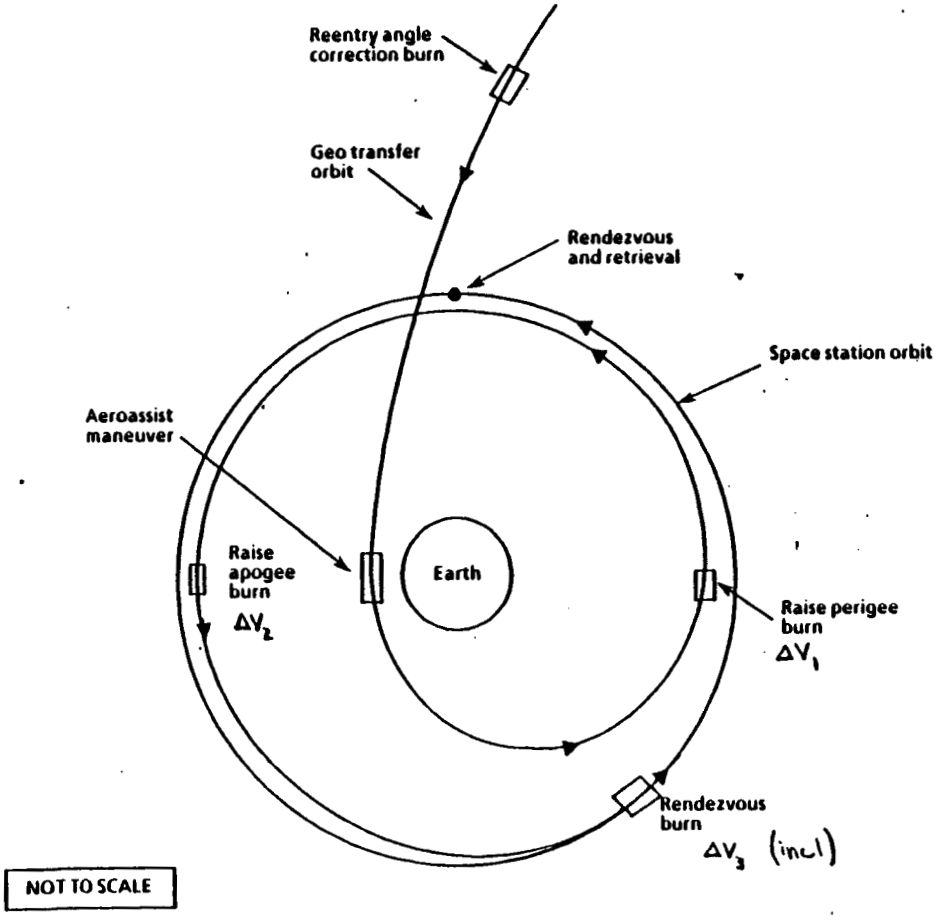

Figure 2.1-2

ENGINEERING TECHNOLOGY

Nominal Mission Altitude/Velocity Profile

Boeing Aerospace Company

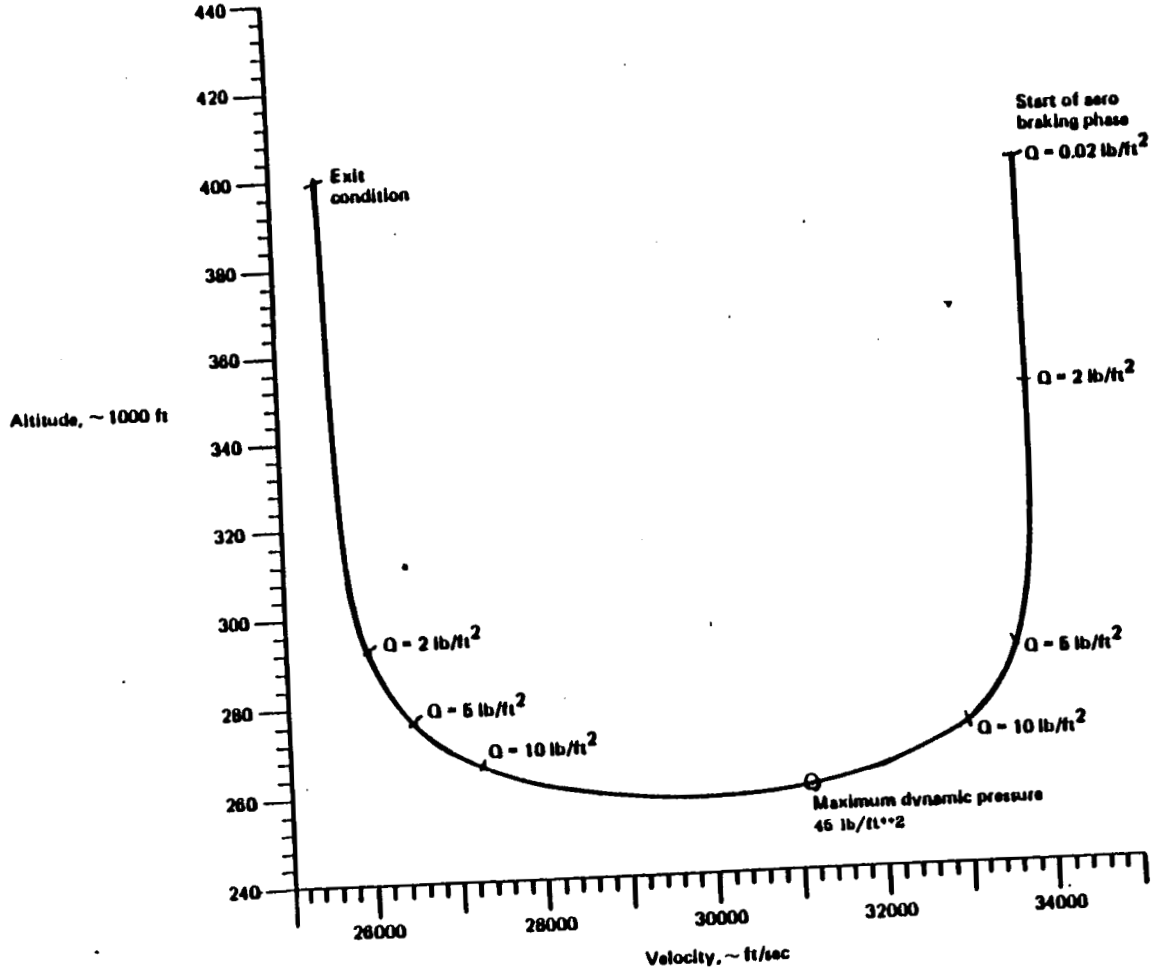

Figure 2.1-3

NOMINAL DYNAMIC PRESSURE PROFILE

Boeing Aerospace Company

ENGINEERING TECHNOLOGY

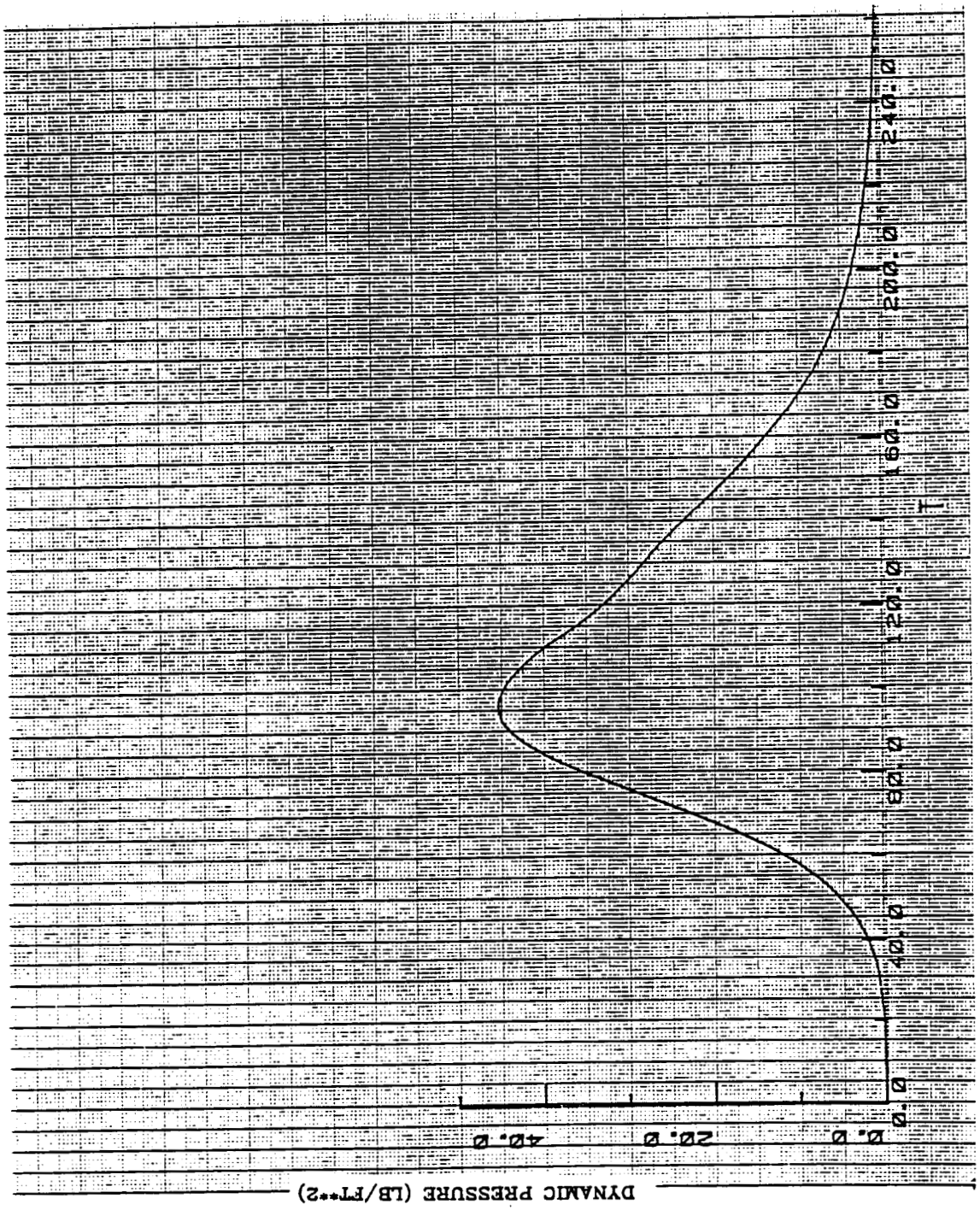

Figure 2.1-4

NOMINAL BANK HISTORY

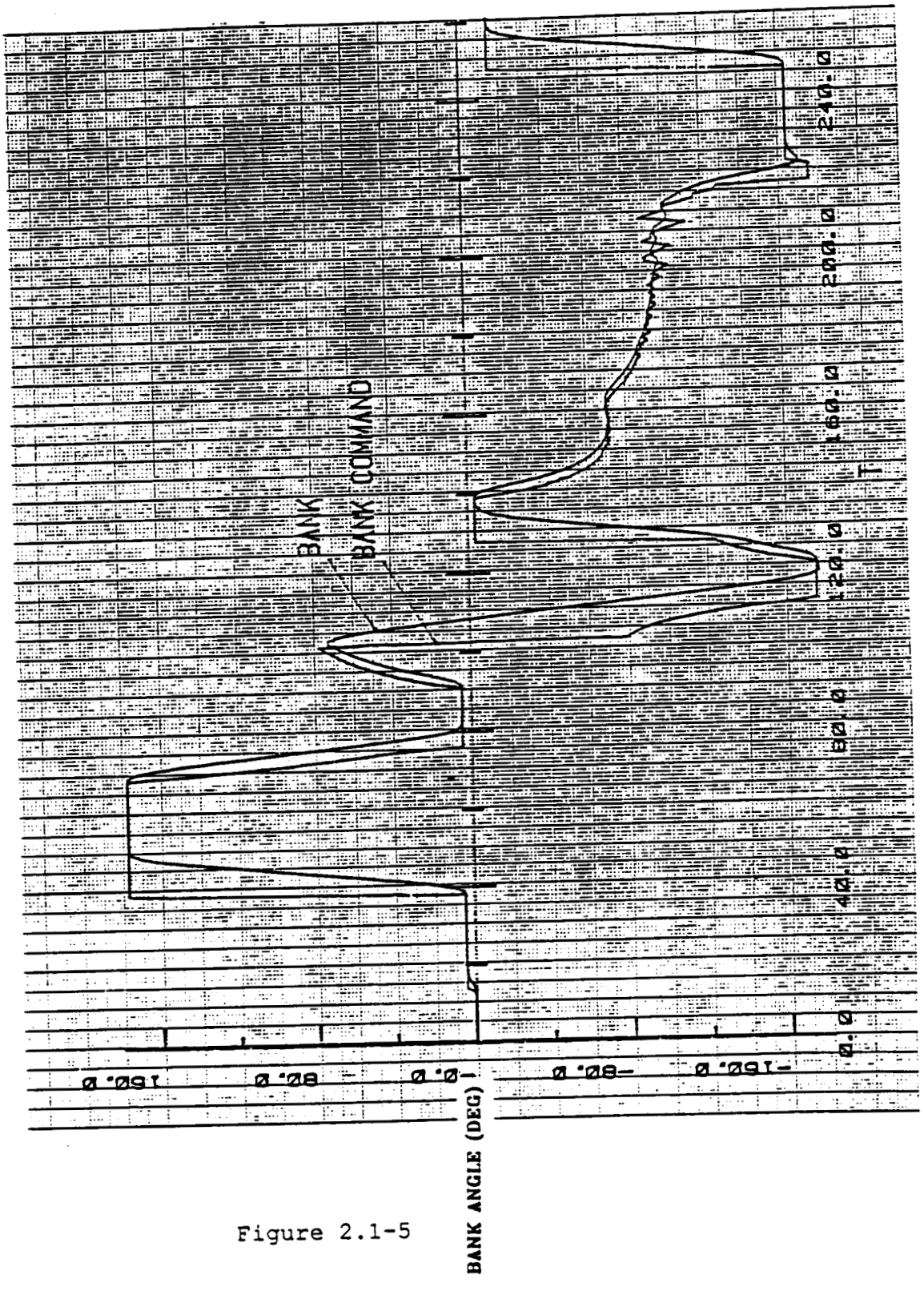

Figure 2.1-5

Shaped Brake Vehicle

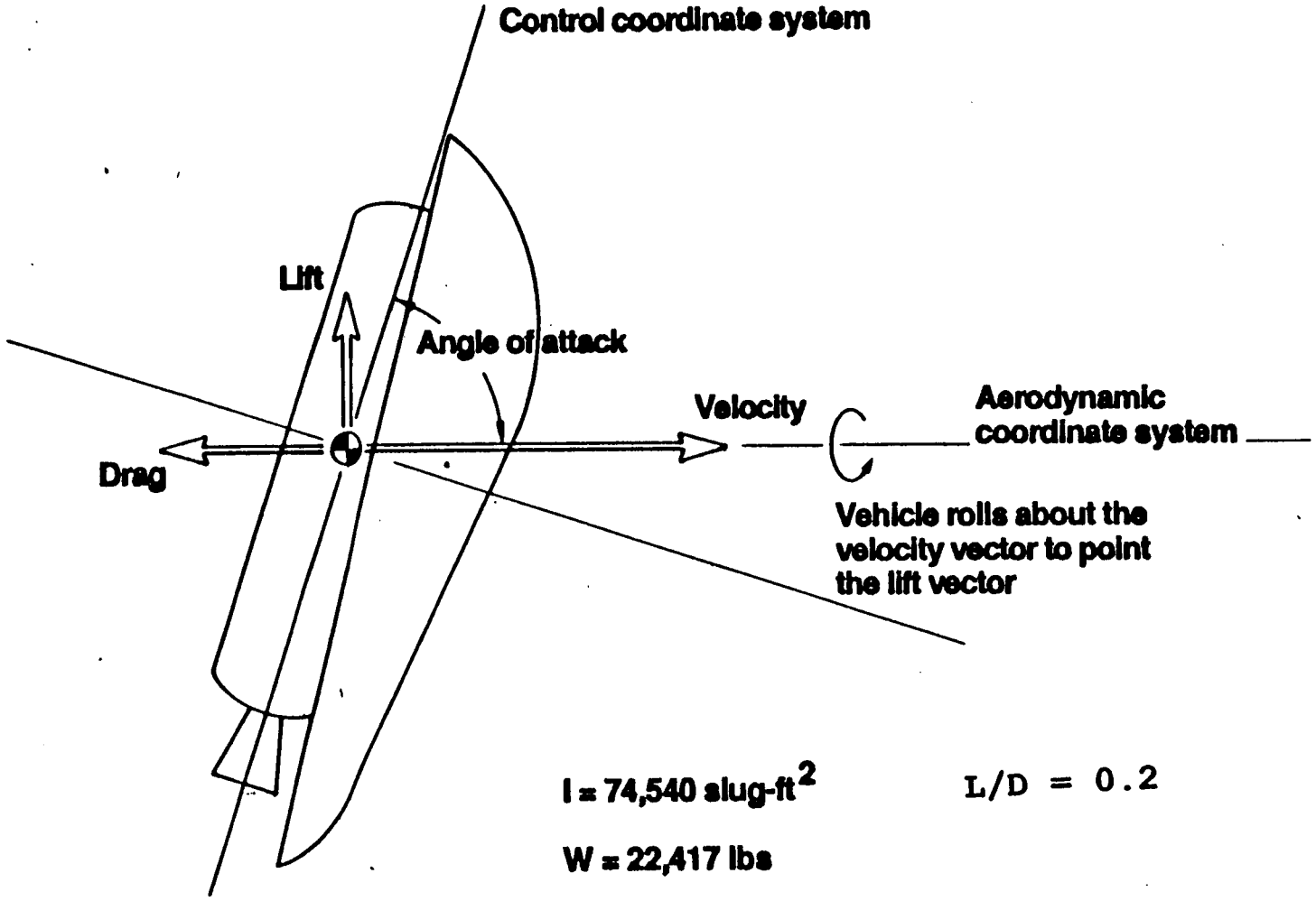

Figure 2.2-1

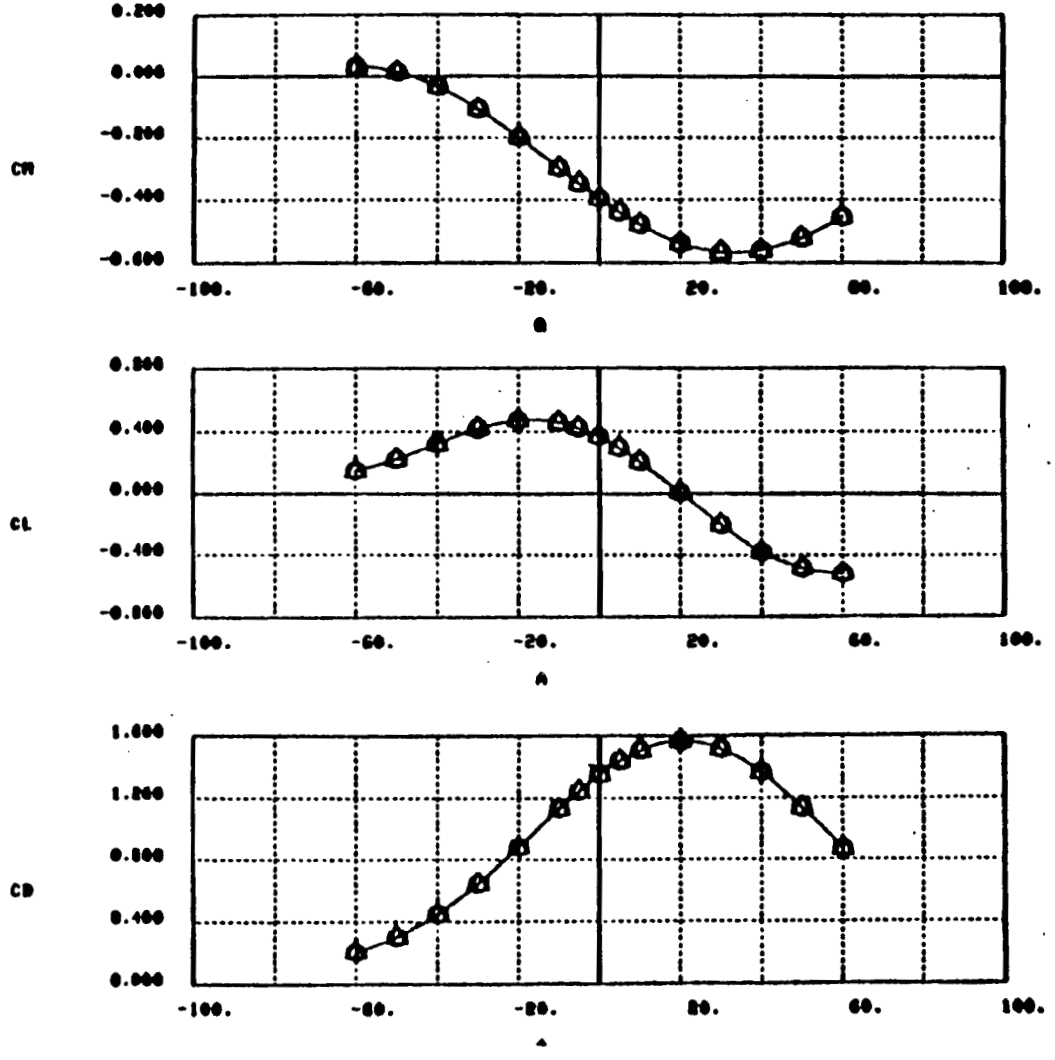
CM
0.200
0.000
-0.200
-0.400
-0.600
-100.
-60.
-20.
20.
60.
100.
α
CL
0.800
0.400
0.000
-0.400
-0.800
-100.
-60.
-20.
20.
60.
100.
α
CD
1.600
1.200
0.800
0.400
0.000
-100.
-60.
-20.
20.
60.
100.
α

Figure 2.2-2

Control Corridor Definition

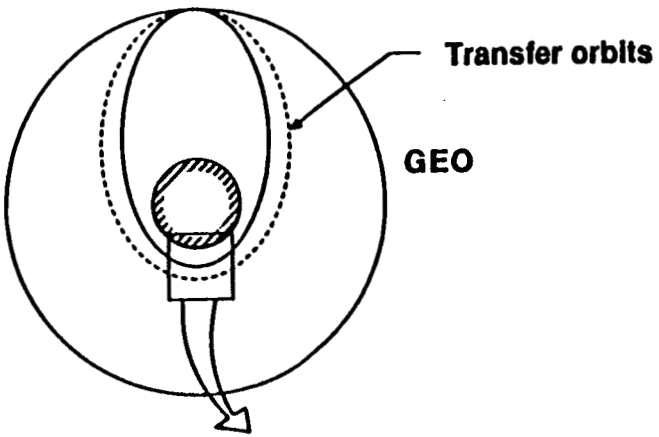

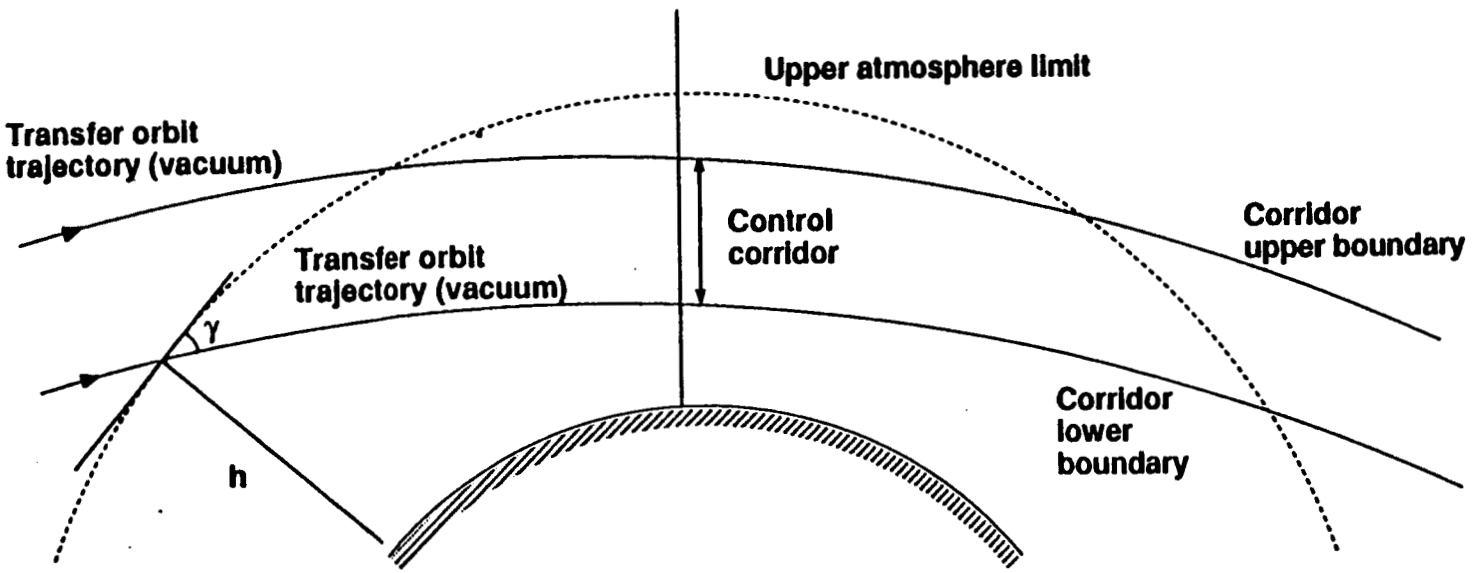

Figure 2.3-1

ΔV Vs. Control Corridor

ENGINEERING TECHNOLOGY — Boeing Aerospace

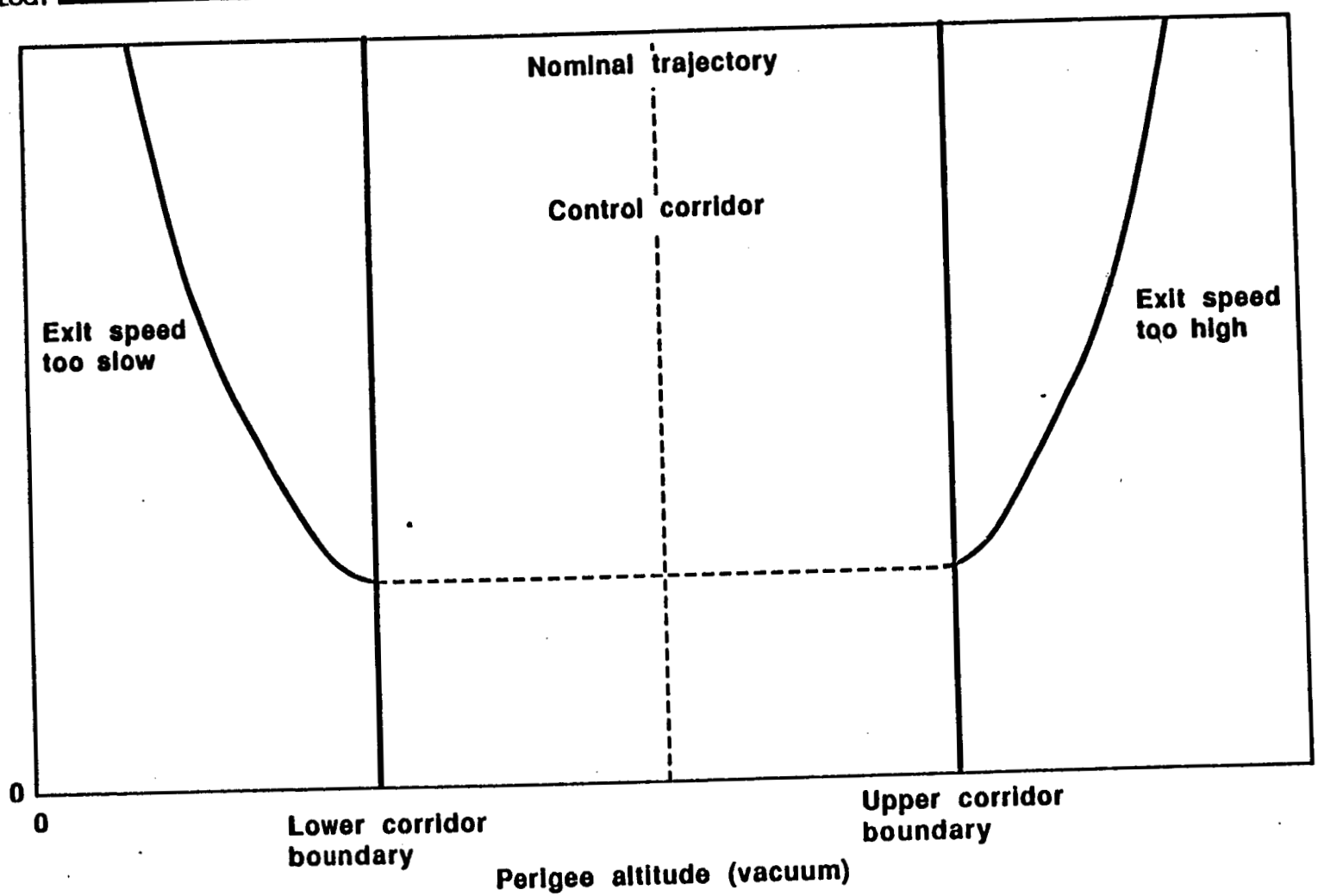

Figure 2.3-2

Control Corridor Width vs. L/D Ratio

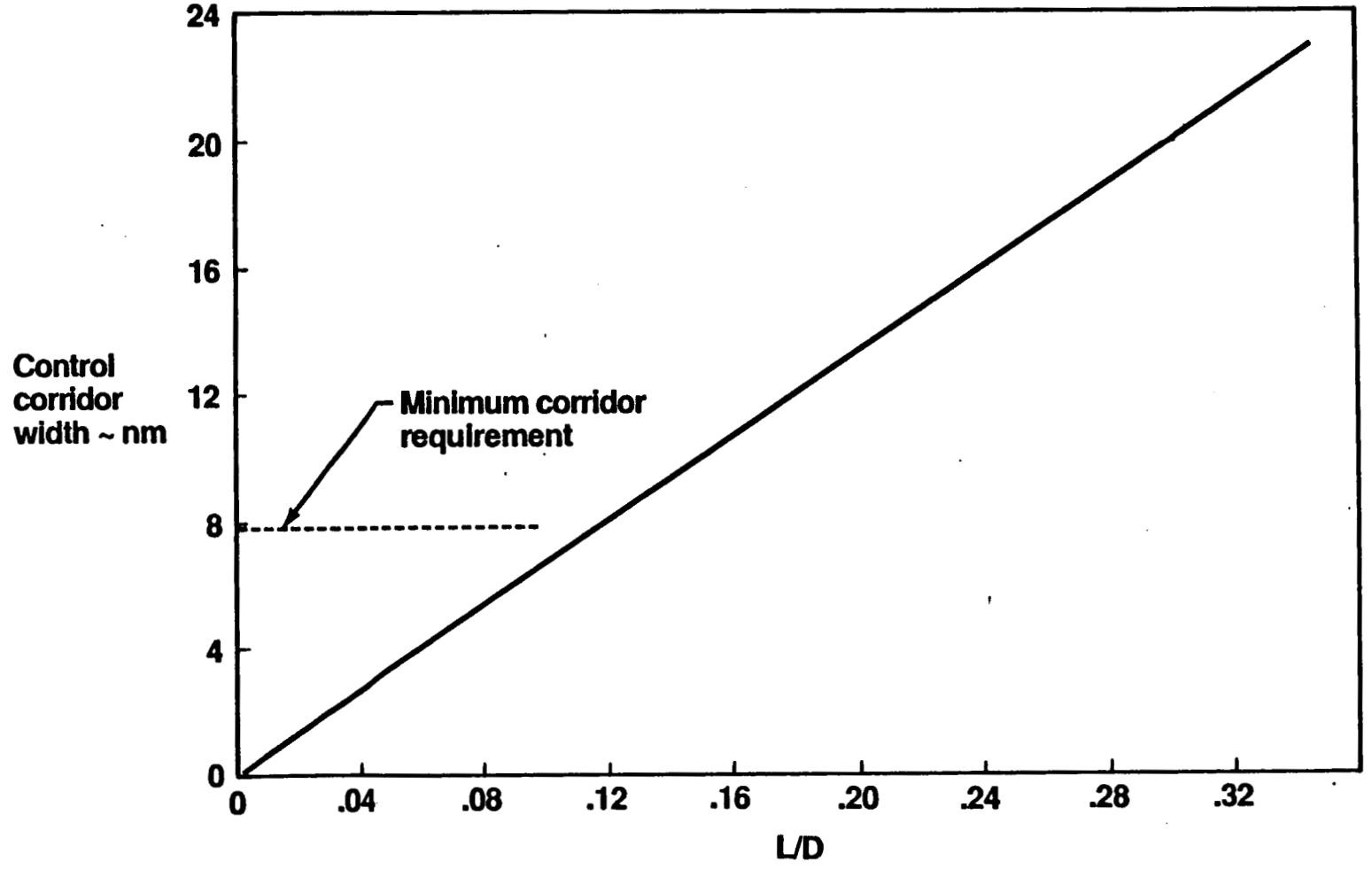

Figure 2.3-3

Minimum Corridor Width Requirement

ENGINEERING TECHNOLOGY

Boeing Aerospace

	Allotted error	Sensitivity N.M./_____	Equivalent corridor width (N.M.)
Navigation error			
Gamma (γ)	0-1 degree	13	1.3
Velocity (V)	500 ft/sec	$3.71 \cdot 10^{-3}$	1.86
Altitude (h)	10,000 ft	$2.2 \cdot 10^{-4}$	2.2
Aerodynamic error			
X C.G.	0.25 ft	2.6	0.65
Z. C.G.	0.25 ft	6.5	1.625
Aero coefficient (L/D)	7%	0.4	2.8
Guidance law effect			2
Inclination	0.5 degree	6	3
Total RSS			RSS = 5.82 N.M
Margin	35%		Minimum corridor width required: 7.86 N.M.

Figure 2.3-4

Orbital Plane Change Capability

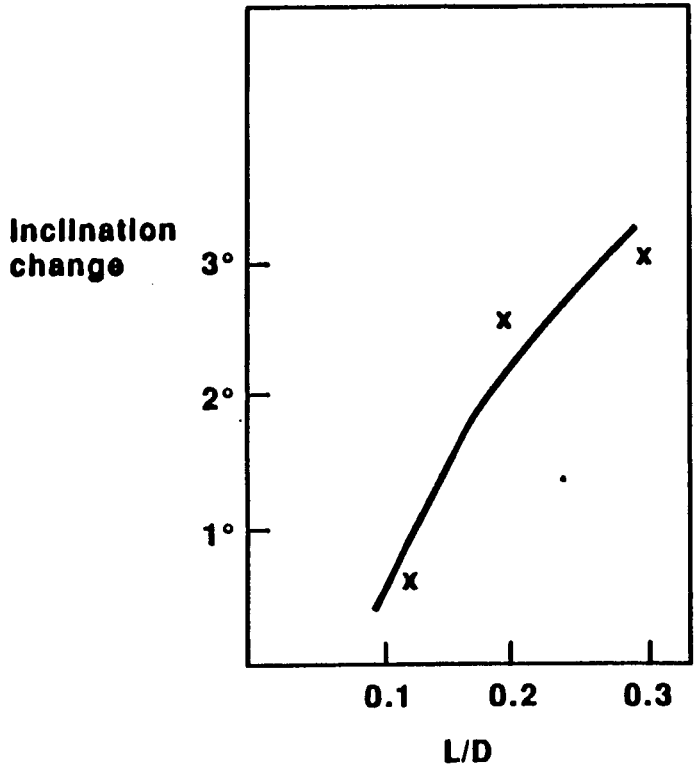

Figure 2.3-5

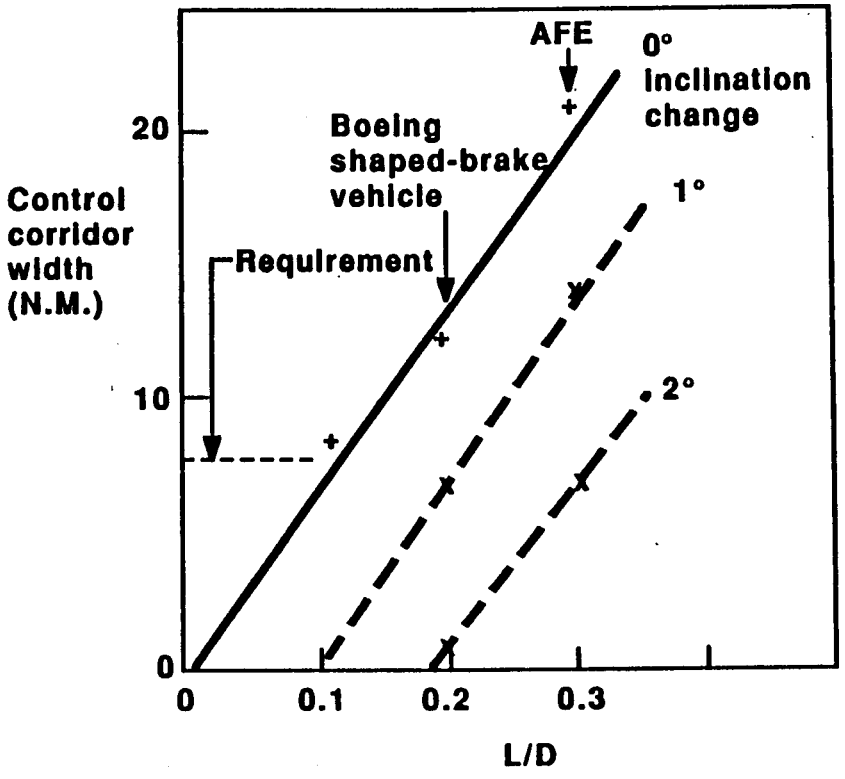

Figure 2.3-6

Bank Angle Command Quadrants

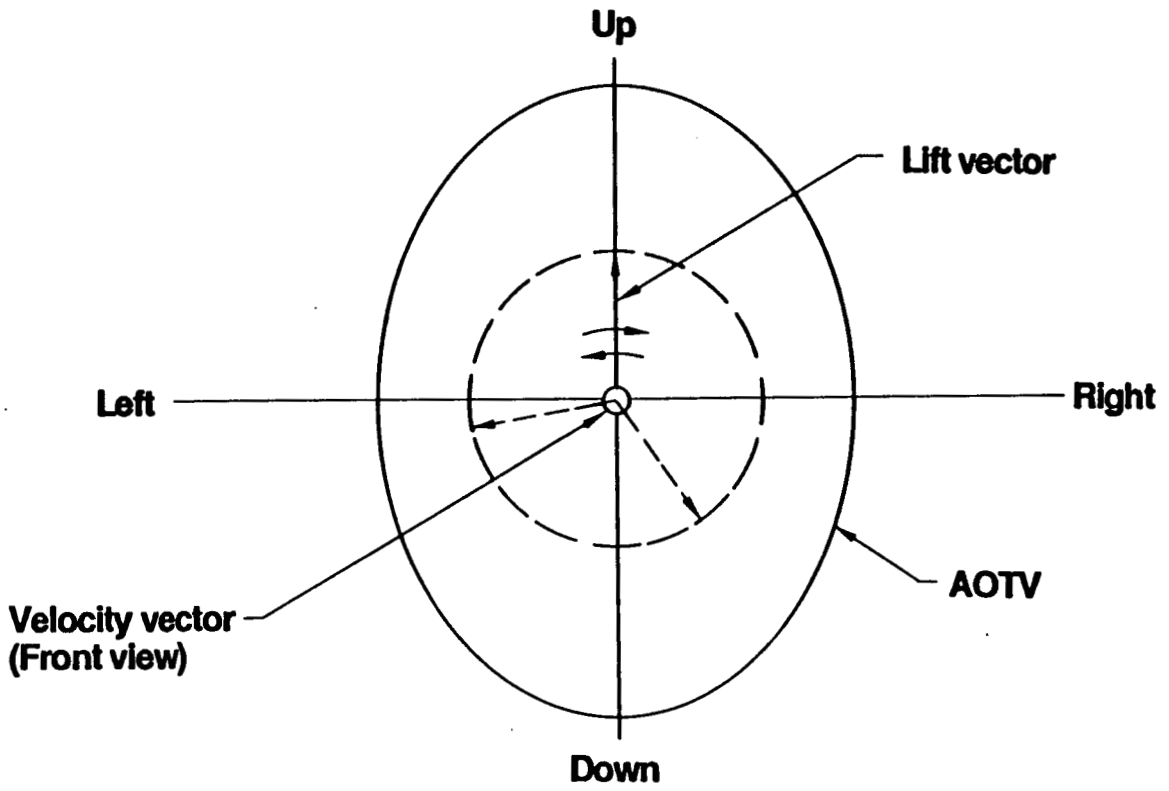

Figure 2.4-1

Control System Block Diagram

ENGINEERING TECHNOLOGY

Boeing Aerospace Company

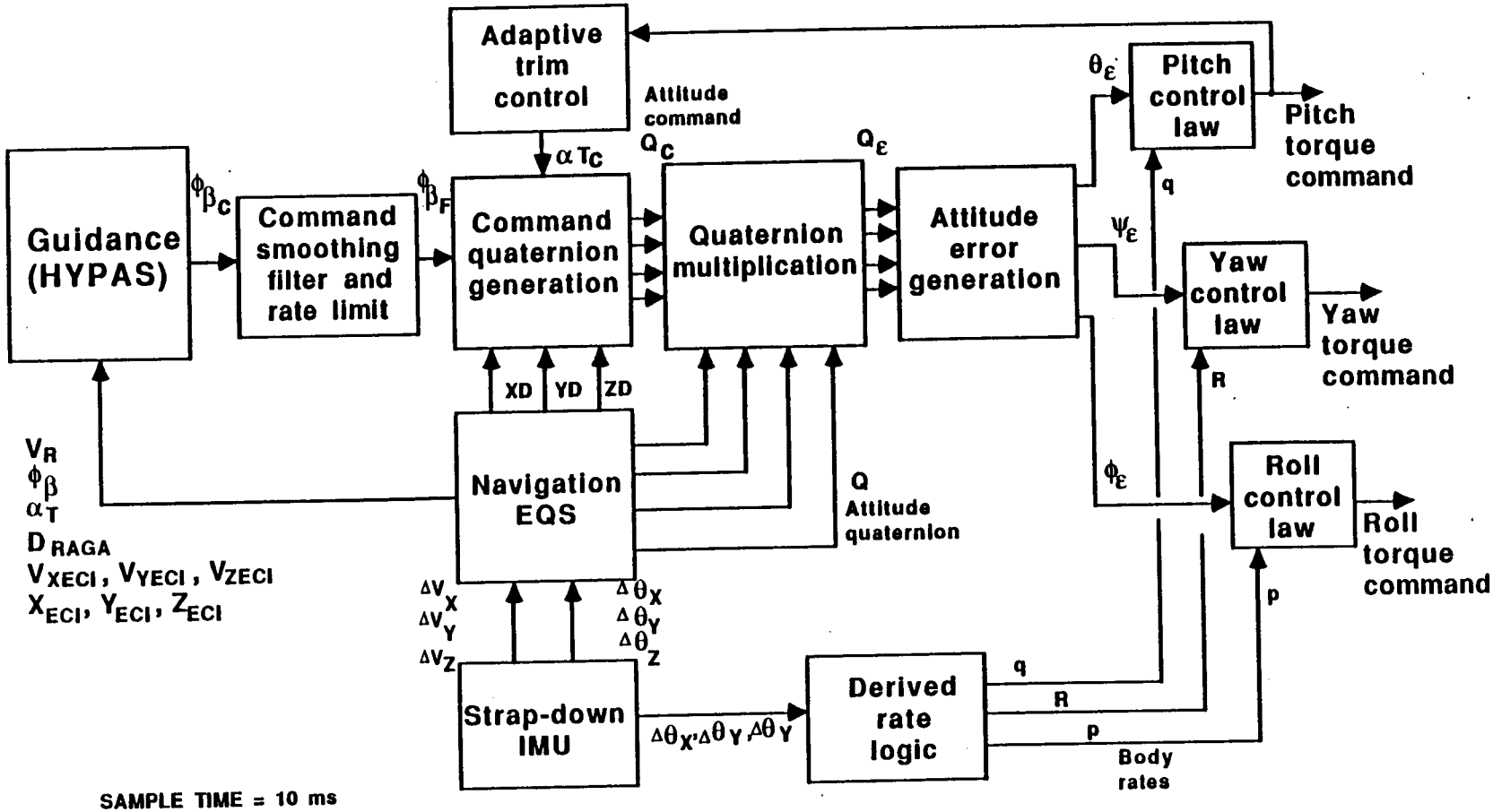

Figure 2.5-1

ENGINEERING TECHNOLOGY

RC Thruster Location (Shaped-Brake AOTV)

Boeing Aerospace Company

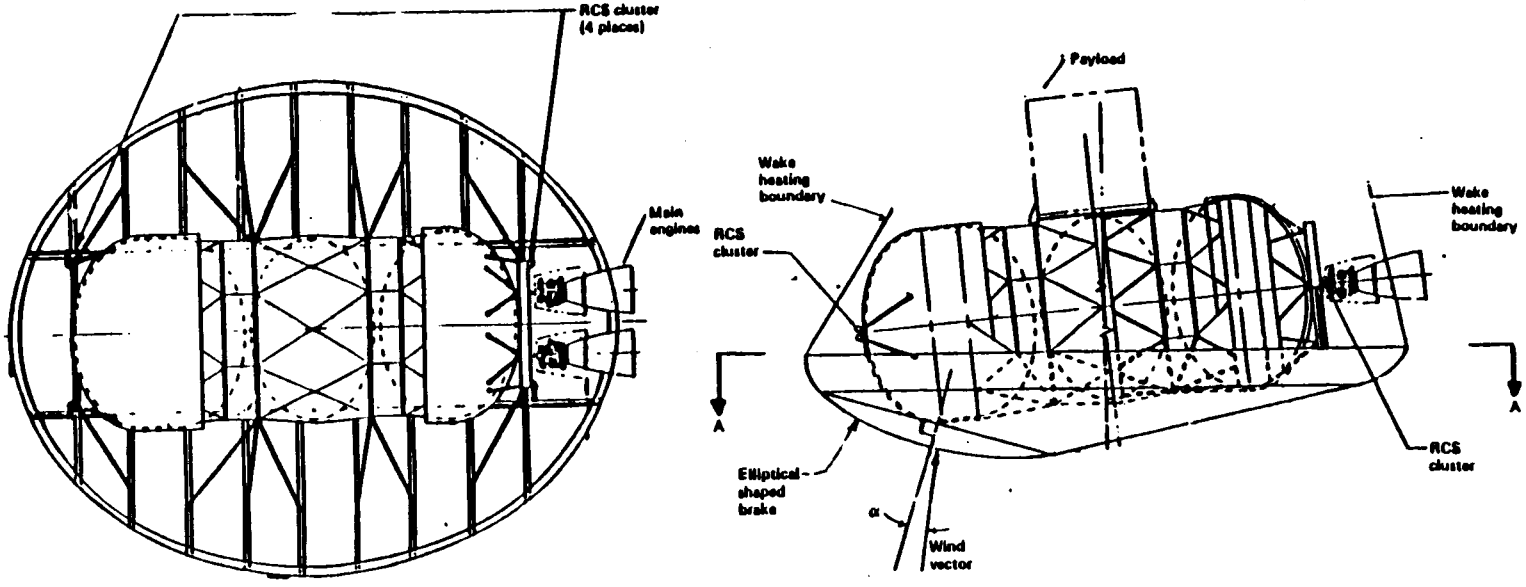

Figure 2.5.1-1

Control Laws

- Proportional

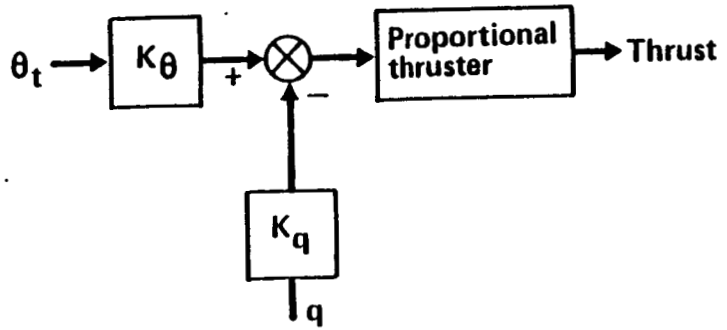

- On-off

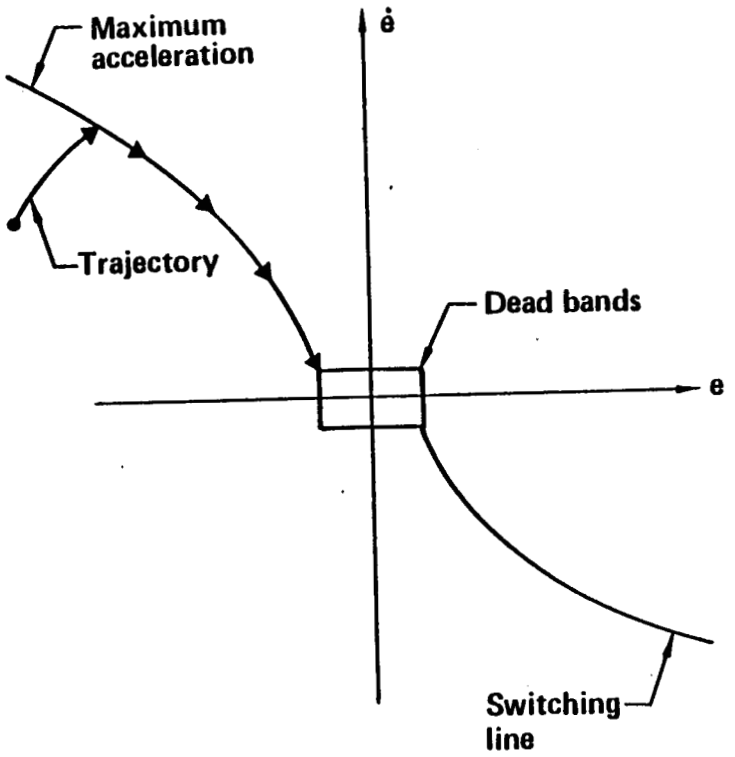

Figure 2.5.2-1

Control Parameters

	Axis	Damping Ratio ξ	Bandwidth W (rad/sec)	Thruster Size (lb)
Proportional Thrusters	Roll	0.8	1.25	250
	Pitch	0.8	1.25	100
	Yaw	0.8	1.25	250

	Axis	Altitude Dead Band (deg)	Rate Dead Band (deg/sec)	Thruster Size (lb)
On-Off Thrusters	Roll	1.5	.1	250
	Pitch	1.5	.1	100
	Yaw	1.5	.1	250

Figure 2.5.2-2

3.0 DESIGN CRITERIA

A set of design criteria, such as the stabilty margins and response times, are usually specified for the control design. The 6DOF simulation with atmosphere and vehicle/hardware uncertainties is then used to evaluate the performance and robustness of the design. This section details the design criteria that were used to develop the AOTV control system.

3.1 Fuel Use And Control Response Requirements

The criteria for the design of the AOTV autopilot were to create a control design that would minimize the fuel burned during the atmospheric maneuvers and also to closely follow the guidance commands to minimize the fuel needed for insertion into the desired orbit. These tend to be opposing criteria since the first objective requires minimal thruster use and the second objective requires significant thruster use to follow rapidly changing large angle guidance commands.

The autopilot must have sufficient bandwidth and accuracy to insure that the total system achieves a desirable post-aeropass velocity and trajectory. An indication of the robustness can be identified in the gain and phase margin of the system. These margin are calculated by opening each loop of the autopilot and analyzing the stability margin. The design goal for each autopilot

loop, opened at the actuator command, is +6 db gain margin and +30 degrees phase margin. The overall system robustness is verified with the sensitivity analysis, wich is measured in terms of fuel consumption and DV.

3.2 Atmosphere Characteristics

Variations in the atmosphere directly affect the AOTV mission. The control system must be able to handle variations in density by as much as twenty percent. The system must also accommodate winds of up to 400 feet per second. Figure 3.2.-1 shows sample air density and wind profiles generated for each season using the GRAM atmosphere model (Global Reference Atmosphere Model).

3.3 Design Uncertainties

The control system must be able to handle uncertainties in the mass distribution, aerodynamic models, and sensor outputs. The following section lists an estimate of the vehicle and hardware uncertainties. The uncertainty values are the result of past experiences on other projects and associated hardware. These values are used in the sensitivity analysis in Section 5.

3.3.1 Mass Properties

In the design phase, the uncertainty in mass properties is large. As the project evolves to the final design and the payload and

mass properties are more accurately determined, the uncertainty value approaches 2-5%. Each payload will alter the c.g. location of the vehicle, which will in turn alter the trim position. The control system must remain stable in the c.g.-shifted condition.

3.3.2 Aerodynamics

Table 3.1 lists estimates of the aerodynamic uncertainties. These tolerances apply to a vehicle which has been aerodynamically wind tunnel tested. The values are associtated with the wind tunnel test accuracy. The uncertainties are small (±5%) for force data, with somewhat larger uncertainty for the moment data. The tolerances are large for the moment cross-coupling term since the nominal values are usually small.

3.3.3 Strapdown Platform Uncertainties

Table 3.2 lists the tolerances associated with a strapdown platform. Values shown are specification values received from strapdown platform vendors. These values are for state-of-the-art missile hardware.

Figure 3.2-1

SAMPLE GRAM ATMOSPHERES

ENGINEERING TECHNOLOGY

Boeing Aerospace Company

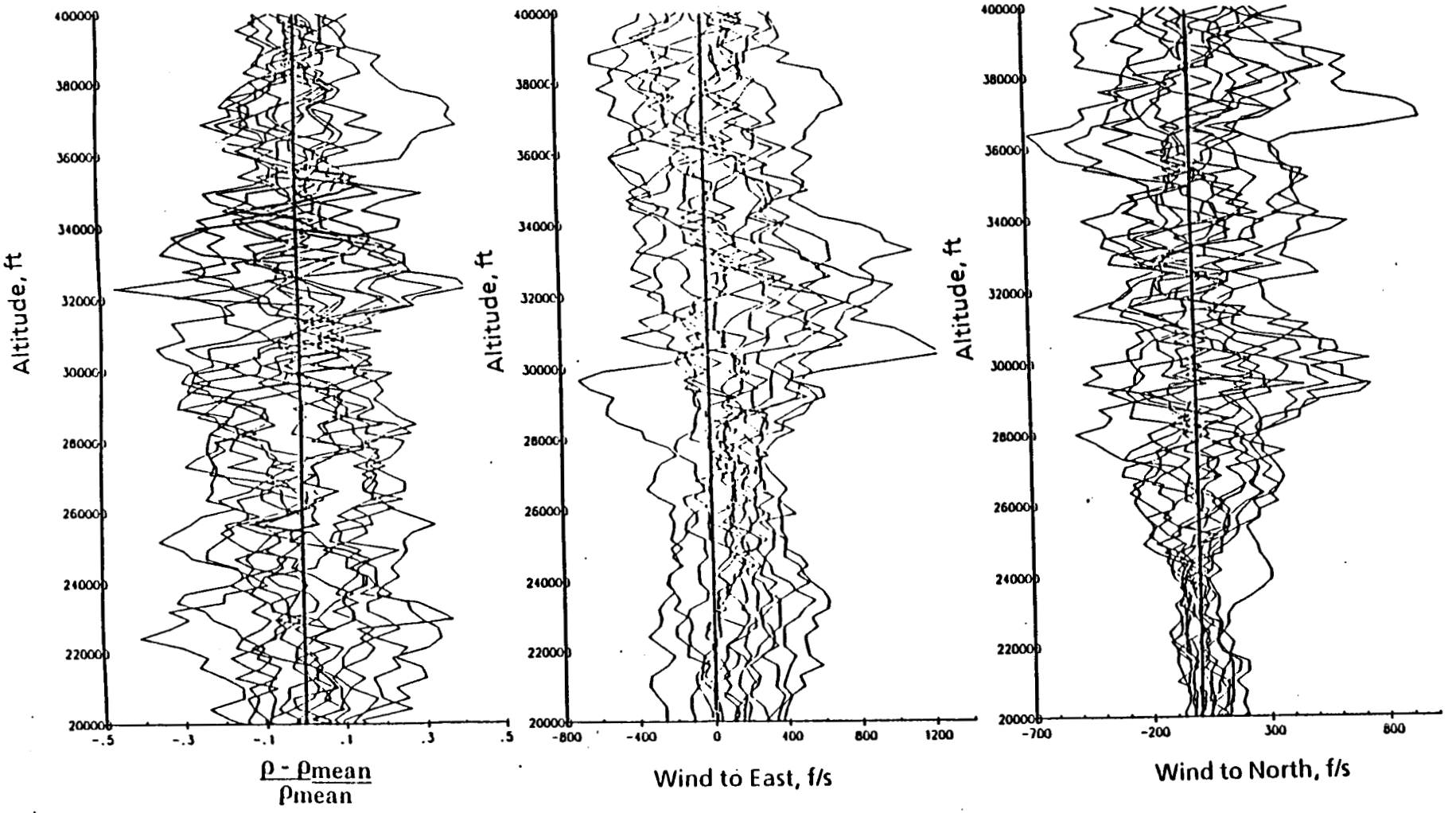

Table 3-1. Aerodynamic Uncertainties

Parameter		Mean Value	3σ Derivation
Aerodynamic Variation	CX	1.0	5%
	CY	1.0	5%
	CZ	1.0	5%
	$C_{m\alpha}$	1.0	5%
	$C_{n\beta}$	1.0	10%
	$C_{l\beta}$	1.0	10%

Parameter		Fortran Variable	Mean Value	3σ Derivation
Rate Gyro Noise	Roll gyro Pitch gyro Yaw gyro	SRTX SRTY SRTZ	0 0 0	.3 deg/sec .3 deg/sec .3 deg/sec
Rate Gyro Bias	Roll gyro Pitch gyro Yaw gyro	BTX BTY BTZ	0 0 0	.0014 deg/sec .0014 deg/sec .0014 deg/sec
Rate Gyro Scale Factor	Roll gyro Pitch gyro Yaw gyro	SFTX SFTY SFTZ	1.0 1.0 1.0	.5% .5% .5%
Rate Gyro Misalignment	Roll gyro Pitch gyro Yaw gyro	PHIG THETAG PSIG	0 0 0	.01 degree .01 degree .01 degree

Parameter		Fortran Variables	Mean Value	3σ Derivation
Rate Gyro Acceleration Sensitivity	Roll sensitivity to $\dot{Q}$ Pitch Sensitivity to $\dot{R}$ Yaw sensitivity to $\dot{Q}$	ATHX ATHZ ATHZ	0 0 0	10 deg/sec/rad/sec^2 10 deg/sec/rad/sec^2 10 deg/sec/rad/sec^2

Table 3-2 Rate Gyro Error Statistics

4.0 DESIGN SYNTHESIS

This section presents the results of the trade studies used to determine the final control system design. The results were used to modify and fine tune the control system and the guidance algorithm to achieve better mission performance.

4.1 Thruster Sizing

Thruster sizes of 100 lbs, 250 lbs, 350 lbs, and 500 lbs were traded to determine the required size. Initially, all axes (roll, pitch, and yaw) used the same size of thruster. In the final design, smaller thrusters were used in the pitch axis because the bank commands from the guidance algorithm involve only the roll and yaw thrusters (for trimmed angle-of-attack).

Rate limits of 15 deg/sec, 17 deg/sec, 20 deg/sec, and 30 deg/sec were used in the autopilots. The rate limits were used to smooth the bank command and eliminate excessive fuel use in the thrusters. Figure 4.1-1 is a block diagram of the digital autopilot design.

The effects of the RCS thruster size and the autopilot rate limit were examined using the total fuel and total ΔV as measures of the sensitivity. Figure 4.1-2 shows the fuel use versus thruster size for all four rate limit configurations. The 15 deg/sec case indicates the lowest fuel use but in fact the lag was so extreme

with respect to the guidance algorithm that the autopilot effectively did nothing. This is reflected in Figure 4.1-3 for the 15 deg/sec curve which shows large ΔV requirements for any thruster size. Larger thrusters combined with the larger rate limits performed better at the expense of more fuel burned. A somewhat "optimal" design can be chosen by trading fuel used for required ΔV. The 20 deg/sec rate limit gives the lowest ΔV for the smaller thruster sizes and the median response for the fuel use. A 250 lb thruster gives a ΔV of around 500 ft/s and uses around 250 lbs of fuel. This design point is shown on Figures 4.1-2 and 4.1-3 by X's.

The operation of the guidance algorithm is the reason for the seemingly large thrusters and large amount of fuel use. The bank commands from the algorithm require large (-165 deg,+165 deg), fast rotational maneuvers of a vehicle with large rotary inertia (74500 slug-ft^2). The smaller thrusters are just capable of following the guidance close enough to reduce the exit condition errors.

Figues 4.1-4, 4.1-5, 4.1-6, and 4.1-7 are time history responses of the 6DOF simulation using the design point with 250 lb thrusters and a 20 deg/sec rate limit in the autopilots. Figures 4.1-4 and 4.1-5 show the altitude versus velocity and altitude versus time trajectories. Figure 4.1-6 is the bank command and actual bank angle. Notice that the actual bank angle lags behind the commanded bank angle. Figure 4.1-7 is the response of one of

the yaw thrusters.

The final design uses 250 lb thrusters for the yaw axis and 100 lb thrusters for the pitch axis. The rate limits were established at 20 deg/sec.

4.2 Control System Trades

Two types of thruster/autopilot systems were included in the six degree-of-freedom simulation, a proportional thruster/autopilot system and a phase-plane/autopilot system. A proportional system is more effective for studying the vehicle sensitivities and the guidance algorithm because of its response characteristics. The proportional system contributes to the dynamic response in a predicable way which makes the other system contributions more distinguishable.

There is an inherent problem created when using a phase-plane/autopilot system and a rapidly changing command source such as HYPAS. Phase-plane systems are usually designed to accommodate a step position command, not follow a series of commands which have faster time constants than the vehicle response time. One way to accommodate these types of commands in a phase-plane system is to use large thrusters to lower the vehicle response time. Without the large thrusters in the roll and yaw axes, the vehicle was not able to follow the guidance well enough to sufficiently reduce the velocity errors at exit.

The phase-plane was designed using parabolic switching curves and a rectangular dead zone for position and rate errors. This phase-plane design always used more fuel than the proportional autopilot for the same flight scenario. Figures 4.2-1, 4.2-2, 4.2-3, and 4.2-4 show the phase-plane verus proportional autopilot fuel trade. Given a specific vehicle design, weight, thruster size, etc., a more elaborate phase-plane could be developed which would approach the proportional autopilot performance.

4.3 Adaptive Angle of Attack Control

An adaptive control scheme was designed to "hunt" for the aerodynamic trim condition in the pitch axis as the center-of-gravity was moved with different payloads. The integrator adjusts the commanded angle-of-attack until the vehicle is trimmed. This would reduce the amount of fuel used by eliminating the need for the pitch thrusters to counter the moment caused by the non-trimmed flight condition.

The technique worked well for some C.G. locations and not for others. In fact, for some C.G. locations the vehicle did not even exit the atmosphere (mission failure). Figure 4.3-1 can be used to explain the effect of the trim integrator on mission performance. The figure shows a plot of the coefficient of lift as a function of angle-of-attack and plots of the trim values of the vehicle for x and z variations in the C.G. location. Notice

that as the x or z location of the C.G. was increased (positive direction) the value of C_1 corresponding to the new trim condition was decreased. Thus at the new trim condition there is significantly decreased lift available to modulate the in- and out-of-plane errors in the trajectory. As the C.G. locations were moved in the negative direction the corresponding values of the lift coefficient increased.

The gains in the guidance algorithm were also modified to be semi-adaptively adjusted as a function of the estimated dynamic pressure. The equations were obtained from documentation on the derivation of the HYPAS guidance scheme [1]. These equations maintain an overdamped (zeta = 1.5) 0.05 hz response in the guidance logic. Other values for the damping and response frequency were tried, but all decreased the performance of the system. The damping ratio was decreased to zeta = 1.0 and the response frequency increased to 0.1 hz with mixed combinations of the two parameters in between. The addition of the equations to the simulation made only a small improvement in the system response. This is to be expected because most of the effective control authority occurs over a very small portion of the trajectory where the dynamic pressure is relatively constant.

4.4 Guidance Law Verification and Sensitivity

Initial comparisons of the 6DOF and 3DOF simulations did not match well. Specifically, the required ΔV's were much larger for the

6DOF simulation. After much tuning and verification of the algorithm, the response was improved but under no circumstances was able to match the performance of the 3DOF version. The basic difference between the two is that the rotary inertia in the 6DOF simulation prevents an exact following of the bank commands. Larger thruster sizes obviously improve the response, but at the expense of more fuel use.

A rate limiting first-order filter set at 0.2 Hz with a 30 deg/sec rate limit was used on the bank command output to smooth the commands. Without the filter the commands drove the RCS autopilots very hard and used excessive fuel. This situation occurs when the guidance alogrithm is not on a hard limit, and issues a ratchety command sequence.

The best performance was obtained by increasing the gain on the vertical plane correction during the entry phase, then decreasing the gain in the exit phase. This effectively creates the situation where the vertical plane components are corrected in the entry phase and the out-of-plane components (inclination) are corrected in the exit phase. This method decreased the required ΔV after exit by several hundred feet per second depending on the autopilot and guidance parameters selected.

The following are the parameters used in the guidance loop for the preliminary sensitivity studies:

GHDOT =.40

GHDOTX =.25

VSAT =26700 ft

VTRIG =29000 ft

AMXER =.63 deg

GN17b =7.6

These parameters were used as the design point for the guidance algorithm for all sensitivity studies.

The HYPAS guidance algorithm was further modified to save fuel by setting the command to zero during the exit phase when the dynamic pressure dropped below .5 lbs/ft^2. Aero maneuvers beyond this point did little to reduce the exit errors.

Rate Limited Filter

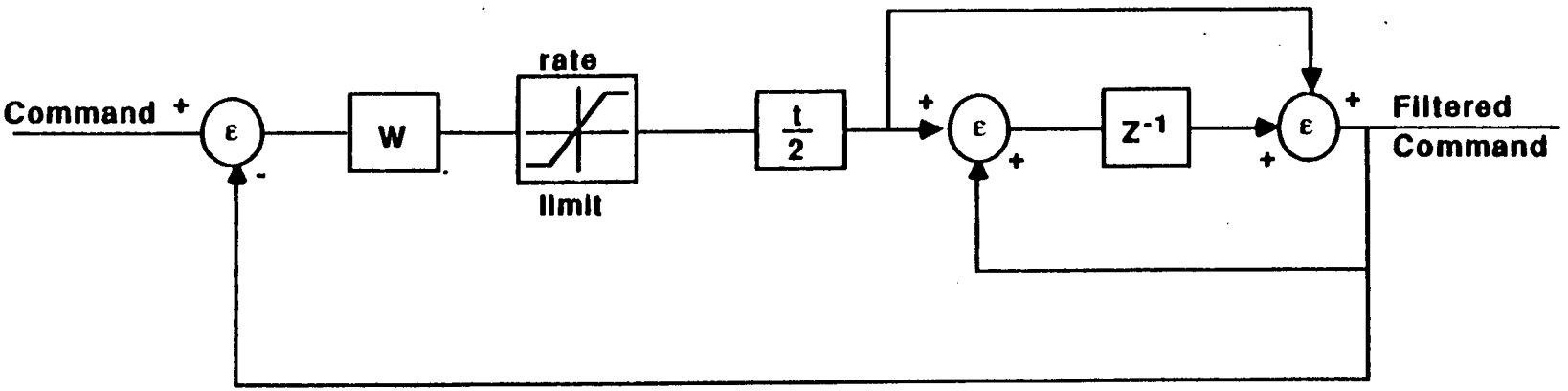

Z^{-1} ⟶ Unit delay

t ⟶ Sample period

W ⟶ Filter gain

88m-34-104c
6-6-88

Figure 4.1-1 Digital Autopilot Filter

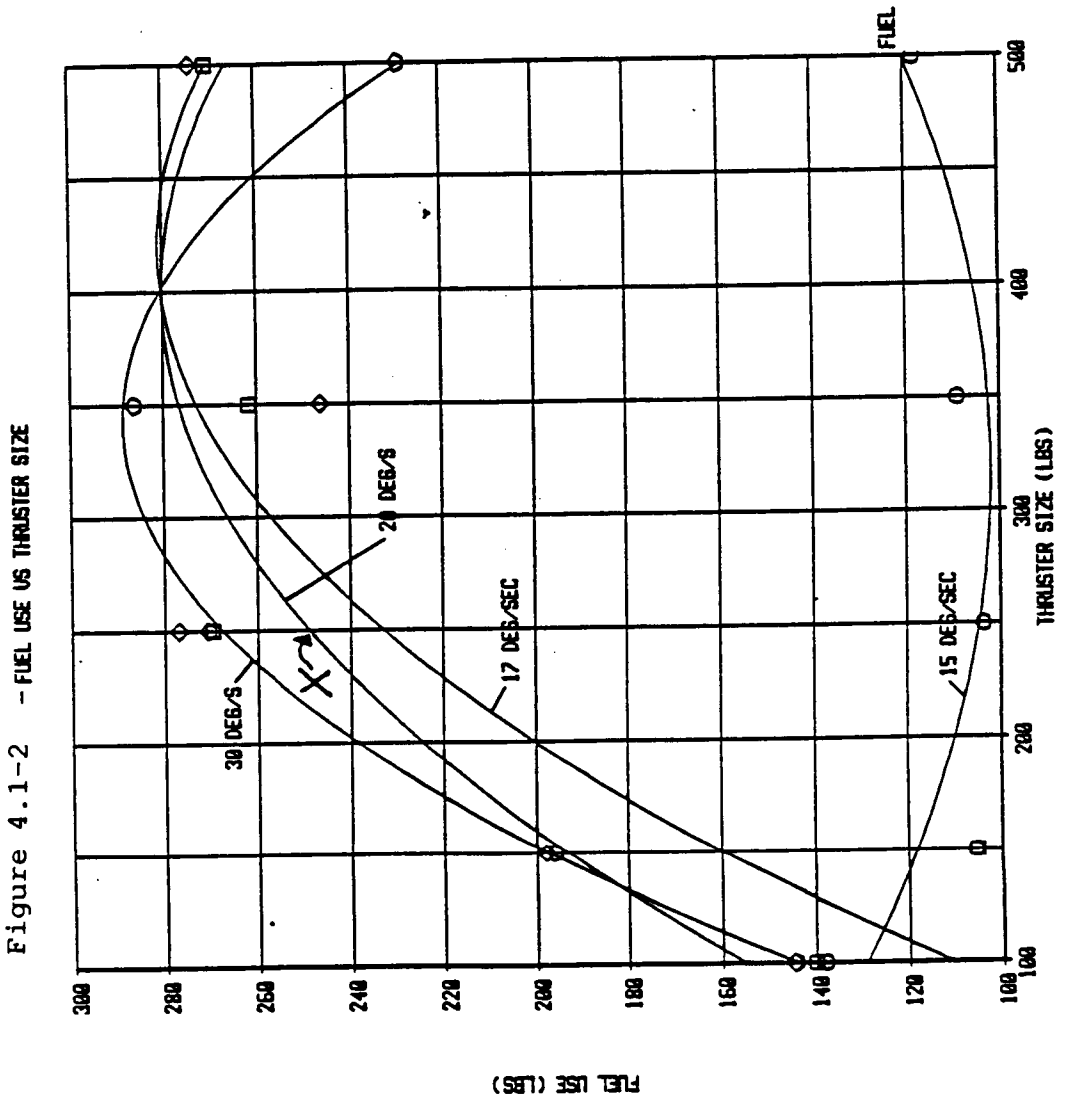

Figure 4.1-2 - FUEL USE VS THRUSTER SIZE

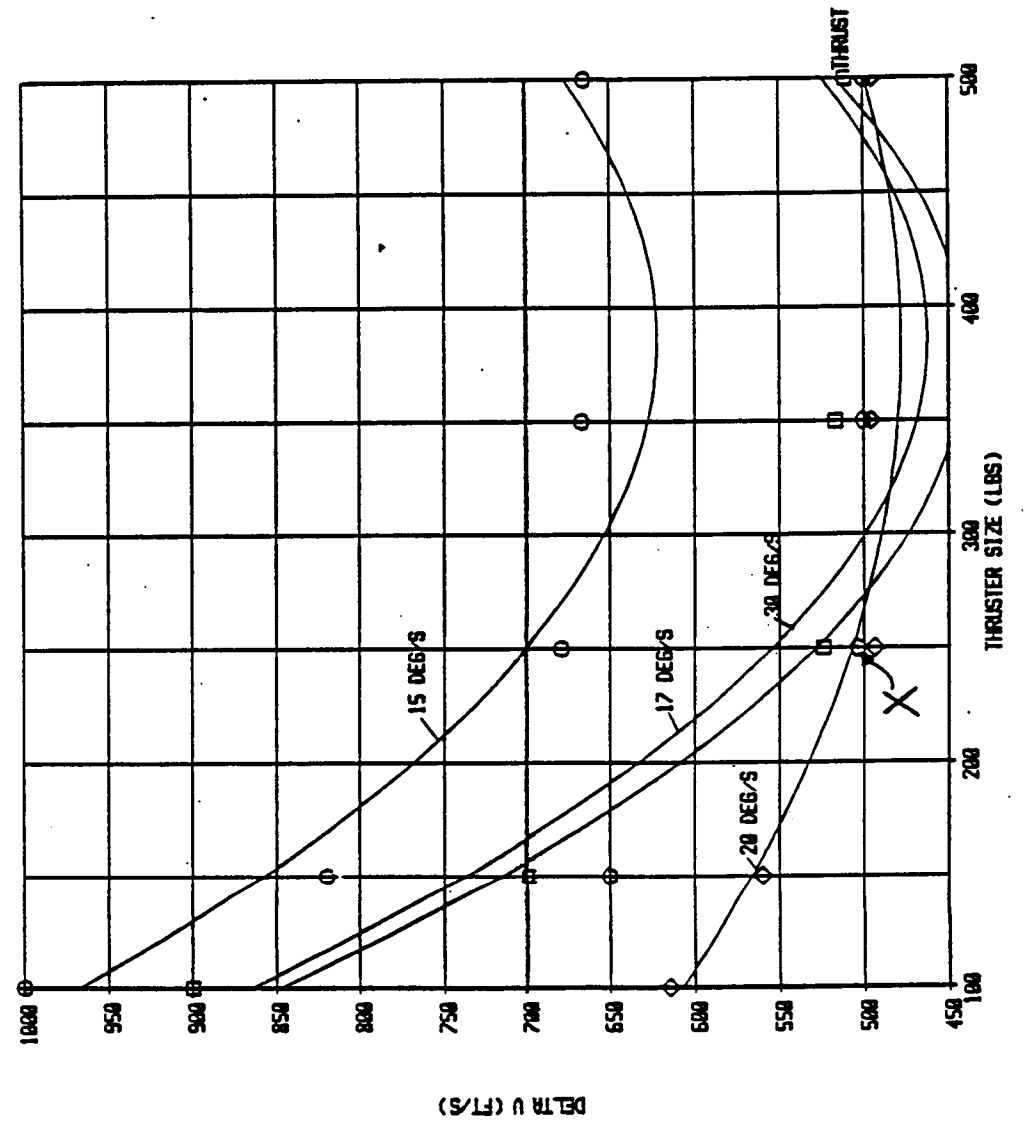

Figure 4.1-3 - DELTAV VS THRUSTER SIZE

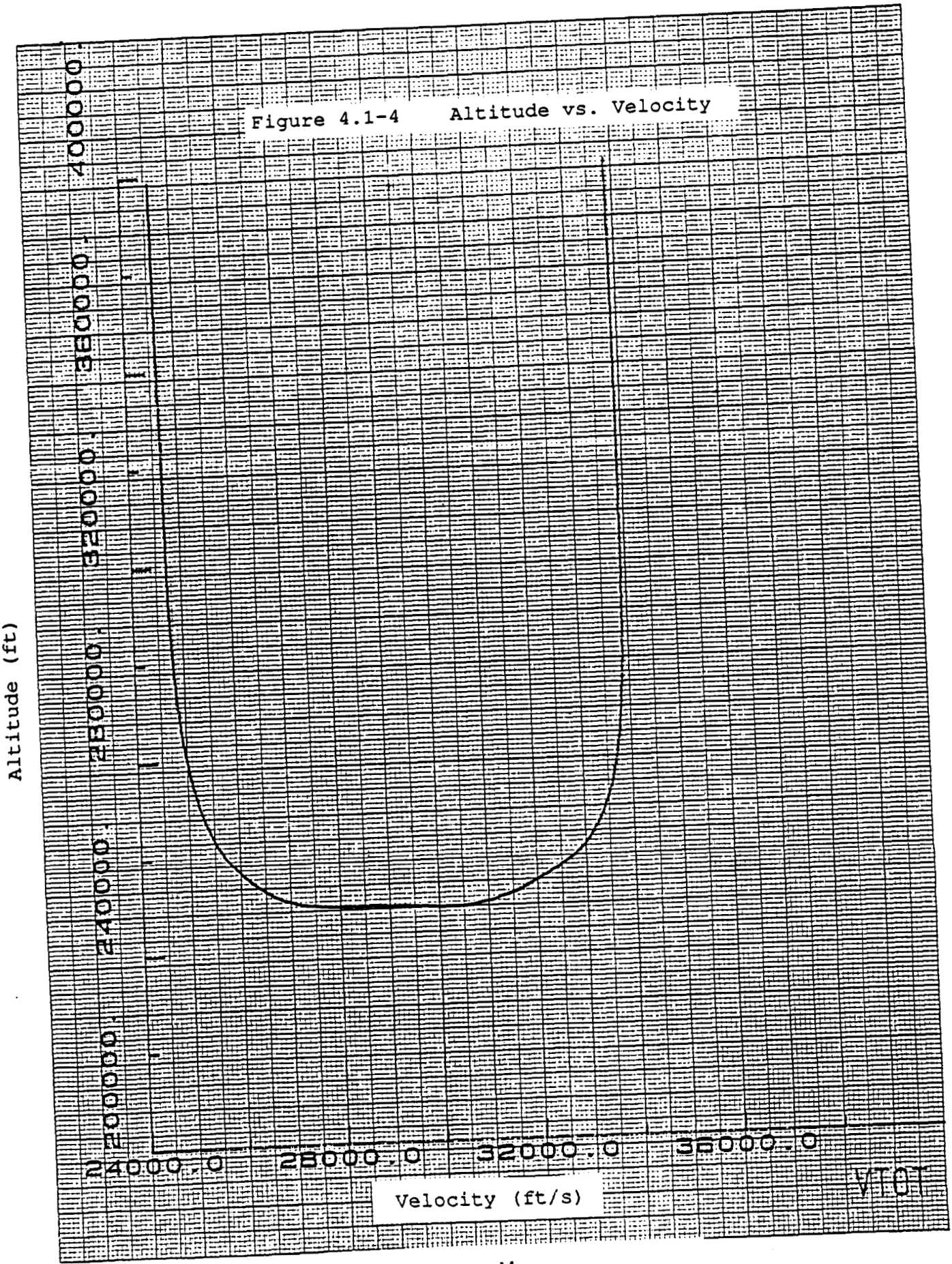

Figure 4.1-4 Altitude vs. Velocity

HEWLETT-PACKARD 9270-1027

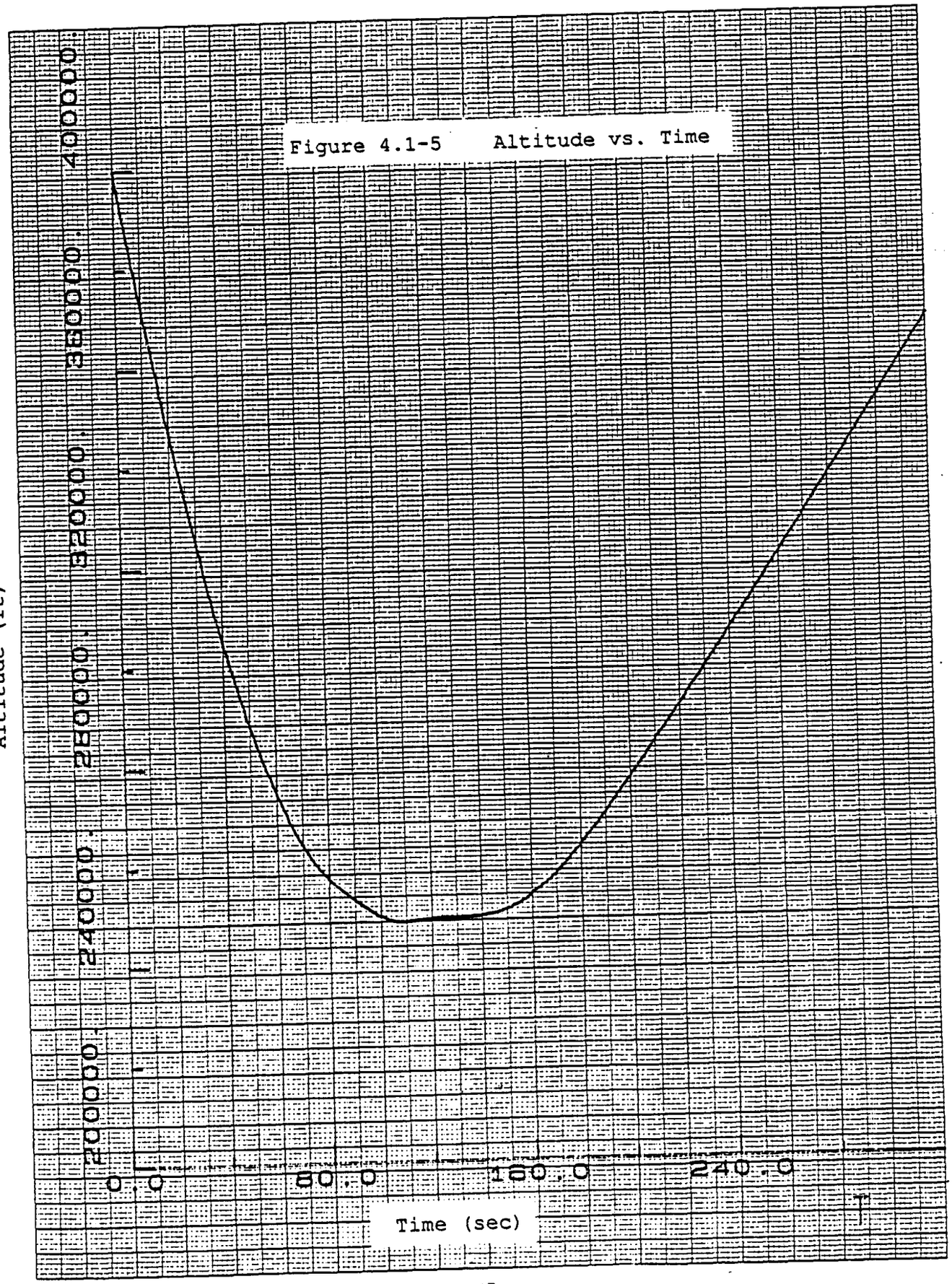

HEWLETT-PACKARD 9270-1027

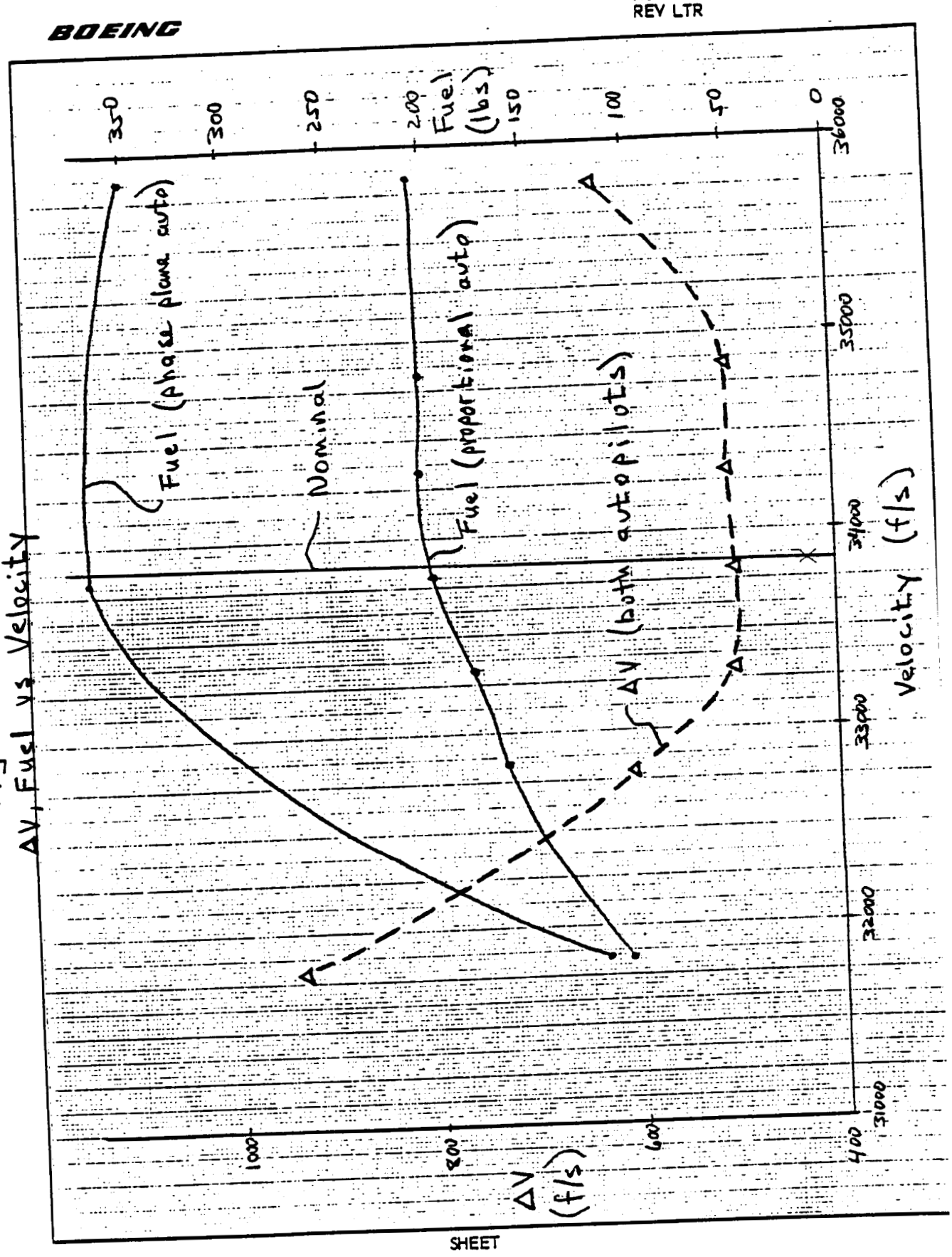

Figure 4.2-1
ΔV, Fuel vs Velocity

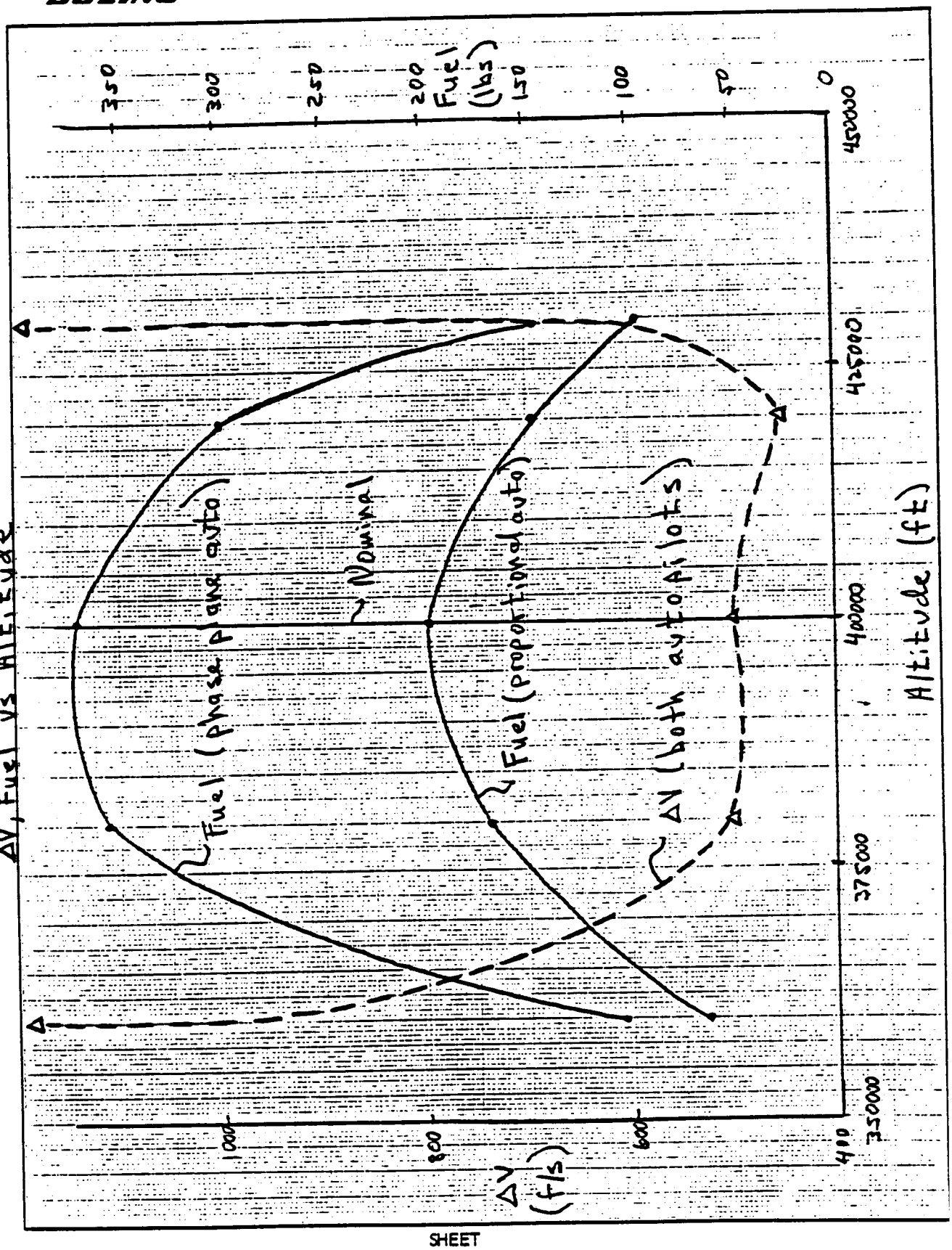

Figure 4.2-2
ΔV, Fuel vs Altitude

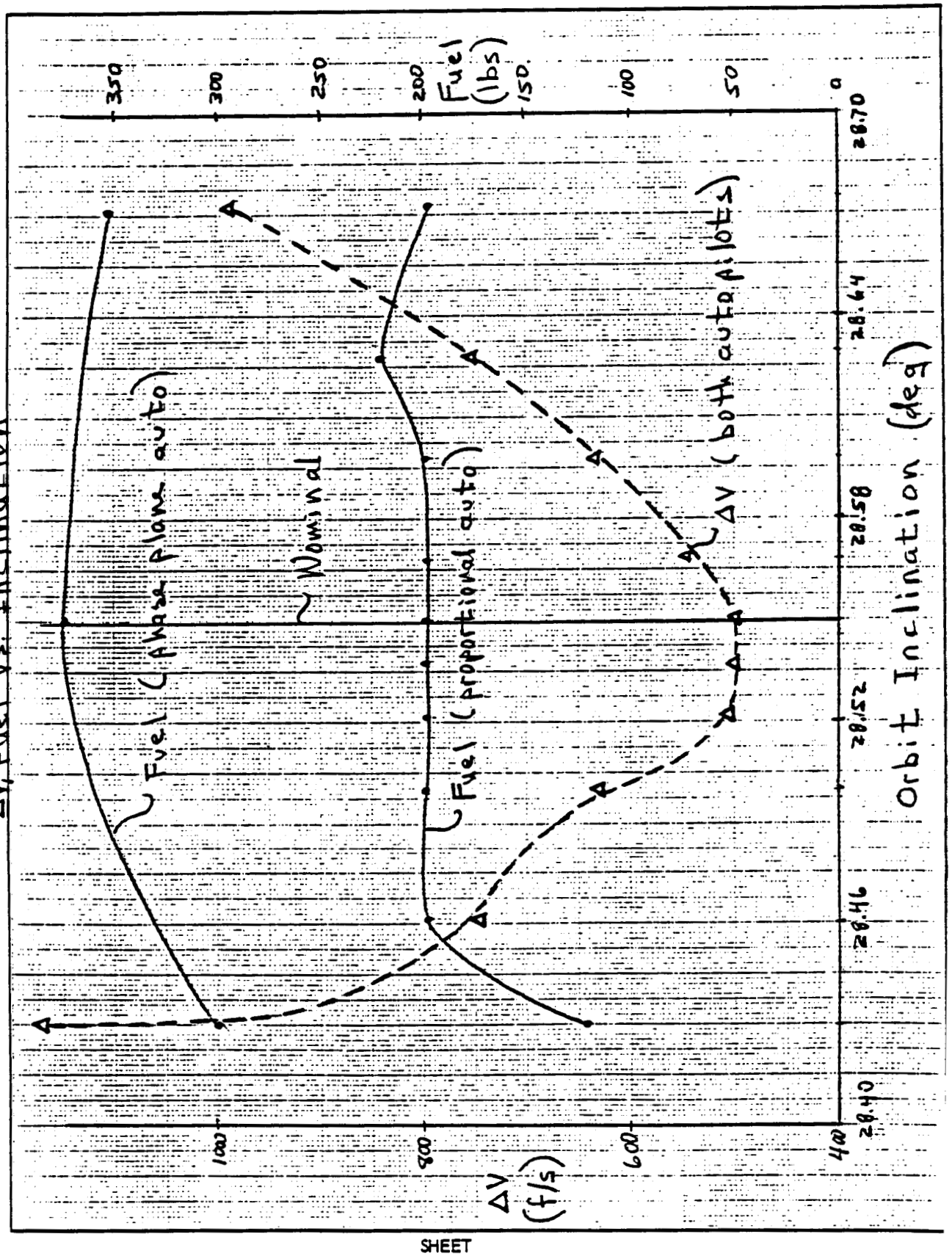

Figure 4.2-3
ΔV, Fuel vs. Inclination

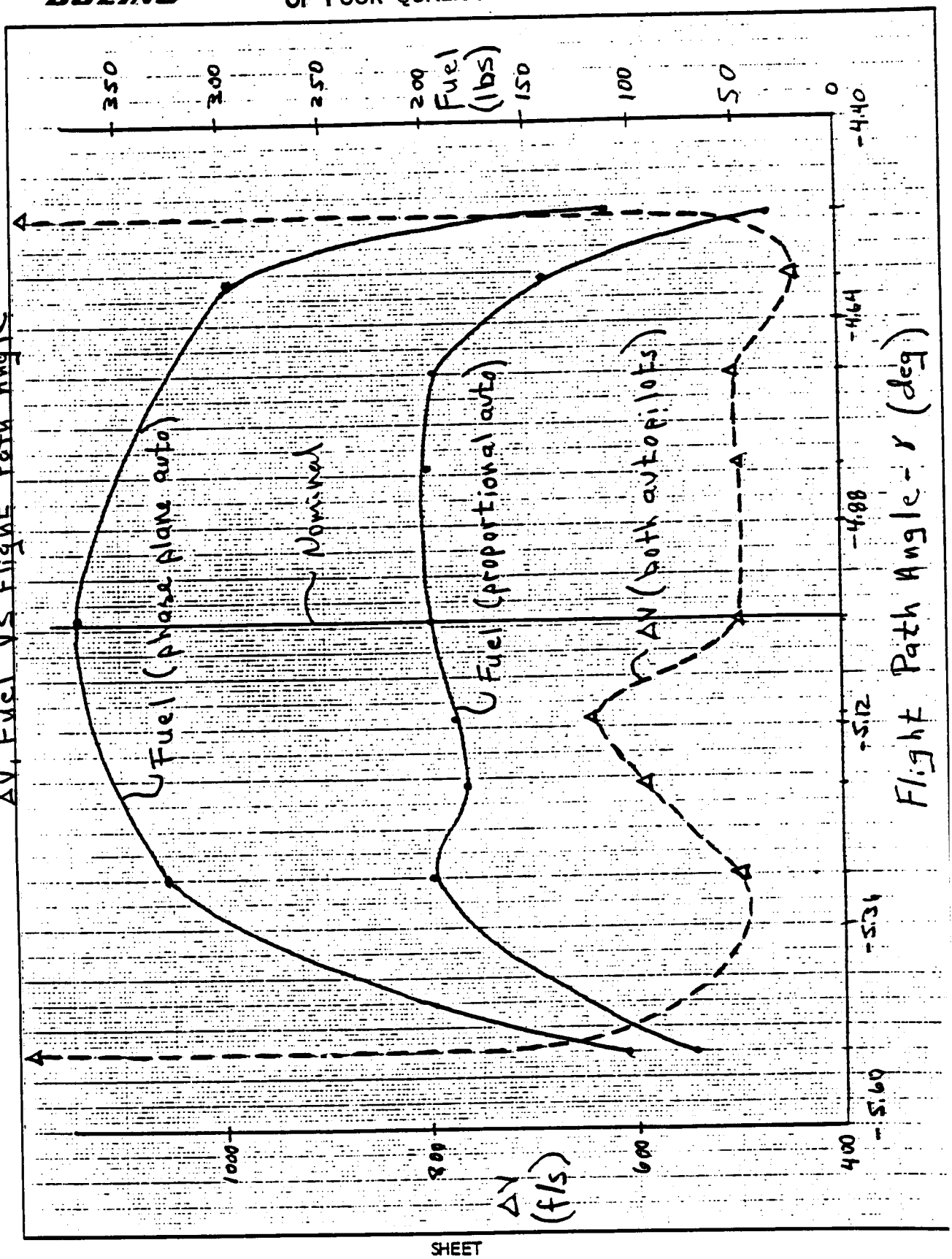

Figure 4.2-4
Δγ, Fuel vs Flight Path Angle

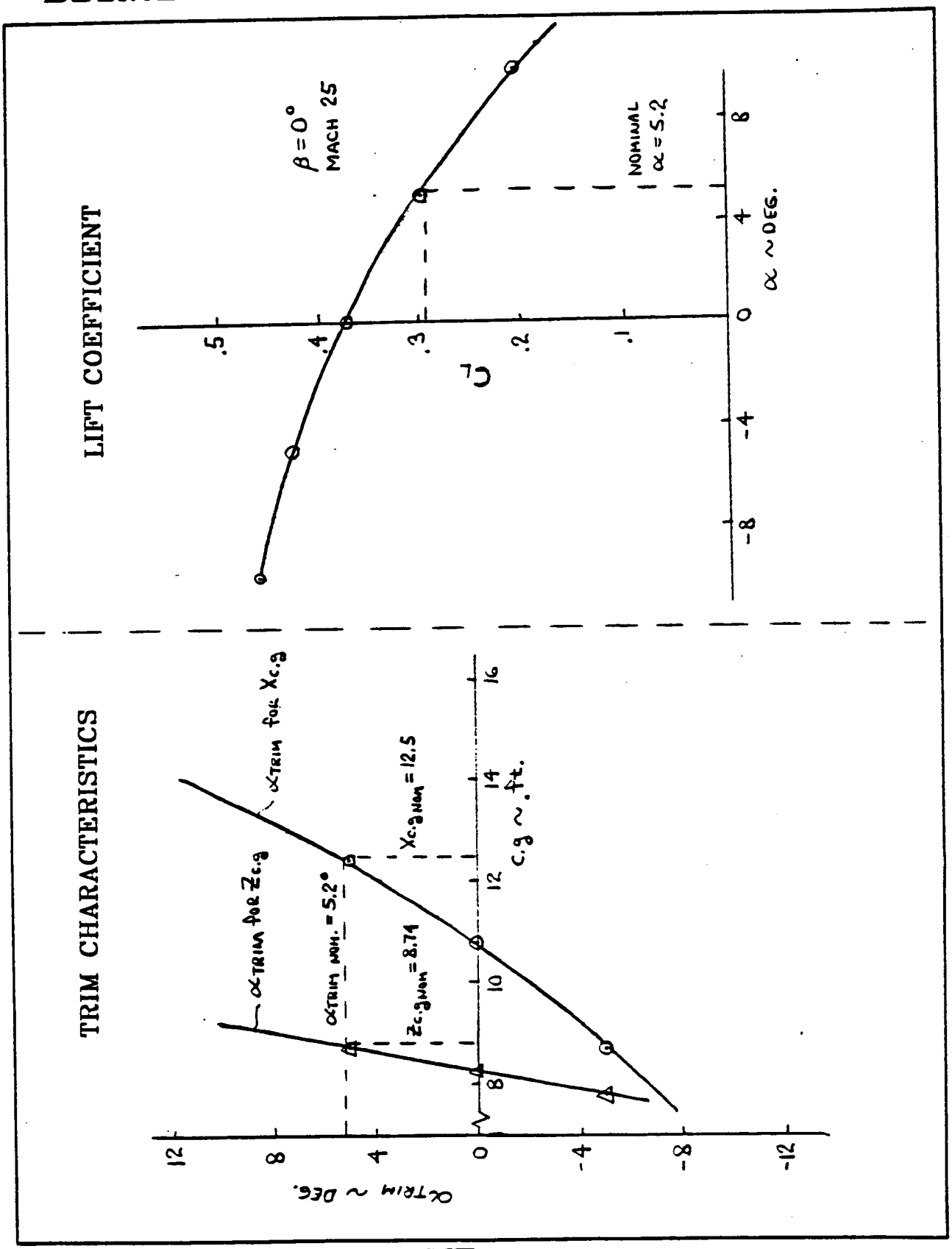
LIFT COEFFICIENT
β=0°
MACH 25
NOMINAL
α=5.2
C_L
.5
.4
.3
.2
.1
0
4
8
-4
-8
α ~ DEG.
TRIM CHARACTERISTICS
α TRIM FOR X_c.g
α TRIM FOR Z_c.g
α TRIM NOM. = 5.2°
X_c.g NOM = 12.5
Z_c.g NOM = 8.74
c.g ~ ft.
16
14
12
10
8
12
8
4
0
-4
-8
-12
α TRIM ~ DEG.

Figure 4.3-1

5.0 SENSITIVITY STUDIES

The 6DOF simulation, including the guidance and control algorithms, was used to evaluate the sensitivity of the AOTV mission to uncertainties in six major categories: 1) mission, 2) entry state, 3) mass properties, 4) atmosphere and winds, 5) aerodynamics, and 6) sensors. The sensitivity analysis for each of the six areas is explained below. Figure 5.0-1 is a summary of the sensitivity analysis.

Sensitivity was measured in three ways. The first measure was the amount of fuel burned during the aeropass. The second measure was the size of the ΔV burns necessary to establish the desired orbit. The third sensitivity measure is the combination of the previous two, yielding a total sensitivity measure.

The three ΔV burns are shown in Figure 5.0-2. The first burn raises perigee, the second burn circularizes the orbit, and the final burn corrects the inclination. Figure 5.0-3 shows the subroutines and logic used to calculate the required burns.

The fuel required for the ΔV burns can be calulated given the mass properties of the OTV the specific impulse of the thruster fuel, and the required velocity change. A ΔV burn corresponds to pounds of fuel through the relationship $lb_f=(m/I_{sp})*\Delta V$, where lb_f is pounds of fuel, m is mass of the vehicle, I_{sp} is the specific impulse of the fuel, and ΔV is the required velocity change.

Using a specific impulse of 250 seconds, and a mass of 22000 slugs we get the formula $lb_f=2.73*\Delta V$. Thus each foot per second of velocity change requires 2.73 pounds of fuel. An effective guidance/control system will try to minimize the ΔV burns and thereby save fuel.

The first sensitivity measure was the amount of RCS fuel used during maneuvers in the atmosphere. The amount of fuel burned in the aeropass can be converted to a ΔV as explained in the previous paragraph. Then the ΔV can be compared to the velocity change of the vehicle due to the atmospheric braking effects. The ratio of the ΔV due to thrusters to the ΔV due to atmospheric effects can be used to measure the effectiveness of the aerobraking scheme. The smaller the ratio the better. For example, a typical mission burns around 225 pounds of fuel with a velocity drop of 9500 feet per second. The fuel translates into a ΔV of 82.4 feet per second and the ratio becomes 0.0086, meaning that the aerobraking maneuver was an effective method of removing velocity.

Parameter variations were accomplished by either adding incremental changes to the variable of interest, or multiplying the variable by a scale factor.

Two FORTRAN subroutines are used to calculate the trajectory orbital parameters and the ΔV burns required to establish the desired orbit. These subroutines and an input/output map are listed in the appendix. Subroutine ORBIT may be called at any

time during the simulation to determine the orbital condition. It must be called when the vehicle reaches the exit condition and previous to the call to subroutine DVEL. Subroutine DVEL will calculate the three trajectory correcting velocity burns which will be required to position the vehicle in the desired orbit. These calculations are based on Hohmann Transfer Orbits followed by a plane correction. The subroutine outputs are used as one sensitivity measure, along with the total fuel used during the atmospheric phase.

5.1 Mission Sensitivities

Two mission profiles were considered. The nominal mission enters the aeropass with no inclination error and attemps to maintain the same inclination in the presence of the rotating earth. The second trajectory enters the aeropass with a 1.5 degree inclination offset and attempts to change the orbital plane to the desired value of 28.5 degrees. The closed and open-loop missions are initiated with the same state vector (total velocity, altitude, heading, flight path angle, inclination). The nominal mission begins with no inclination error. The nominal trajectory results in large rotational motions to correct small inclination errors. This action burns the majority of the fuel used during the aerobraking phase.

The second trajectory was generated using the 3DOF simulation, with a 1.5 degree initial inclination error. The intent was to

find a trajectory which does not start with zero inclination error and examine the system performance. The guidance tries to eliminate the inclination error, which requires the vehicle to remain on one side of the bank plane for the majority of the mission. Fuel use was reduced from 225 pounds for the nominal system to 161 pounds for the out-of-plane trajectory. Figure 5.1-1 is a plot of the bank angle and bank angle command for the out-of-plane trajectory. Notice that the bank angle and command are one-sided. Figure 5.1-2 shows the orbital inclination during the aerobraking phase. The desired inclination (28.5 degrees) is reached during the late phase of the mission.

All remaining sensitivity studies were conducted with the nominal trajectory (no initial out-of-plane error).

5.2 Entry State Sensitivities

The mission sensitivity to total velocity, altitude, inclination, and flight path angle errors are shown in Figures 5.2-1, 5.2-2, 5.2-3, 5.2-4, respectively. The left-hand axis and the dashed line on the plot correspond to ΔV measurements. The right-hand axis and the solid lines correspond to the RCS fuel used during the aerobraking phase. Each of the parameters exhibit similar sensitivity patterns, a relatively flat zone in the middle with rapid divergence when the parameter is too far off nominal. The sensitivity bounds are approximately ±6% off nominal for the velocity, ±8% for altitude, ±.4% for inclination, and ±9% in

flight path angle. By far the most sensitive parameter is the orbital inclination.

5.3 Mass Property Sensitivities

The mission sensitivities to uncertainty in vehicle weight, inertia, and x and z c.g. location are shown in Figures 5.3.-1, 5.3-2, 5.3-3, and 5.3-4.

Variations of the weight by as much as ±27% resulted in changes in fuel use by at most ±23% and in the ΔV measurement by at most ±17%. In summary, while the mission performance is affected by the vehicle weight, it is not nearly as sensitive to weight as it is to the entry state parameters.

Increasing the inertia resulted in a proportional increase in the fuel. The ΔV curve should be viewed in light of the scales. A ±40% variation in the inertia resulted in a ±2.4% variation in the ΔV measurement. In summary, the mission is not highly sensitive to inertia and the effect is predictable.

Figures 5.3-3 and 5.3-4 are plots of the sensitivities to x and z variations in the c.g. location and will be discussed together. The two solid lines in each plot are the fuel used with and without the integrator logic. The two dashed lines are the ΔV measurements with and without the integrator measurements. From the figure we can see that the mission is least sensitive to

variations in the x direction without the integrator. Addition of the integrator increases the performance if the c.g. is moved in the negative direction and causes the system to fail if the c.g. is moved too far in the positive direction. Too much variation of the c.g. in the z direction (either direction) causes the system to fail without the integrator. The addition of the integrator increases the performance if the c.g. is moved in the negative direction and quickly causes the system to fail if the c.g. is moved in the positive z direction. This is easily explained by looking at the aerodynamic data and Figure 4.3-1. If the c.g. is moved in the negative direction, the trimmed angle of attack decreases, which results in an increased lift capability.

5.4 Atmospheric Sensitivities

The atmospheric sensitivity studies included the effect of density variation and winds. Sixteen random atmosphere models were generated using the GRAM (Global Reference Atmospheric Model) atmosphere program. The models include random variations in density and wind profile. Figure 5.4-1 is a plot of the density, north-south, and east-west winds as a function of altitude. The sixteen atmospheres were chosen as four worst cases from each season - summer, fall, winter, and spring. The four cases for each season are maximum dynamic pressure (MQ), worst winds (WW), most northerly (MN), and most southerly (MS). The nomenclature used to identify the winds is a four letter name with the type of model first and the season as the second two letters. For example

a most southerly fall profile would be MSFA. Summer is (SU), winter is (WI), and spring is (SP). Figure 5.4-2 shows the fuel and ΔV numbers for the nominal trajectory using the sixteen atmospheres, with and without winds. No general trends are discernible because the atmosphere models are random in nature. However, the vehicle remains stable and completes the mission profile for all of the different atmosphere models.

5.5 Aero Coefficient Sensitivities

The mission sensitivity to uncertainty in the aerodynamic coefficients was determined by multiplying the aero coefficients by a scale factor. The nominal scale factor value was one. Sensitivity studies were conducted on the force (C_x, C_y, C_z), static stability (Cm_a, Cn_B), and yaw/roll coupling (Cl_B) aero coefficients.

Figure 5.5-1 shows the sensitivities for the three force coefficients. The horizontal axis has units of percent uncertainty from the nominal condition. The combined sensitivity measure clearly shows that the effect of off-nominal C_y is negligible, as is negative variation of the C_z coefficient. Positive variations in the C_z coefficient are more pronounced but do not cause the control/guidance systems to fail. The C_x coefficient has a stable sensitivity range of -15% to +5% off the nominal condition.

Figure 5.5-2 is a plot of the Cn_B, Cl_B, and Cm_a sensitivities.

Notice that the Cl_B and Cn_B curves are overlayed. The vehicle is insensitive to these parameters. The two remaining sets of curves show the Cm_a sensitivities with and without the pitch axis integrator. The integrator has a stabilizing effect for positive variations of the coefficient. For negative variations the integrator quickly causes the system to diverge. This is due to the decreased control authority at the reduced angle of attack. Figure 5.5-3 is a plot of the combined sensitivity measure for these parameters. The effect of the integrator can be seen very clearly.

5.6 Sensor Sensitivities

The mission sensitivity to noise and bias in the strap-down sensor package was evaluated by including a detailed model of a rate gyro package in the 6DOF simulation.

Figure 5.6-1 shows the model for rate gyro errors. Five error sources have been modeled: misalignment of the rate gyro package, bias and scale factor error, additive noise in each channel, and the gyro cross-axis effects. The axes of the gyros in the package were assumed perfectly orthogonal, with the alignment error defined from the package roll, pitch, and yaw axes to the true body axis. Table 5-1 lists the expected 3σ statistic value for each parameter. The listed values apply to missile systems. For space hardware, the requirements are more stringent because mission durations are usually much longer.

Figure 5.6-2 shows the sensitivity for the gyro parameters except for noise. The plots show that the system is relatively insensitive to errors in the rate gyro. The amount of fuel burned due to the errors is small (less than 5 percent). The rate gyro errors are principally manifested in the increase of ΔV measurement. The increase is comparatively small (less than 13 percent).

The system is also insensitive to noise in the rate gyro channel, as the dynamic response of the vehicle acts as a low pass filter in removing most of its effect. The effect of gyro noise can be seen, however, in the increased thruster activity level, which translates to an increase in fuel burned during maneuver phase. The fuel burned due to 3σ noise level in the roll, pitch and yaw rate gyro channels are 269, 255 and 254 lbs respectively, compared to 244 lbs of fuel for a nominal flight. Again, the increase in fuel burned is small.

In conclusion, the mission is most sensitive to parameters that directly affect the guidance alogorithm, such as inclination error. The control systems developed for the AOTV were stable for all parameter variations. The performance decreases were principally due to the minimal control authority which was only significant during the one to two minutes of highest dynamic pressure.

The HYPAS guidance algorithm is listed in the appendix for reference and comparison.

Sensitivity Matrix

Parameter	Variable	Tolerance
Entry state	Velocity Flight path angle Altitude Inclination	± 6% ± 9% ± 8% ± .4%
Atmosphere	Winds Density	Random ± 400 f/s Random ± 20%
Mass properties	Weight Center of gravity Moment of inertia	± 23% X > ± 20% Z = ± 14% > ± 20%
Aerodynamics	C_x, C_y, C_z $C_{m\alpha}$, $C_{n\beta}$ $C_{l\beta}$	+10%, -20% Large > ± 20% +15%, -10% Large Large
Sensors	Bias Cross coupling Scale factor Misalignment Noise	> ± .0014 deg/sec (3σ) > ± .1 (3σ) > ± .005 (3σ) > ± .1 deg (3σ) > ± .3 deg/sec (3σ)

Figure 5.0-1

MEASURE OF SYSTEM EFFECTIVENESS

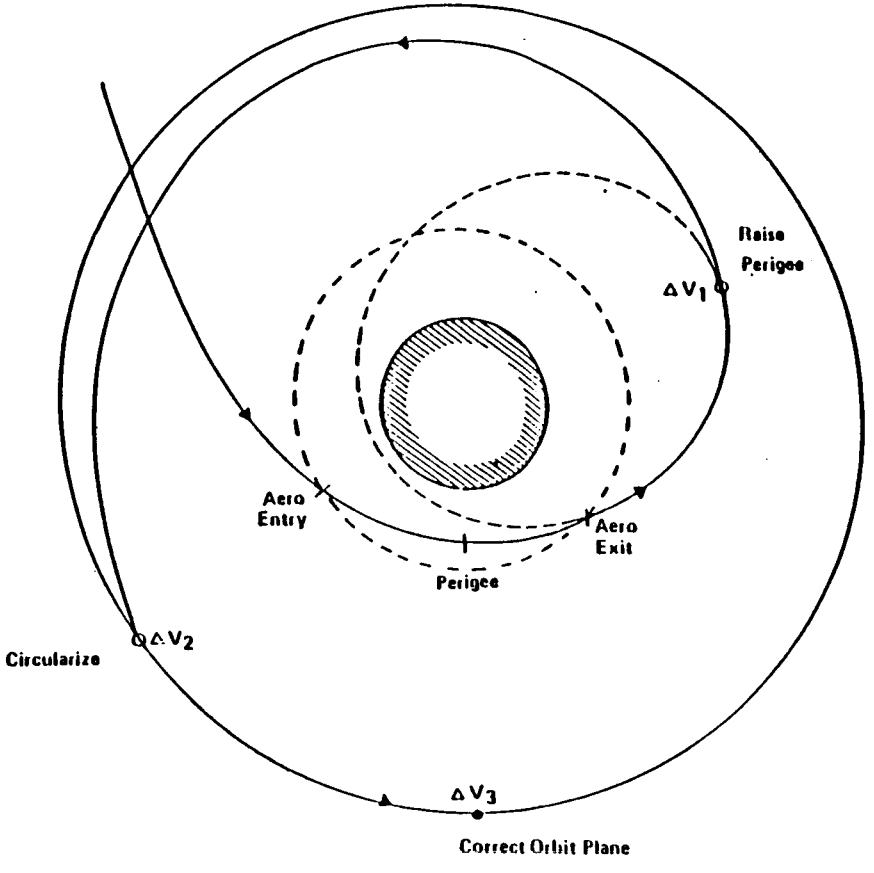

Impulsive velocity changes to insert into desired orbit

- ΔV_1 - Raise perigee to desired altitude
- ΔV_2 - Circularize orbit
- ΔV_3 - Correct orbit plane
- ΔV - Total ΔV to insert into desired orbit

Figure 5.0-2

Orbit Correction Burns

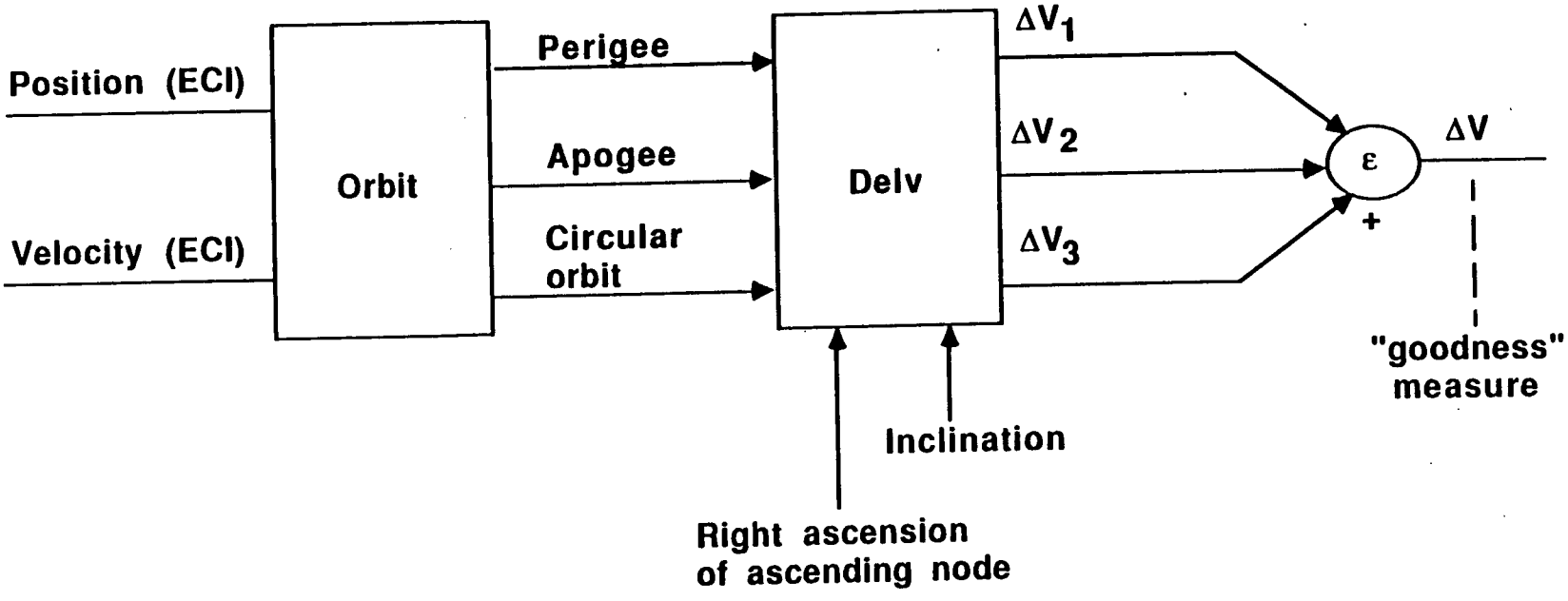

Figure 5.0-3

Subroutine DELV

inputs:	RP1 -->	radius at perigee (feet)
	RA1 -->	radius at apogee (feet)
	RCIRC -->	radius circular orbit (feet)
	RAAN -->	right accension of acending node (deg)
	RINC -->	orbit inclination (deg) (28.5)
outputs:	DV1 -->	burn to correct perigee
	DV2 -->	burn to correct inclination
	DV3 -->	burn to circularize
	DVEL -->	total delta velocity

Subroutine ORBIT

inputs:	$Reci_{x,y,z}$ -->	ECI position vector (feet)
	$Veci_{x,y,z}$ -->	ECI velocity vector (feet/sec)
outputs:	RPER -->	radius at perigee (feet)
	RAPO -->	radius at apogee (feet)
	RCIRC -->	radius of circular orbit (feet)

Figure 5.0-3 cont.

Subroutines Input/Output Map

```
      SUBROUTINE ORBIT
C
$ADD V:AOTVCM
C
C MOMENTUM VECTOR AND MAGNITUDE
      HX=RECIY*VECIZ-VECIY*RECIZ
      HY=RECIZ*VECIX-VECIZ*RECIX
      HZ=RECIX*VECIY-VECIX*RECIY
      HMAG=SQRT(HX**2+HY**2+HZ**2)
C NODAL VECTOR AND MAGNITUDE
      RNX=-HY
      RNY=HX
      RNZ=0.0
      RNMAG=SQRT(RNX**2+RNY**2+RNZ**2)
C ECCENTRICITY VECTOR AND MAGNITUDE
      VSQRD=VECIX**2+VECIY**2+VECIZ**2
      RDOTV=RECIX*VECIX+RECIY*VECIY+RECIZ*VECIZ
      TEMPZ=VSQRD-RMU/(-ZP)
      EX=1./RMU*(TEMPZ*RECIX-RDOTV*VECIX)
      EY=1./RMU*(TEMPZ*RECIY-RDOTV*VECIY)
      EZ=1./RMU*(TEMPZ*RECIZ-RDOTV*VECIZ)
      EMAG=SQRT(EX**2+EY**2+EZ**2)
C APOAPSIS AND PERIAPSIS CALCULATIONS
      SLR=HMAG**2/RMU
      IF(HMAG .NE. 0.0) RINC=ACOS(HZ/HMAG)*Z57P3
      IF(RNMAG .NE. 0.0) RLAN=ACOS(RNX/RNMAG)*Z57P3
      RPER=SLR/(1.0+EMAG)
      RAPO=SLR/(1.0-EMAG)
      RPERN=(RPER-REARTH)/60776.1155
      RAPON=(RAPO-REARTH)/60776.1155
      RCIRC=REARTH+APOTG*60776.1155
      RETURN
      END
```

Figure 5.0-3 cont.

```
      SUBROUTINE DELV(RP1,RA1,RCIRC,RINC,RAAN,DV1,DV2,DV3,DVEL)
C
C           XMU:  GRAVITATIONAL PARAMETER IN FT**3/SEC
C
      DATA XMU /1.4076E+16/
      DATA Z57P3 /57.29578/
C
C       EXIT ORBIT VELOCITY AT APOGEE:
C
      VA1=SQRT(2.*XMU*(1/RA1-1/(RP1+RA1)))
C
C        TRANSFER ORBIT VELOCITY AT APOGEE:
C
      VA2=SQRT(2.*XMU*(1/RA1-1/(RA1+RCIRC)))
C
C        DELTA V REQUIRED FOR EXIT TO TRANSFER ORBIT CHANGE:
C
      DV1=ABS(VA2-VA1)
C
C        CIRCULAR ORBIT VELOCITY:
C
      VCIRC=SQRT(XMU/RCIRC)
C
C        TRANSFER ORBIT VELOCITY AT PERIGEE
C
      VP2=SQRT(2.*XMU*(1/RCIRC-1/(RA1+RCIRC)))
C
C        DELTA V REQUIRED FOR TRANSFER TO CIRCULAR ORBIT CHANGE:
C
      DV2=ABS(VCIRC-VP2)
C
C        CALC PLANE CHANGE DELTA V (TARGET ORBIT INCLINATION AND RIGHT
C        ACCENSION OF ACENDING NODE ARE HARD CODED AT 28.5 DEG AND Ø
C        RESPECTIVELY
C
      RINCR=RINC/Z57P3
      RINCRF=28.5/Z57P3
      RAANR=RAAN/Z57P3
      IF (ABS(RAAN) .LT. 1.E-8) THEN
         PLNCHG=ABS(RINCR-RINCRF)
      ELSE
         PCCOS=COS(RINCR)*COS(RINCRF)+SIN(RINCR)*SIN(RINCRF)*COS(-RAANR)
         PLNCHG=ACOS(PCCOS)
      END IF
C
      DV3=ABS(2.*VCIRC*SIN(PLNCHG/2.))
C
C        TOTAL DELTA V
C
      DVEL=DV1+DV2+DV3
      RETURN
      END
```

Figure 5.0-3 cont.

BANK ANGLE AND COMMAND

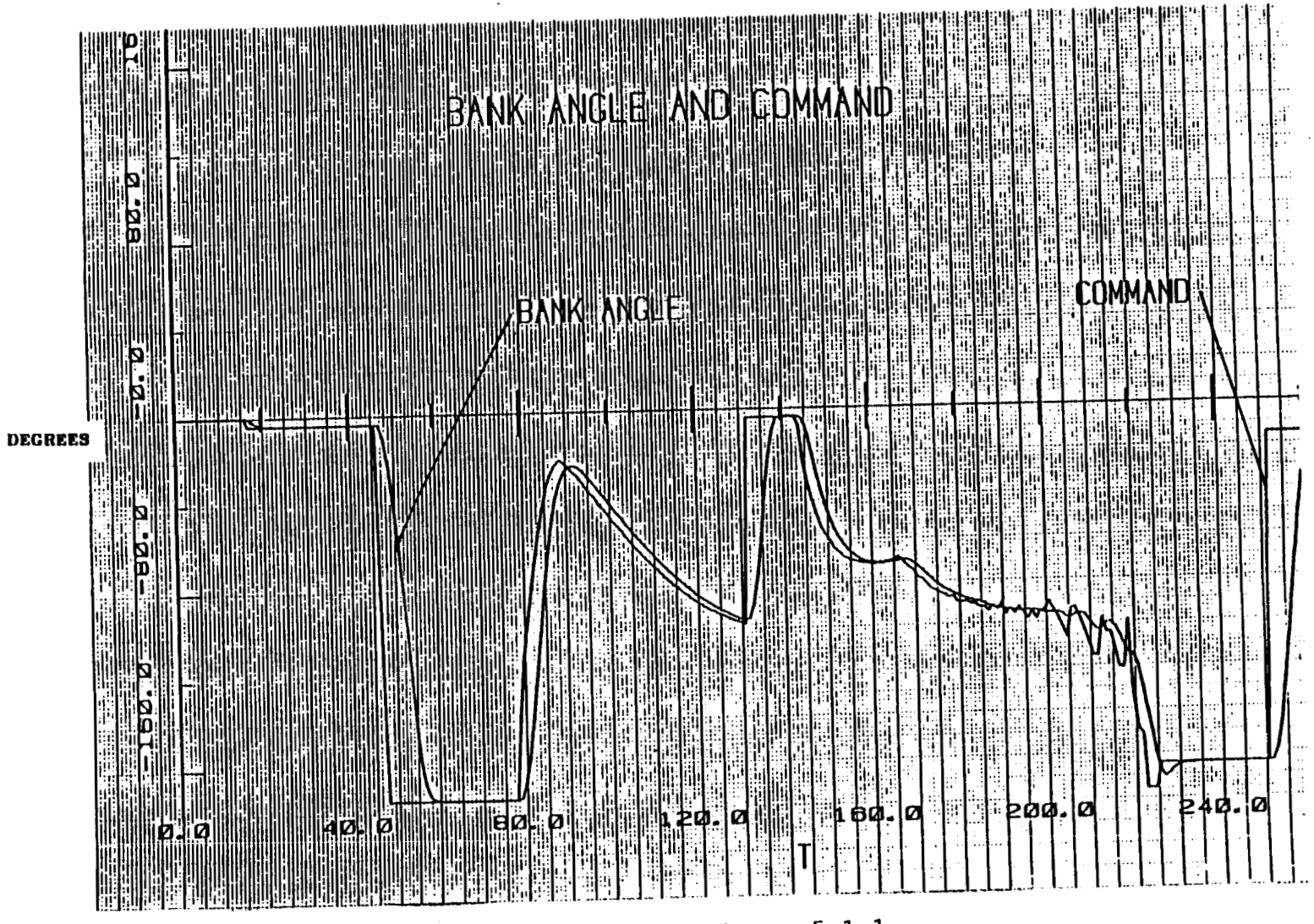

Figure 5.1-1

ORIGINAL PAGE IS
OF POOR QUALITY

Figure 5.1-2

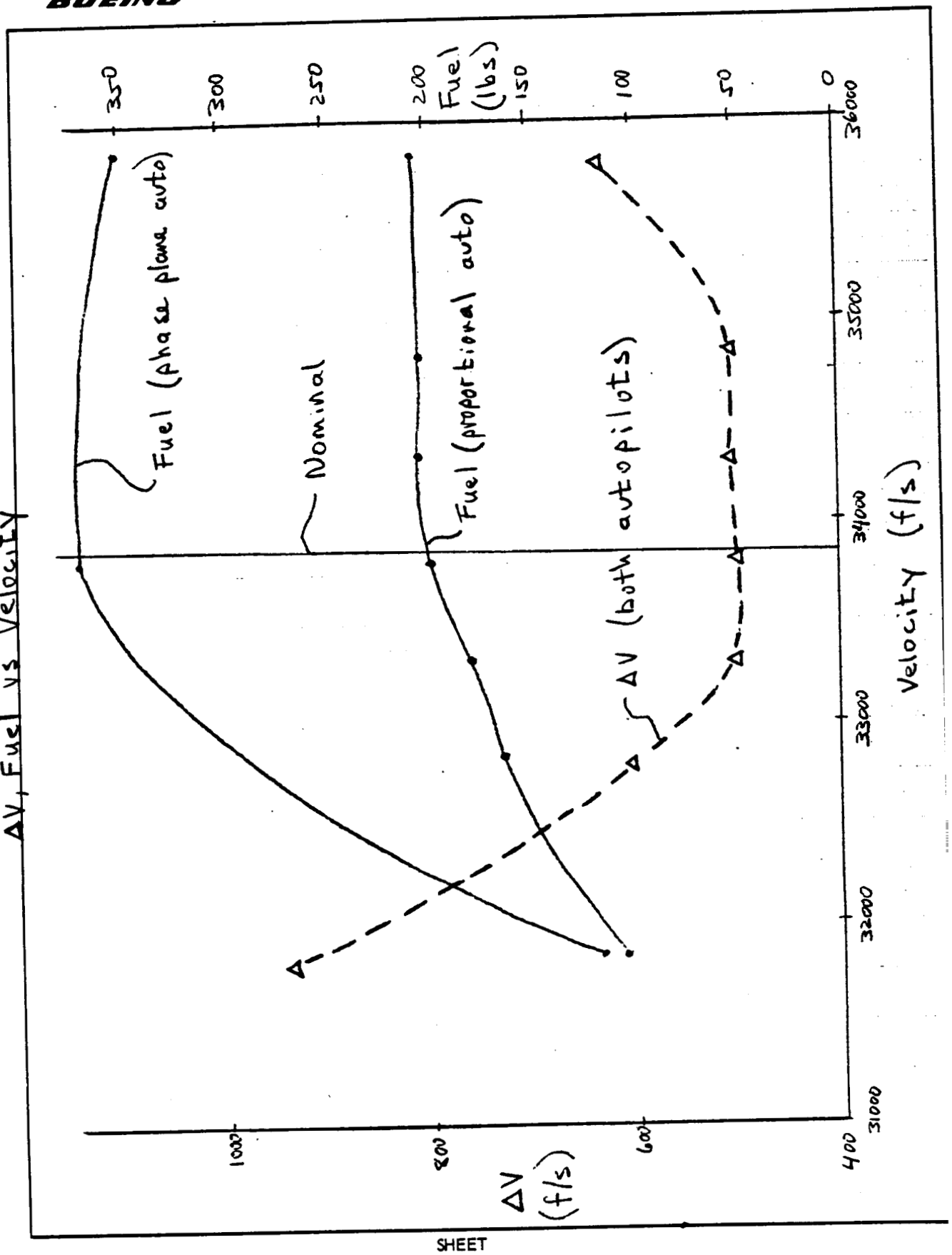

Figure 5.2-1
ΔV, Fuel vs Velocity

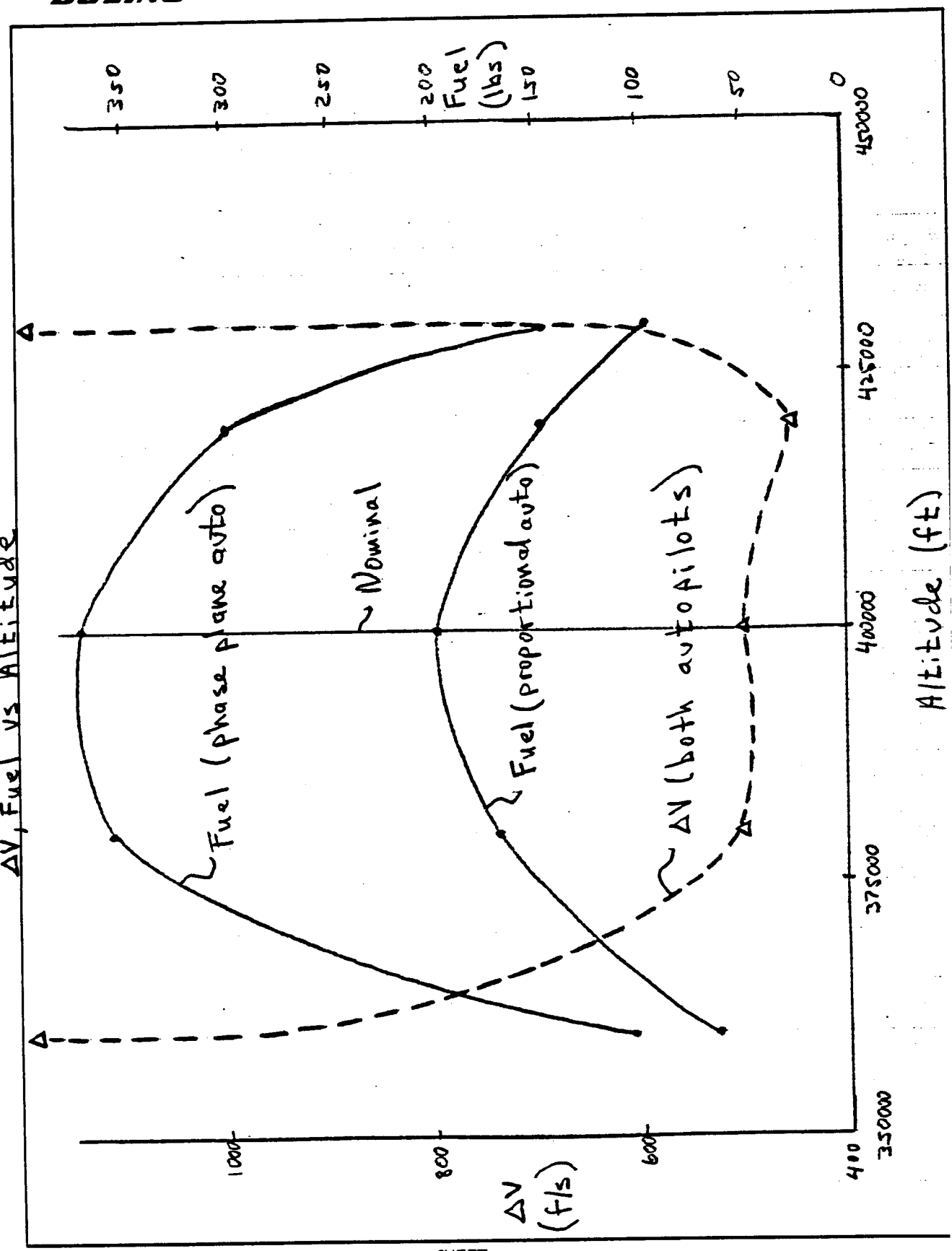

Figure 5.2-2
ΔV, Fuel vs Altitude

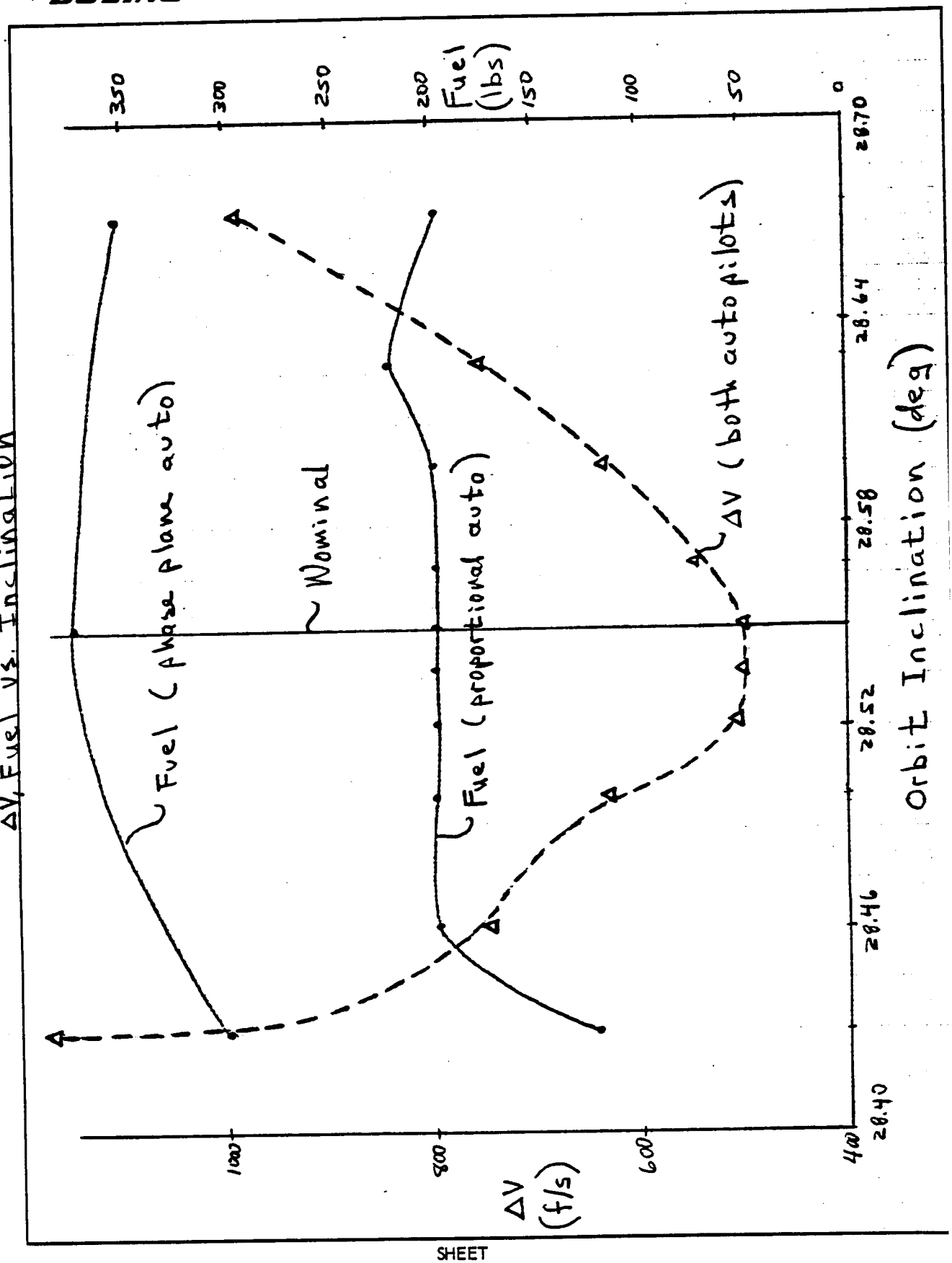

Figure 5.2-3
ΔV, Fuel vs. Inclination

Figure 5.2-4
ΔV, Fuel vs Flight Path Angle

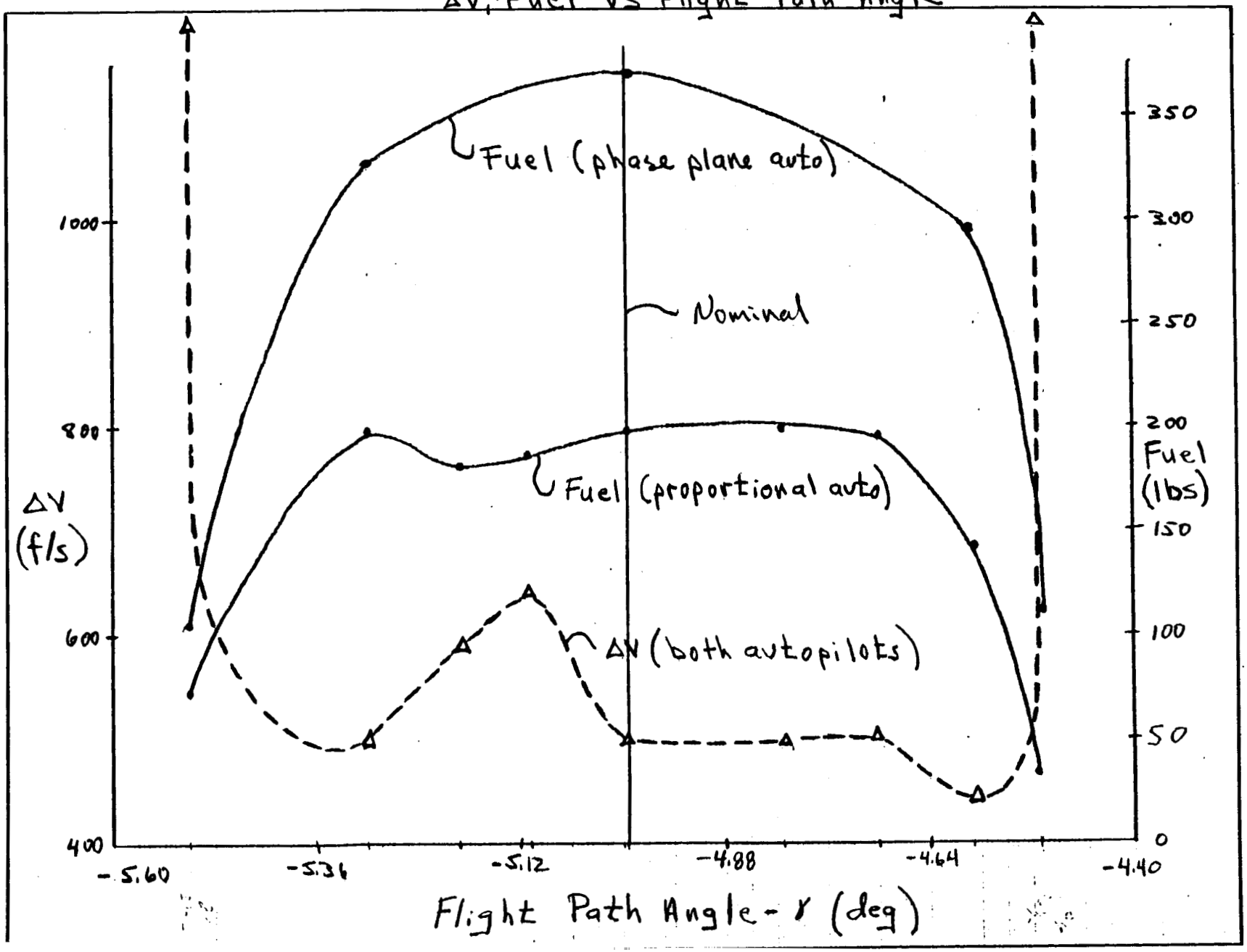

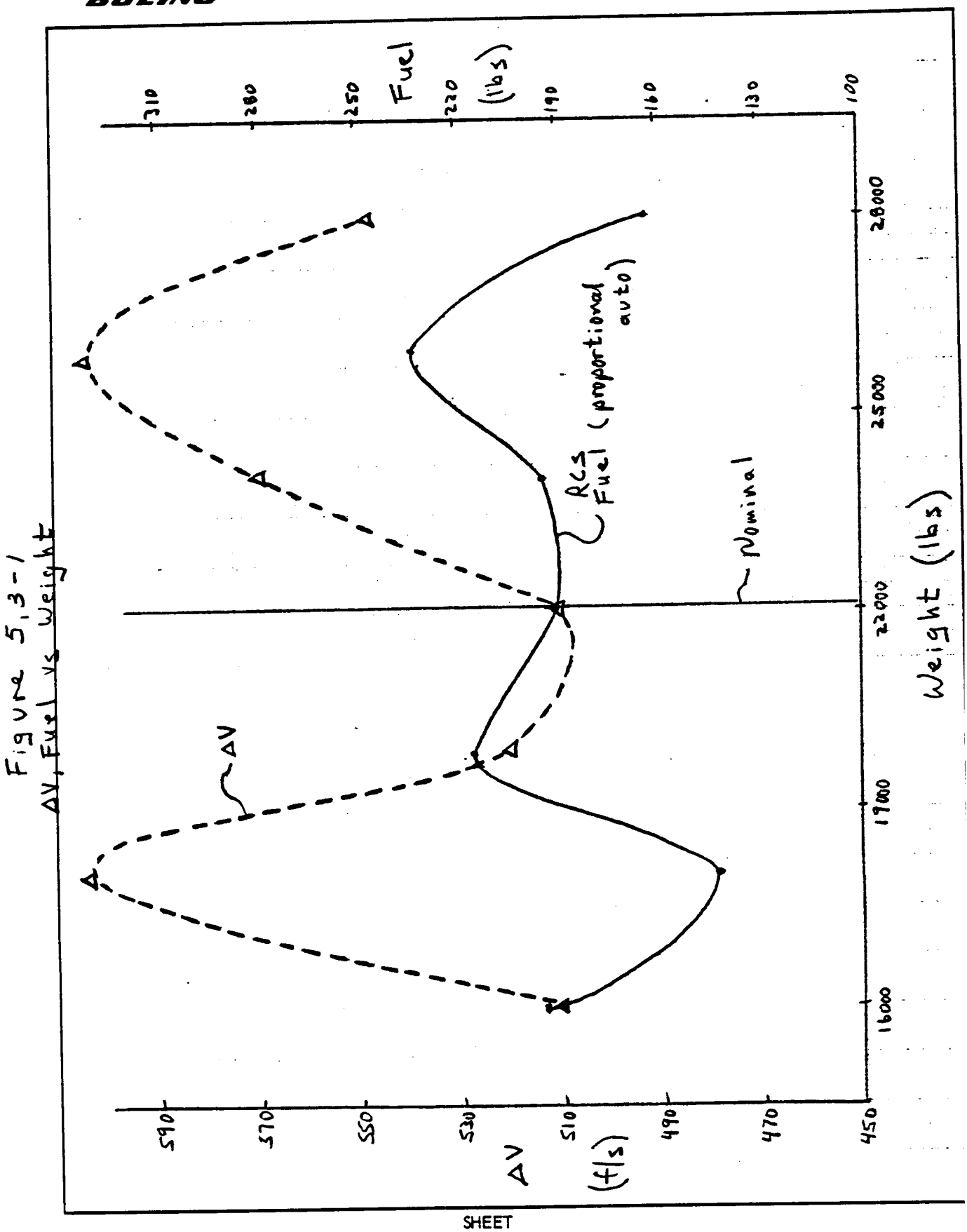

Figure 5.3-1
ΔV, Fuel vs Weight

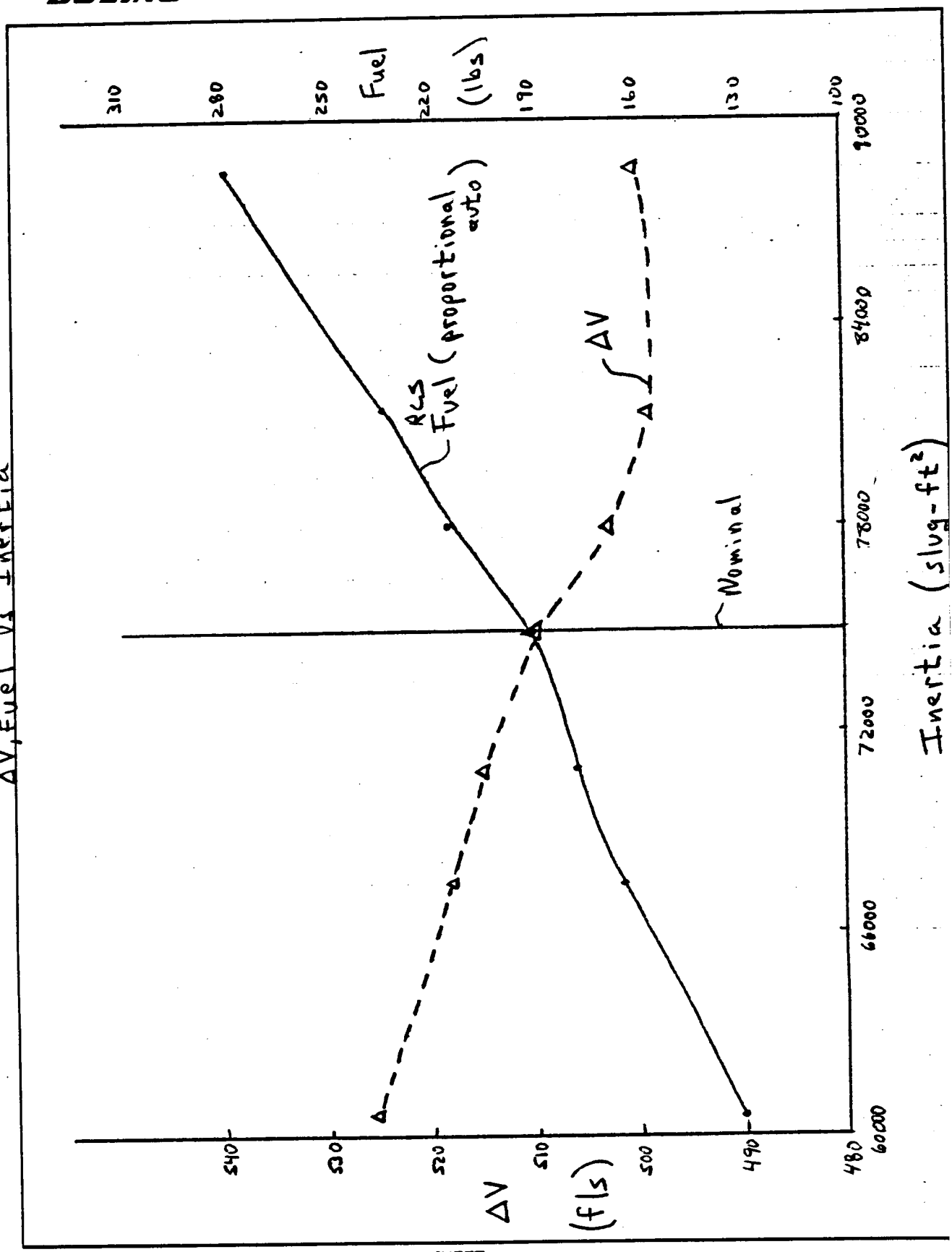

Figure 5.3-2
ΔV, Fuel Vs Inertia

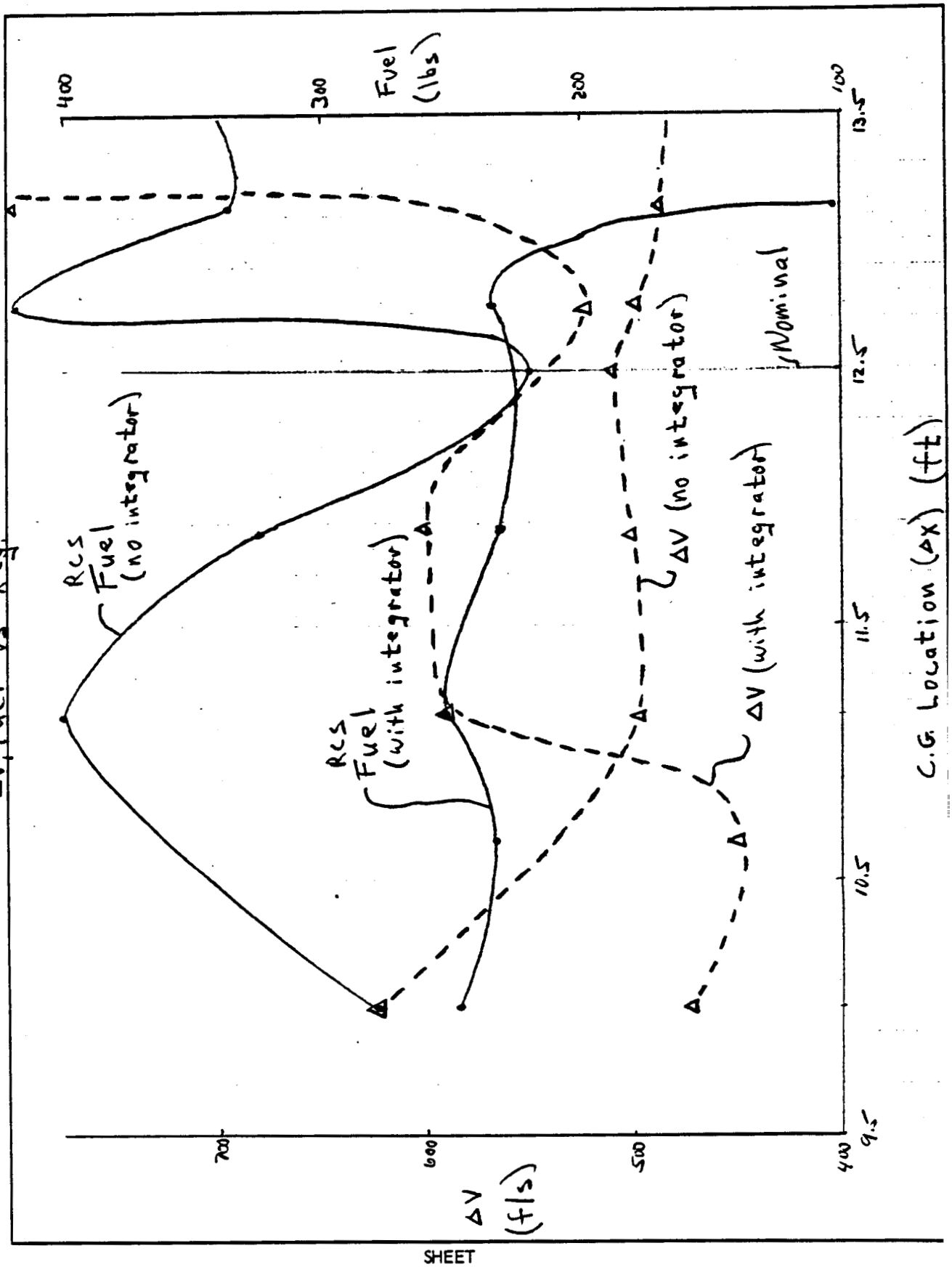

Figure 5.3-3
ΔV, Fuel vs X cg

Figure 5.3-4

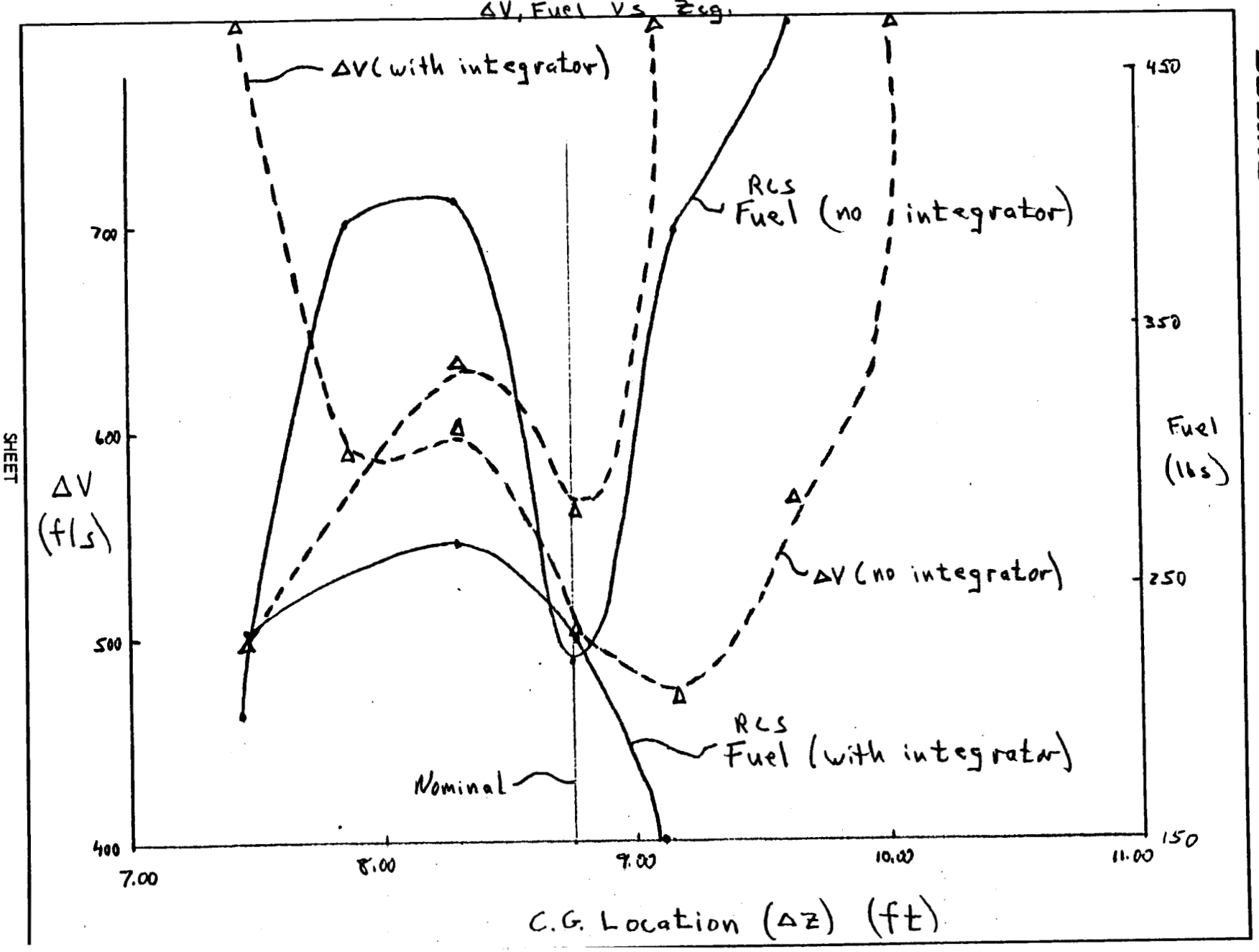
ΔV, Fuel Vs Zcg.
ΔV (with integrator)
RCS Fuel (no integrator)
ΔV (no integrator)
RCS Fuel (with integrator)
Nominal
ΔV (fps)
Fuel (lbs)
700
600
500
400
450
350
250
150
7.00
8.00
9.00
10.00
11.00
C.G. Location (Δz) (ft)

Figure 5.4-1

Atmospheric Density and Wind Profiles

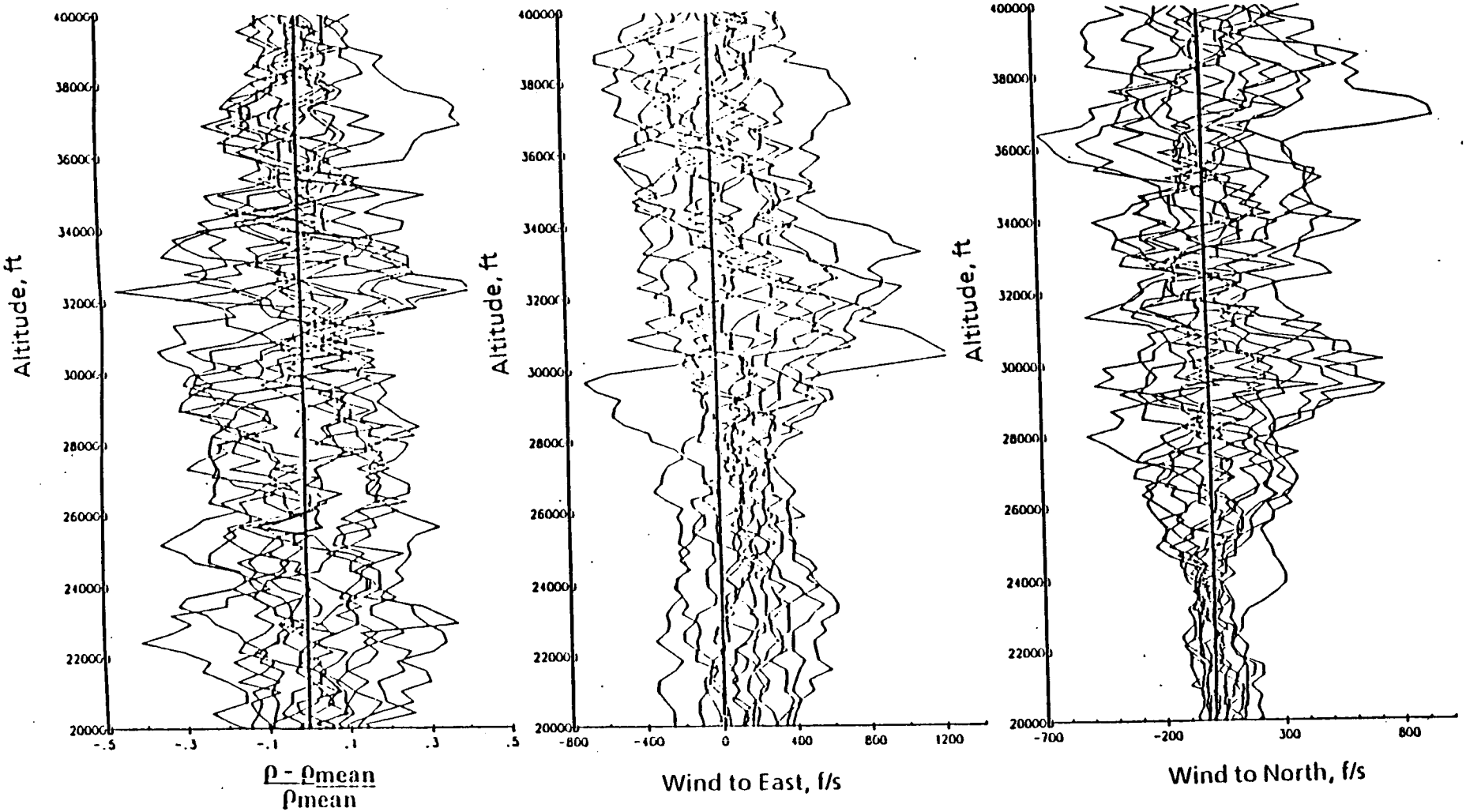

ATMOSPHERIC SENSITIVITY RESULTS

Atmosphere	Winds		No Winds	
	ΔV (ft/s)	Fuel (lb)	ΔV (ft/s)	Fuel (lb)
Atmos 62	525	219	—	—
MNSU	509	314	623	326
MNWI	1068	201	1168	278
MNFA	518	322	544	257
MNSP	618	197	618	231
MQFA	514	310	491	314
MQSU	503	261	509	271
MQWI	602	326	592	322
MQSP	633	340	619	328
WWSP	848	212	831	235
WWWI	572	362	553	482
WWFA	549	213	556	228
WWSU	571	283	534	305
MSSP	489	318	494	375
MSFA	523	354	508	363
MSWI	535	330	533	338
MSSU	554	210	556	222

Figure 5.4-2

Figure 5.5-1
Total Fuel Vs Cx, Cy, Cz

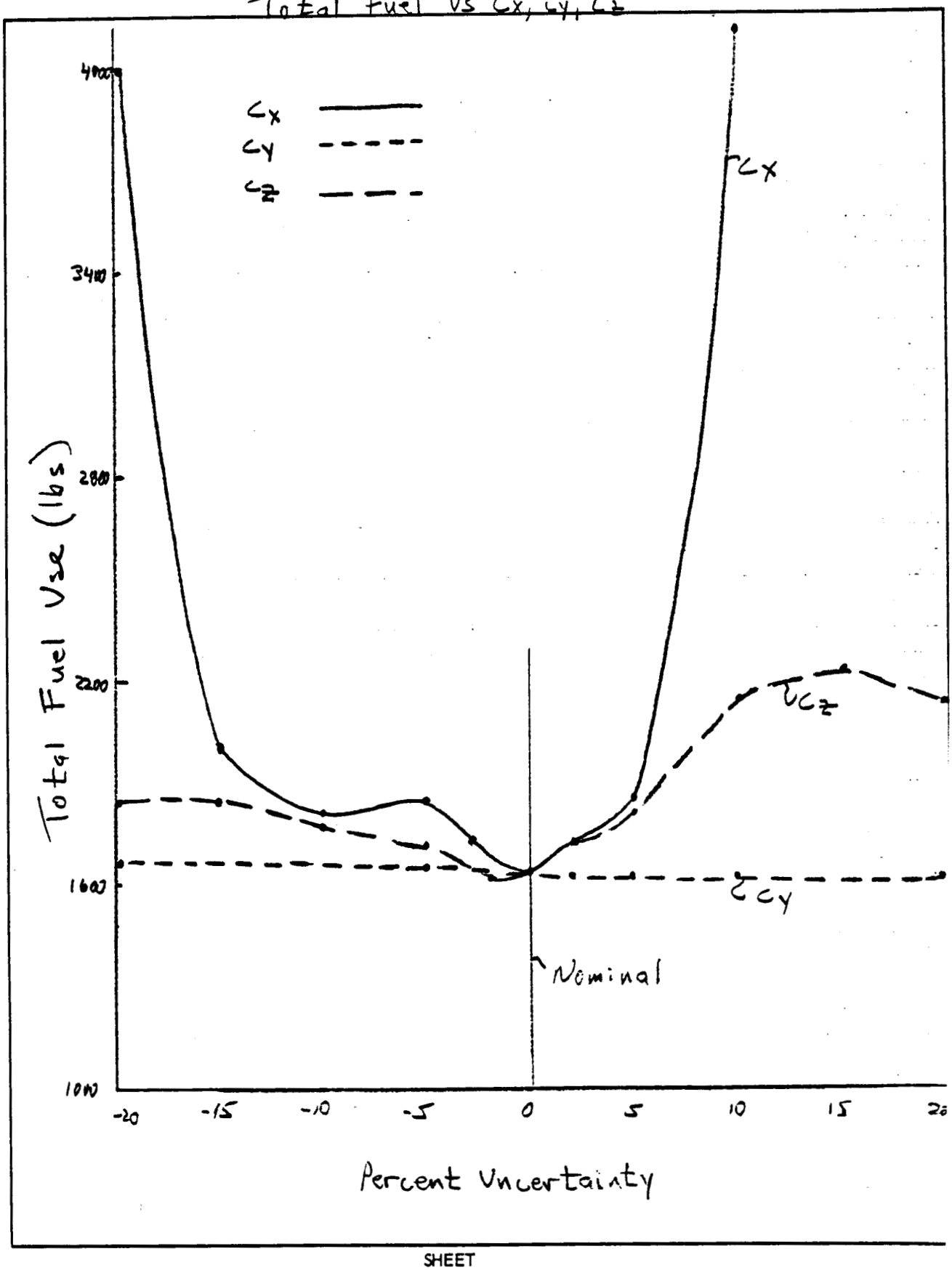

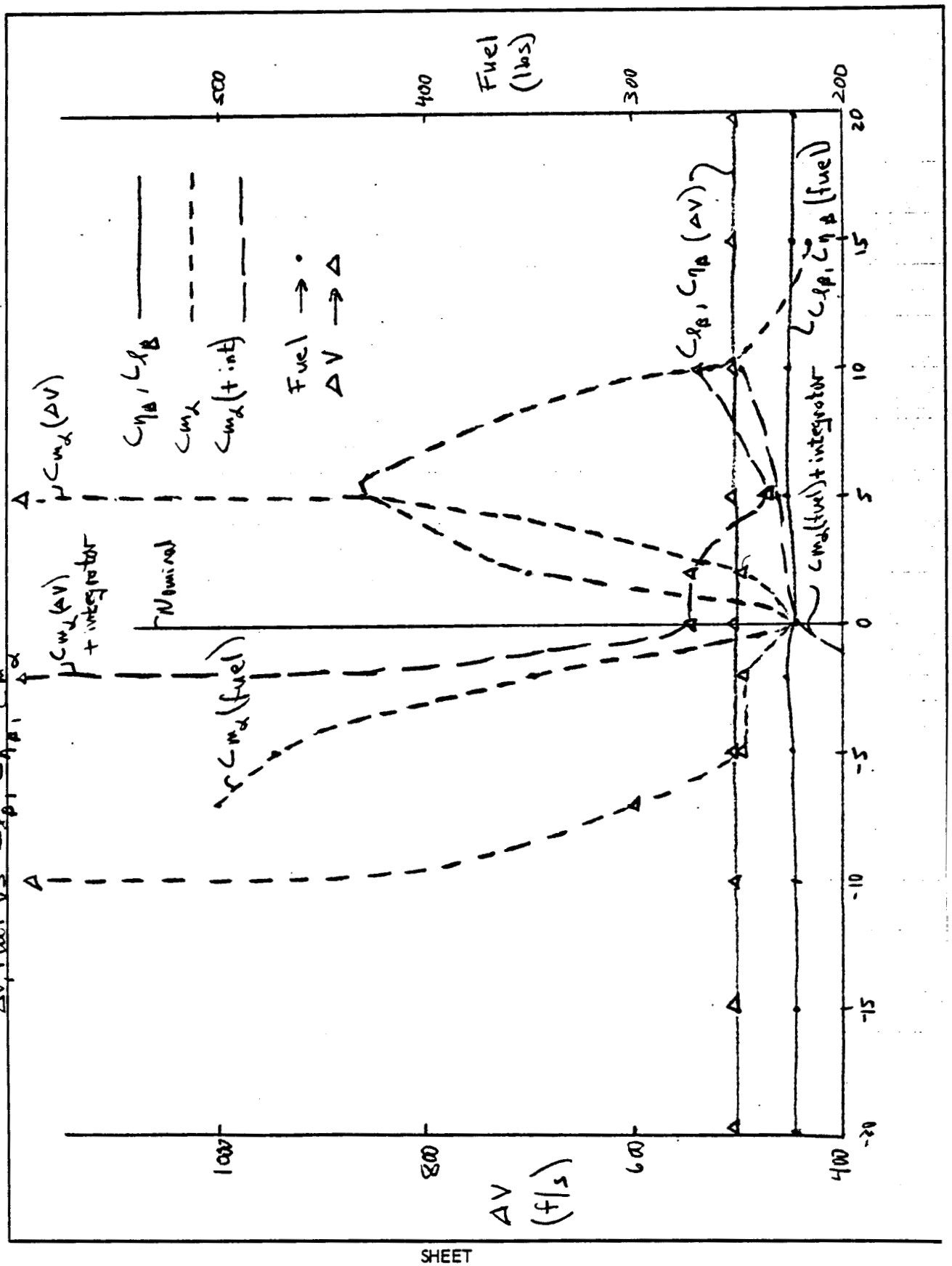
ΔV, Fuel vs $C_{\eta\beta}$, $C_{\eta\beta}$, C_{m_α}
Fuel (lbs)
500
400
300
200
ΔV (ft/s)
1000
800
600
400
20
15
10
5
0
-5
-10
-15
-20
$\mu C_{m_\alpha}(\Delta V)$
$C_{\eta\beta}, C_{y_\beta}$
C_{m_α}
C_{m_α} (+ int)
Fuel → •
ΔV → Δ
$\mu C_{m_\alpha}(\Delta V)$ + integrator
$N_{nominal}$
$-C_{m_\alpha}$ (fuel)
$C_{y_\beta}, C_{\eta\beta}$ (ΔV)
C_{m_α}(fuel)+integrator
$C_{y_\beta}, C_{\eta\beta}$ (fuel)

Figure 5.5-2

Figure 5.5-3 Total Fuel vs C_{n_β} C_{l_β}, C_{m_α}

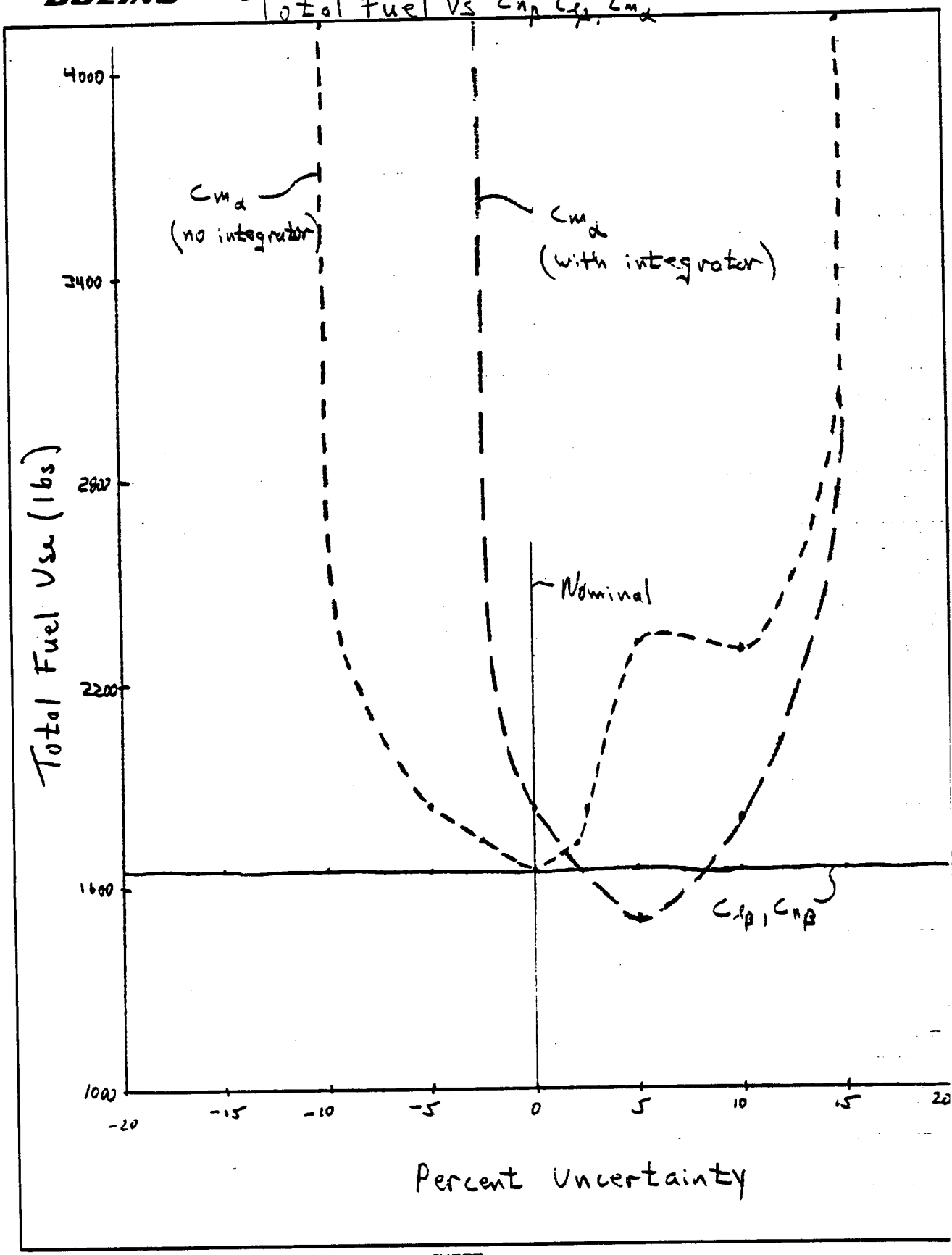

Figure 5.6-1. Rate Gyro Package Modifications for Sensitivity Studies

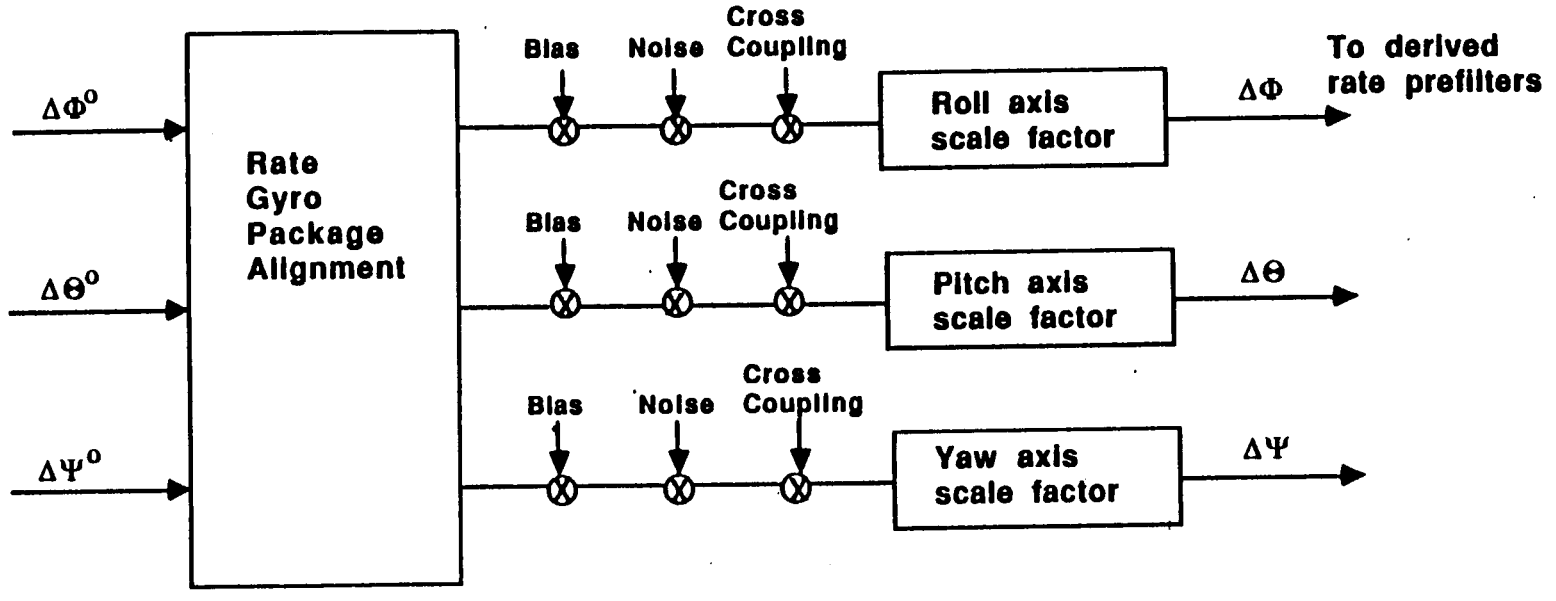

SENSOR ERROR STATISTICS

Parameter		Fortran Variable	Mean Value	3σ Derivation
Rate Gyro Noise	Roll gyro	SRTX	0	.3 deg/sec
	Pitch gyro	SRTY	0	.3 deg/sec
	Yaw gyro	SRTZ	0	.3 deg/sec
Rate Gyro Bias	Roll gyro	BTX	0	.0014 deg/sec
	Pitch gyro	BTY	0	.0014 deg/sec
	Yaw gyro	BTZ	0	.0014 deg/sec
Rate Gyro Scale Factor	Roll gyro	SFTX	1.0	.5%
	Pitch gyro	SFTY	1.0	.5%
	Yaw gyro	SFTZ	1.0	.5%
Rate Gyro Misalignment	Roll gyro	PHIG	0	.01 degree
	Pitch gyro	THETAG	0	.01 degree
	Yaw gyro	PSIG	0	.01 degree

Parameter		Fortran Variables	Mean Value	3σ Derivation
Rate Gyro Acceleration Sensitivity	Roll sensitivity to $\dot{Q}$	ATHX	0	10 deg/sec/rad/sec^2
	Pitch Sensitivity to $\dot{R}$	ATHZ	0	10 deg/sec/rad/sec^2
	Yaw sensitivity to $\dot{Q}$	ATHZ	0	10 deg/sec/rad/sec^2

Table 5-1

5.5-2

Figure ~~7.1-5~~ Rate Gyro Sensitivities

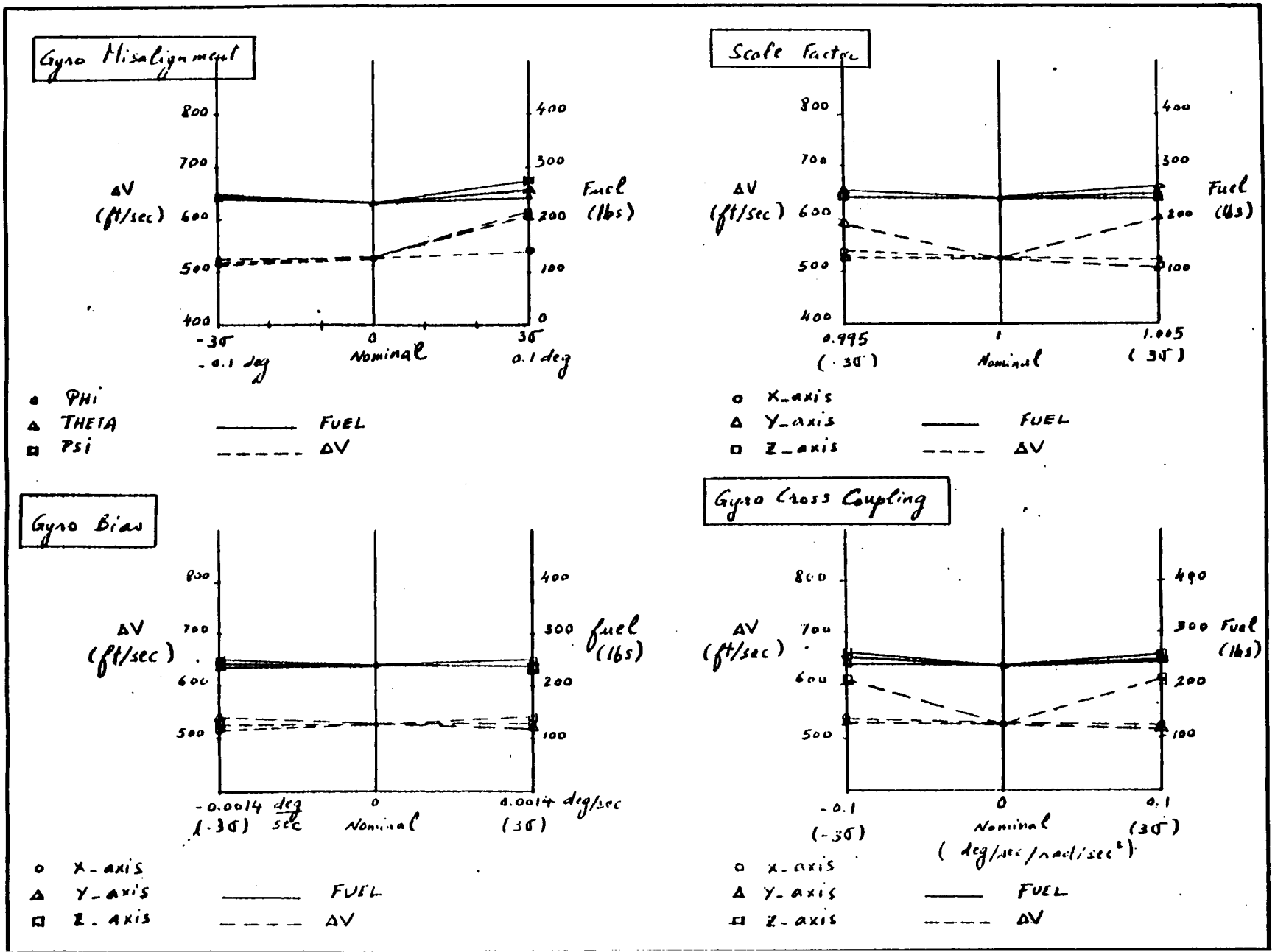

D1-8213-2001 REV. 11/84

SHEET 86

BOEING

NUMBER
REV LTR

ORIGINAL PAGE IS
OF POOR QUALITY

6.0 ADVANCED CONTROL SYSTEM CONCEPTS

Advanced control concepts are used to obtain improved system performance and robustness, relative to established control techniques and designs. These advanced concepts may include an adaptive element which is used to identify unknown or uncertain parameters in the system. For example, an adaptive algorithm might fine tune a control system by identifying the actual drag coefficient, as opposed to using the value generated by the aerodynamic model.

Another group of advanced control techniques includes the so-called "modern methods," which address the multiple-input, multiple output control problem. The thrust of these techniques is generally to minimize some form of a cost function, which varies for each technique. A well known example is the quadradic cost function of the Linear Quadradic (LQ) technique, which may be configured to minimize time, fuel, distance, or other important parameters.

The object of the aerobraking scheme is to maximize the energy "bleed-off" during the aeropass while minimizing the exit window error such that minimum fuel is required for orbit correction burns. An additional objective is to minimize the fuel burned during the aeropass. The first objective translates into a guidance requirement, i.e., use of an algorithm that will "bleed-off" energy and minimize exit window errors. The second

objective can be addressed using classical or modern control methods.

The following paragraphs describe the design and implementation of a semi-adaptive pitch axis controller. A new adaptive scheme which control combines aspects of each the techniques to achieve improved performance, robustness, and efficiency is presented in Section 6.2.

6.1 Semi-adaptive Pitch Axis Control System

The pitch axis rotational dynamics can be characterized with the second order transfer function

$$\frac{\theta}{\delta} = \frac{M_\delta}{(s^2 - M_\alpha)}$$

where θ is the angular position and δ is the commanded angular acceleration. M_α and M_δ are the moment sensitivities, which for this vehicle reduce to

$$M_\alpha = \frac{Cm_\alpha * Q * S * D * 57.3}{I_{yy}} = \frac{-K}{I_{yy}}$$

$$M_\delta = \frac{57.3}{I_{yy}}$$

where 57.3 is used to keep the units consistent (degrees). K may be viewed as the system "stiffness" which varies with dynamic pressure.

The natural frequency is given by the square root of M_α (defined above) . Over the course of the AOTV mission the natural frequency ranges from 0.0 to 2.1 radians per second, a function of the dynamic pressure. An autopilot designed to keep the pitch axis well damped at low Q will have a decreased damping ratio as Q increases, see Figure 6.1-1. The semi-adaptive control scheme estimates dynamic pressure using the X or Z axis accelerometer measurement and the corresponding aero coefficient, and then adjusts the control gains and bandwidth to keep the vehicle damping ratio at .8 throughout the entire mission. At the large angle of attack (72 or 74 degrees) the X measurement is principally a lift measurement and the Z measurement is principally a drag measurement. Figure 6.1-2 is a block diagram of the dynamic pressure estimation logic and the semi-adaptive gain adjustment. The X axis acceleration measurement is depicted.

The bandwidth of the semi-adaptive scheme is shown in Figure 6.1-3 for the nominal mission. As the bandwidth increases the pitch axis thrusters are more active and more fuel is used. The semi-adaptive scheme uses 56 pounds more fuel than the nominal fixed gain controller (increase of 25 percent). The semi-adaptive scheme also causes the required ΔV burns to increase from 521 feet per second to 530 feet per second (increase of 1.7 percent). This

increase comes from the additional Z axis loadings by the thrusters.

Figure 6.1-4 shows the pitch axis thruster firings for the adaptive and fixed gain autopilots.

6.2 Adaptive Control Concepts

The goal when using adaptive control techniques is to obtain acceptable levels of performance and stability with a changing or unknown plant. In the case of the AOTV vehicle, the parameters of most concern are the atmospheric variations and the c.g. shifts due to payload uncertainty. The atmospheric variations affect the guidance (HYPAS) and control, which both use an open-loop estimation scheme (see Figure 6.1-2) for dynamic pressure based on assumed knowledge of the aerodynamic coefficients. The c.g. shifts cause the trim position of the vehicle to change, requiring excessive thruster firings to maintain a specified trim angle. These two parameters represent the largest uncertainties and sensitivities in the system, and are therefore the most viable parameters to be identified in an adaptive control scheme.

Model Reference Adaptive Control (MRAC) is most applicable to deterministic tracking problems, i.e., when the desired output responses are known functions. For example, an advanced fighter aircraft can be made to handle like a training aircraft using MRAC. In this case, the desired response (trainer) is known

C-2

through on-board simulation, and the difference between the actual response (fighter) and the desired response can be calculated and used to influence the control, see Figure 6.2-1. The MRAC technique tries to minimize the error in the controlled variables, which for the example might be the normal acceleration, angle of attack, or pitch rate. Since there is no defined response function for the shaped-brake vehicle, this method is not recommended for the AOTV.

Self Tuning Control (STC) modifies the control as the unknown or uncertain parameters in the plant are identified. The technique attempts to achieve improved control through minimization of a performance index. Example cost functions may include minimization of any function of the system parameters; for example minimum fuel use or minimum deviation from a desired set point. The STC methods usually include an identification algorithm such as the "least squares technique" which must identify the unknown system parameters in real time. These algorithms can be greatly simplified by keeping the parameters to be estimated to a minimum. Variations of this technique are recommended for the AOTV vehicle because useful cost functions such as minimum fuel are important to mission performance.

The following is a proposed adaptive control design for the AOTV vehicle which uses a variation of the STC technique combined with a second non-adaptive controller and an optimization algorithm. Under this approach, a non-adaptive control system is designed

using classical or modern techniques (Linear Quadratic, H-Infinity, Eigenstructure, Optimal Projection, etc.) using expected values of the vehicle and mission parameters. This system is simulated and analyzed for stability. This is considered the base design.

For each specific mission there may be new parameters/constraints such as payload requirements, atmospheric conditions, or maximum thruster size. The base design is then altered to accommodate the new parameters using the nonlinear optimization program QDES. QDES (Q-Design) is a computer aided design tool developed at Stanford by Boyd [2]. The QDES program reformulates the control problem using coprime factorization and searches for an optimal solution in the defined convex search space. If an optimal solution exists, the algorithm is guaranteed to converge to the global optimum.. The constraints which may be included in the optimization process are frequency domain type constraints such as phase and gain margins, bandwidth, and settling time. Using this program, the base design can be augmented in an optimal way to handle the new requirements.

Up to this point no adaptive techniques have been incorporated. To this end, a Self Tuning Controller can be included in the above design for in-flight fine tuning of the control as better estimates of the true plant become available. The advantage of using the ST to fine tune the optimized base design over a purely adaptive control scheme is that the base design is already a

stable control system and the adaptive system does not need to identify the system to maintain stability. Thus the adaptive portion of the algorithm only fine tunes an already stable design for improved performance.

The basis of the self tuning algorithm is similar to that of the QDES program, both being derived from a parameterization of the class of all stabilizing controllers as found in Vidyasagar [3]. Moore [4,5] has extended the parameterization technique to the class of all stabilizing, time-varying controllers for time-varying plants. Using the techniques of Moore, the stable transfer function matrix designed with the QDES program can be augmented with a time varying stable transfer matrix, which must be calculated in real-time.

This advanced adaptive scheme has several advantages over a purely adaptive control scheme. First, the knowledge base of past experience can be built into the base design. This provides a fail-safe level of control which can be used as a default if the adaptive algorithm fails to perform. Second, the control system is easily modified for different mission requirements without requiring extensive analysis for stability and performance. Third, the self tuning adaptive element attempts to tweak the control system to obtain optimal performance during the mission, but is not required to identify a large number of parameters and also guarantee stability.

The diagram in Figure 6.2-3 shows the structure of the proposed control system. Notice that Q and Q′ can be zeroed out and the remaining control is the base feedback design closed through the X and Y^{-1} blocks (coprime factors). With a nonzero Q and a zeroed out Q′ the system has been augmented to handle the modified performance requirements. Q′ is implemented in real-time and is the adaptive element in the system. This evolved control design is utilized to accommodate unknown system and mission parameters and achieve an acceptable level of performance.

ROOT LOCUS FOR FIXED GAIN SYSTEM

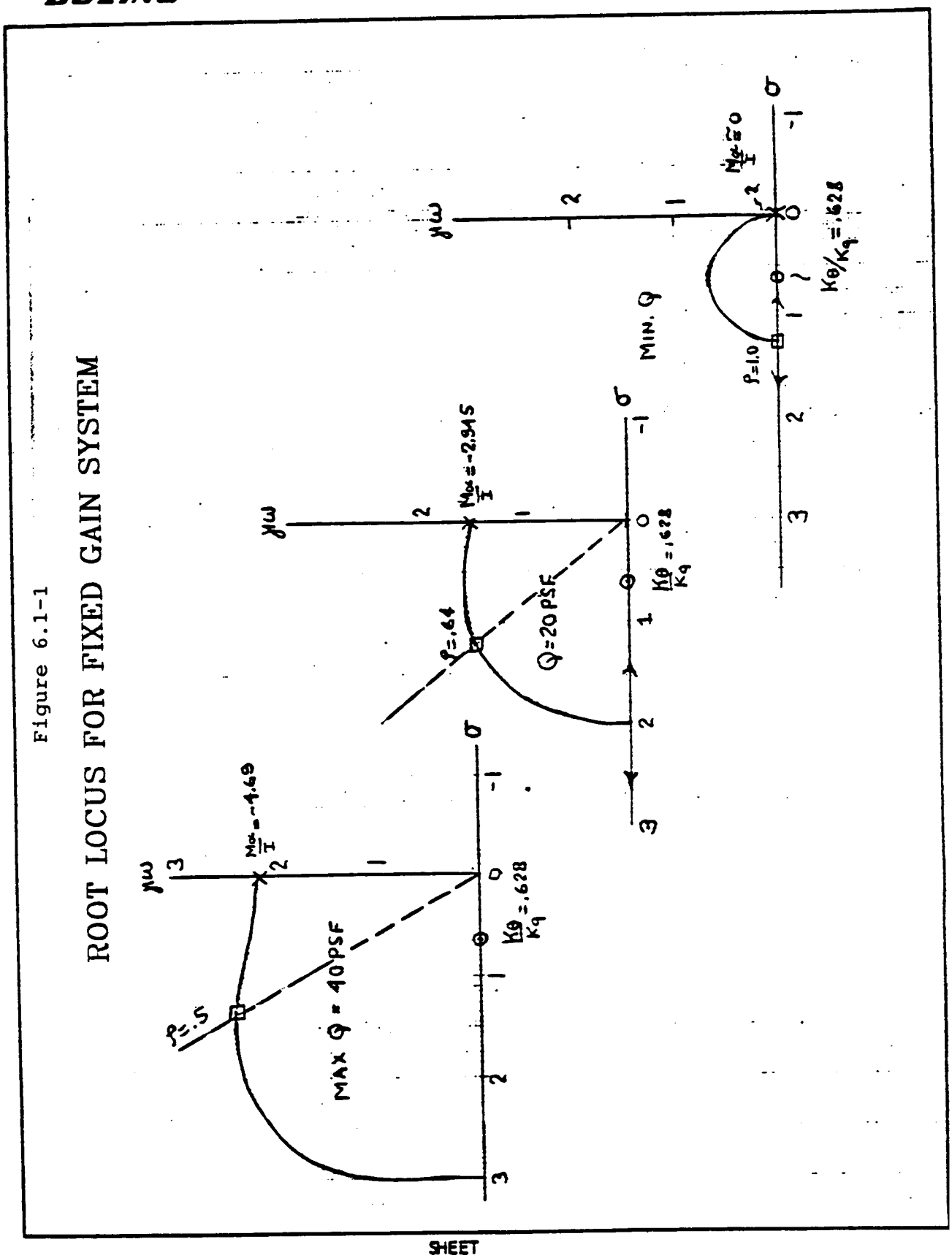

Figure 6.1-1

Estimation/Adaptation Algorithm

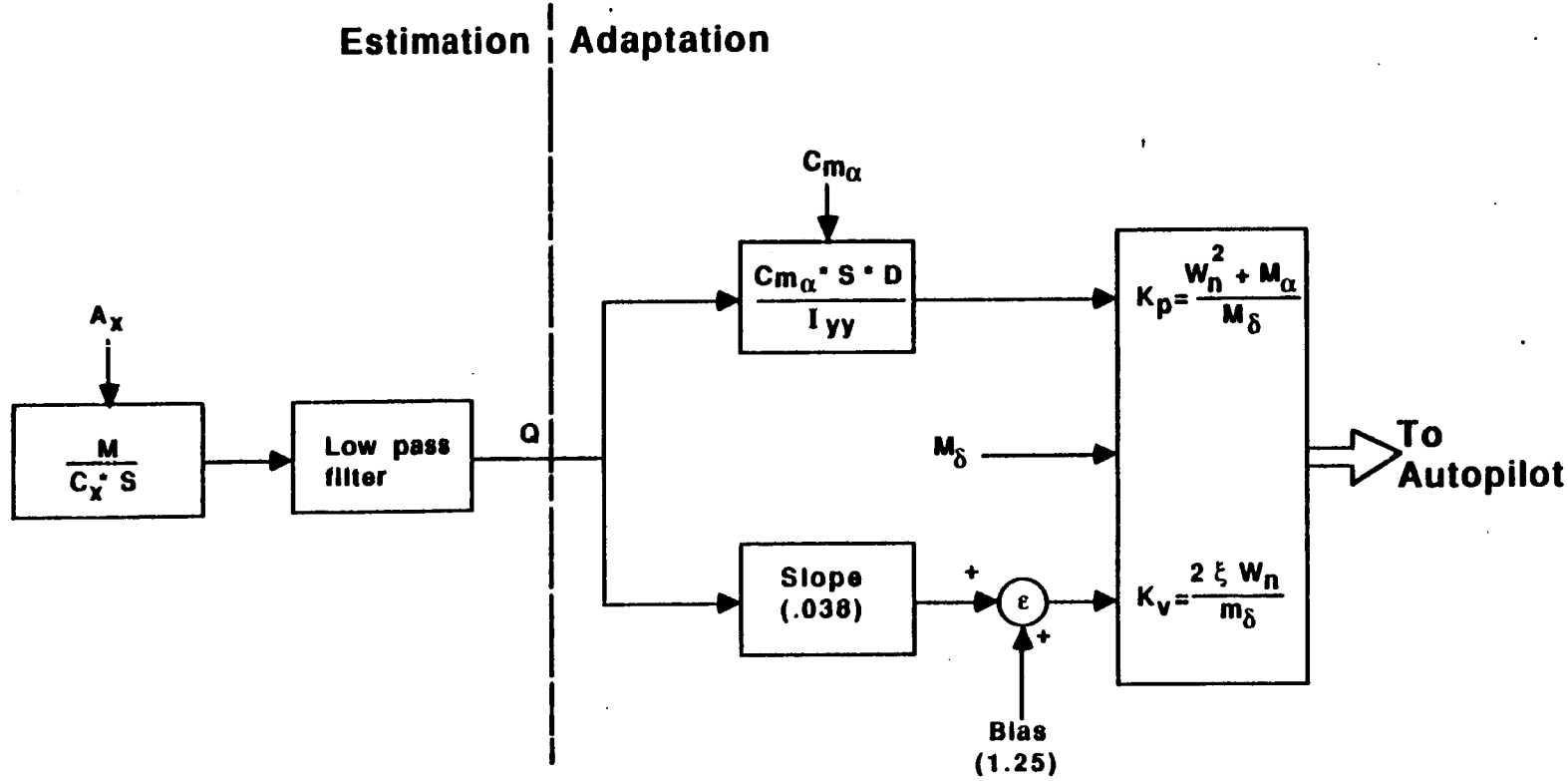

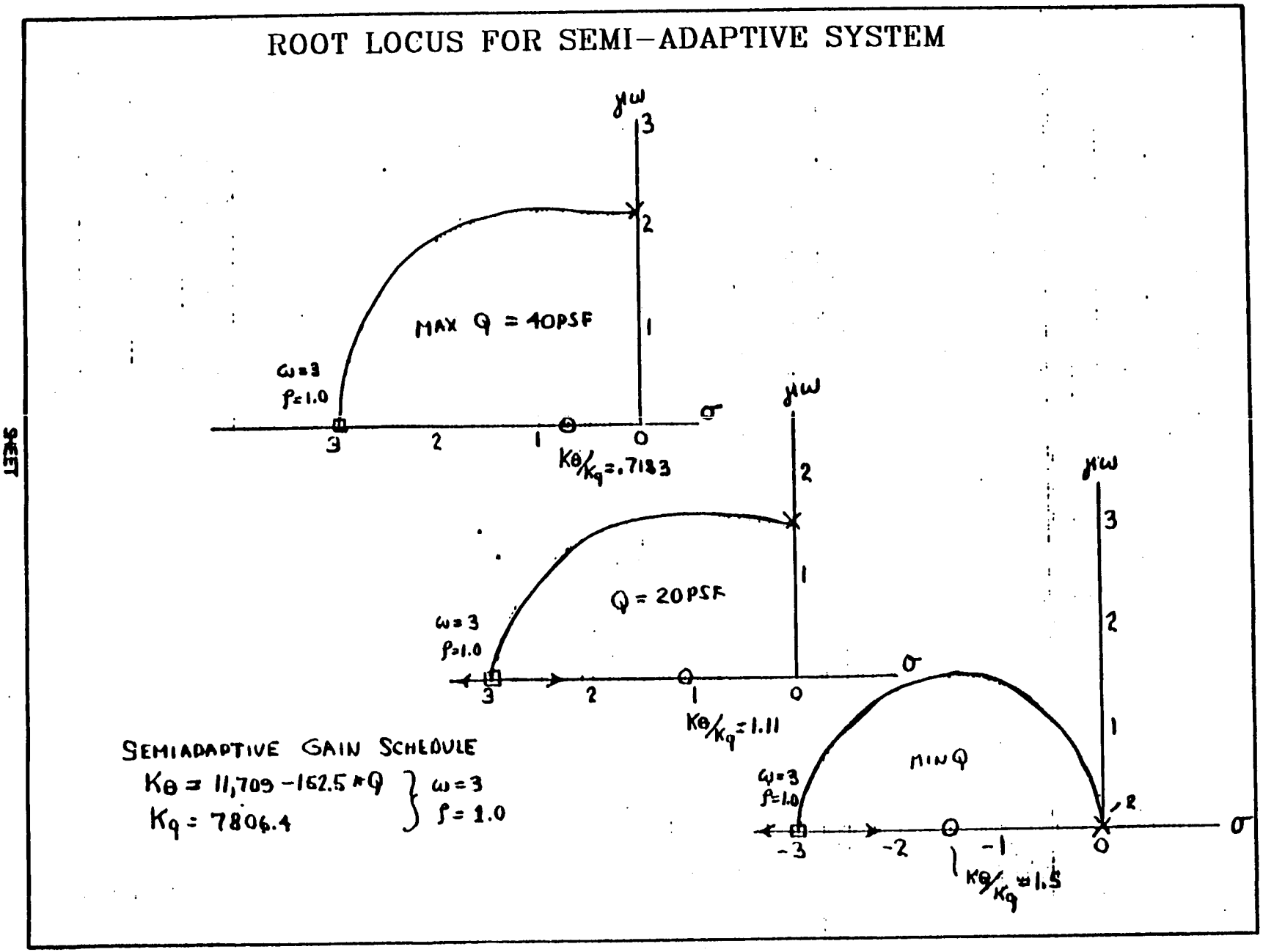

Figure 6.1-2 cont.

BANDWIDTH VS TIME

Boeing Aerospace Company

ENGINEERING TECHNOLOGY

ACTUAL AND COMMANDED THRUST

ENGINEERING TECHNOLOGY

Boeing Aerospace Company

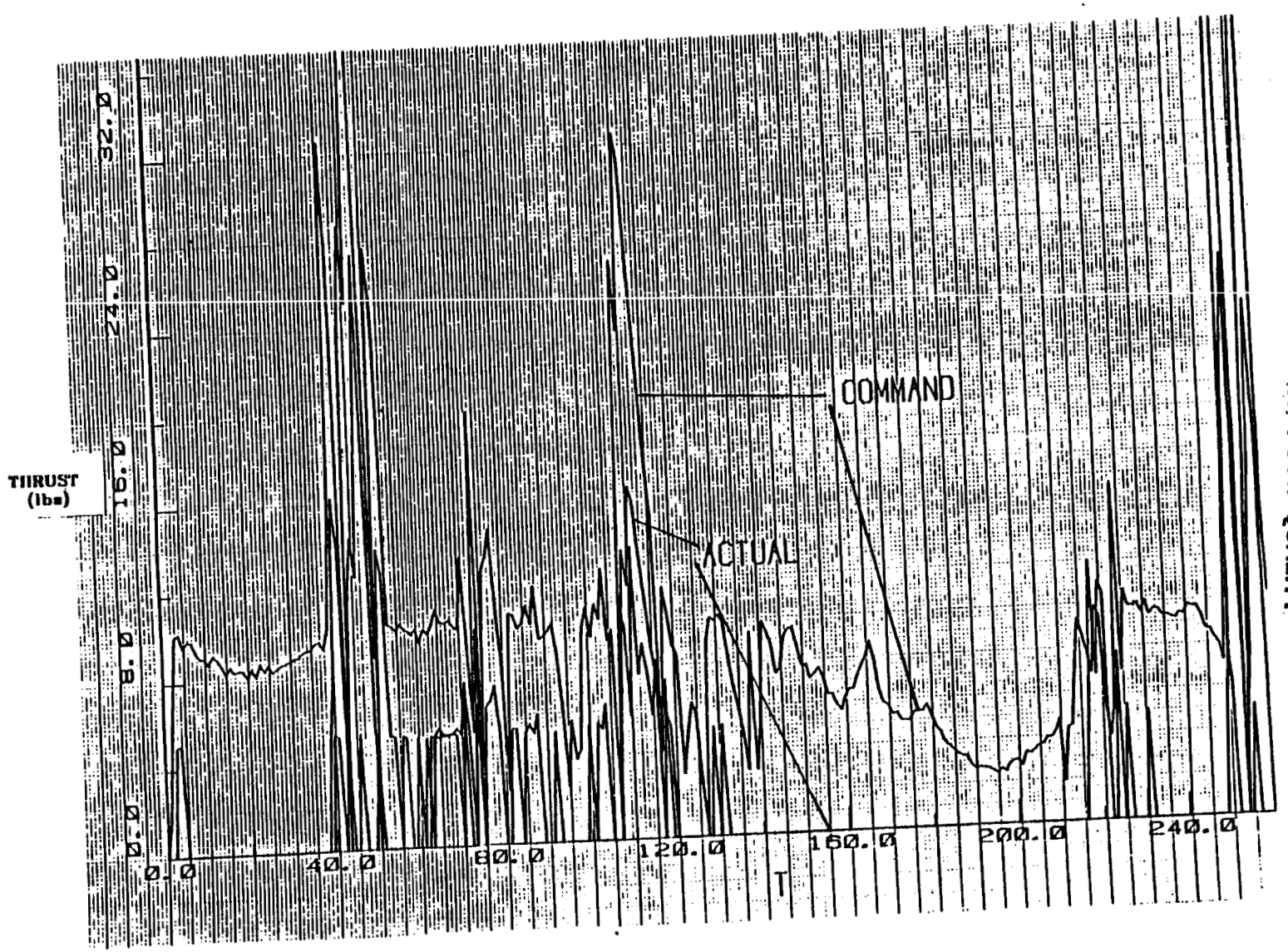

ORIGINAL PAGE IS
OF POOR QUALITY

MODEL REFERENCE CONTROL SYSTEM

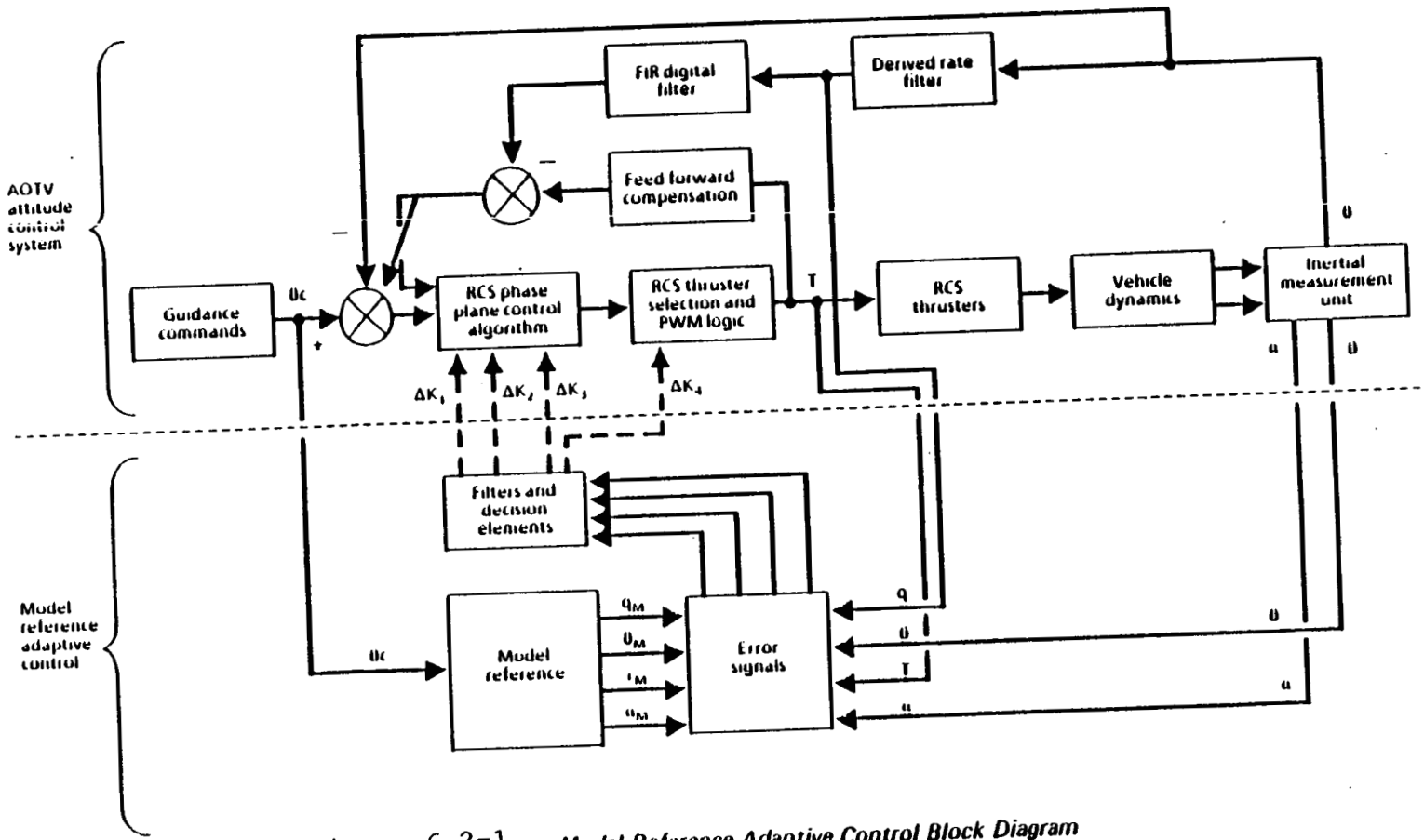

Figure 6.2-1 *Model Reference Adaptive Control Block Diagram*

SEMI–ADAPTIVE CONTROL SYSTEM

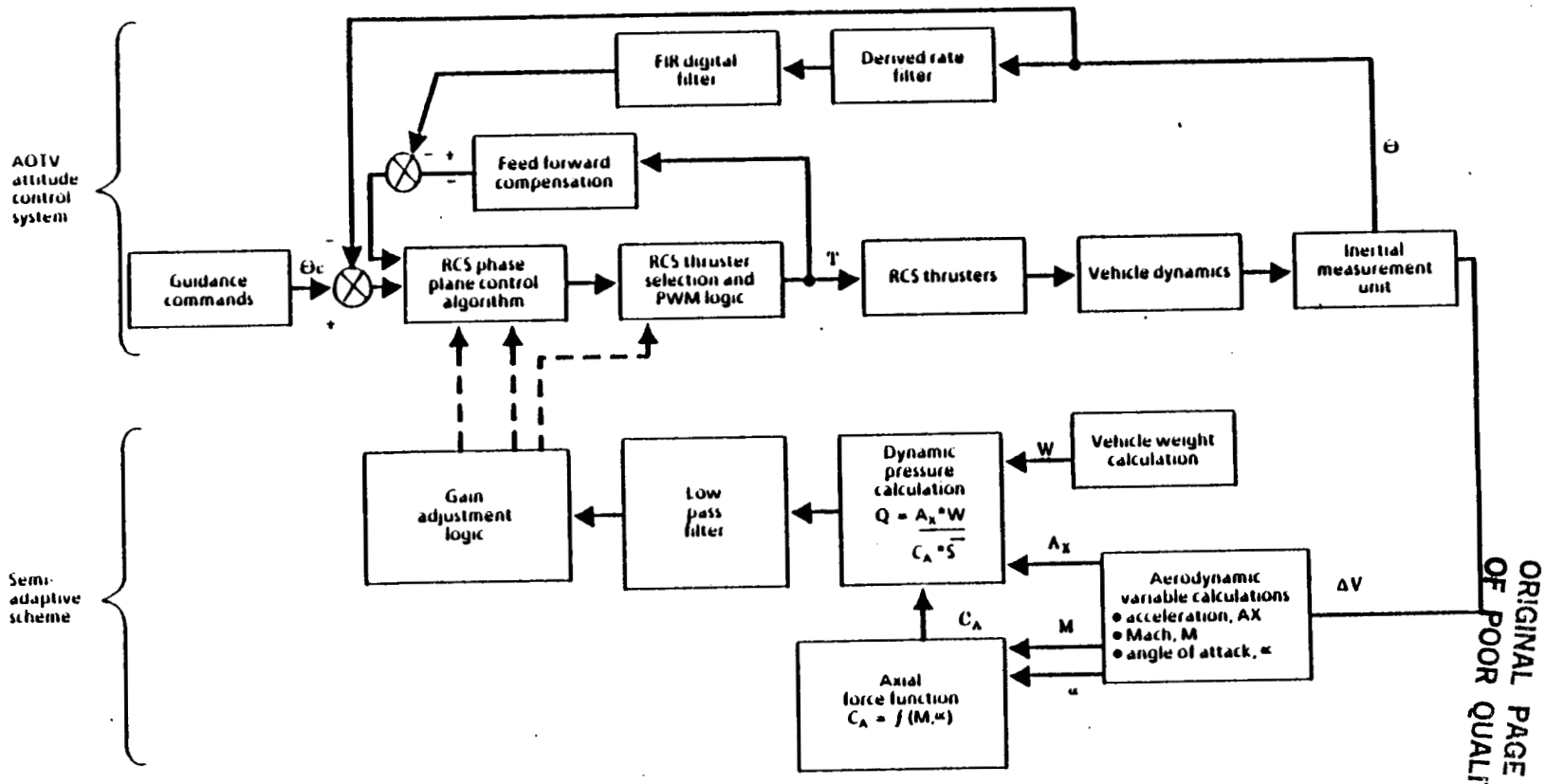

Figure 6.6-2 *Semiadaptive Control Based on Dynamic Pressure*

THREE TIERED APPROACH

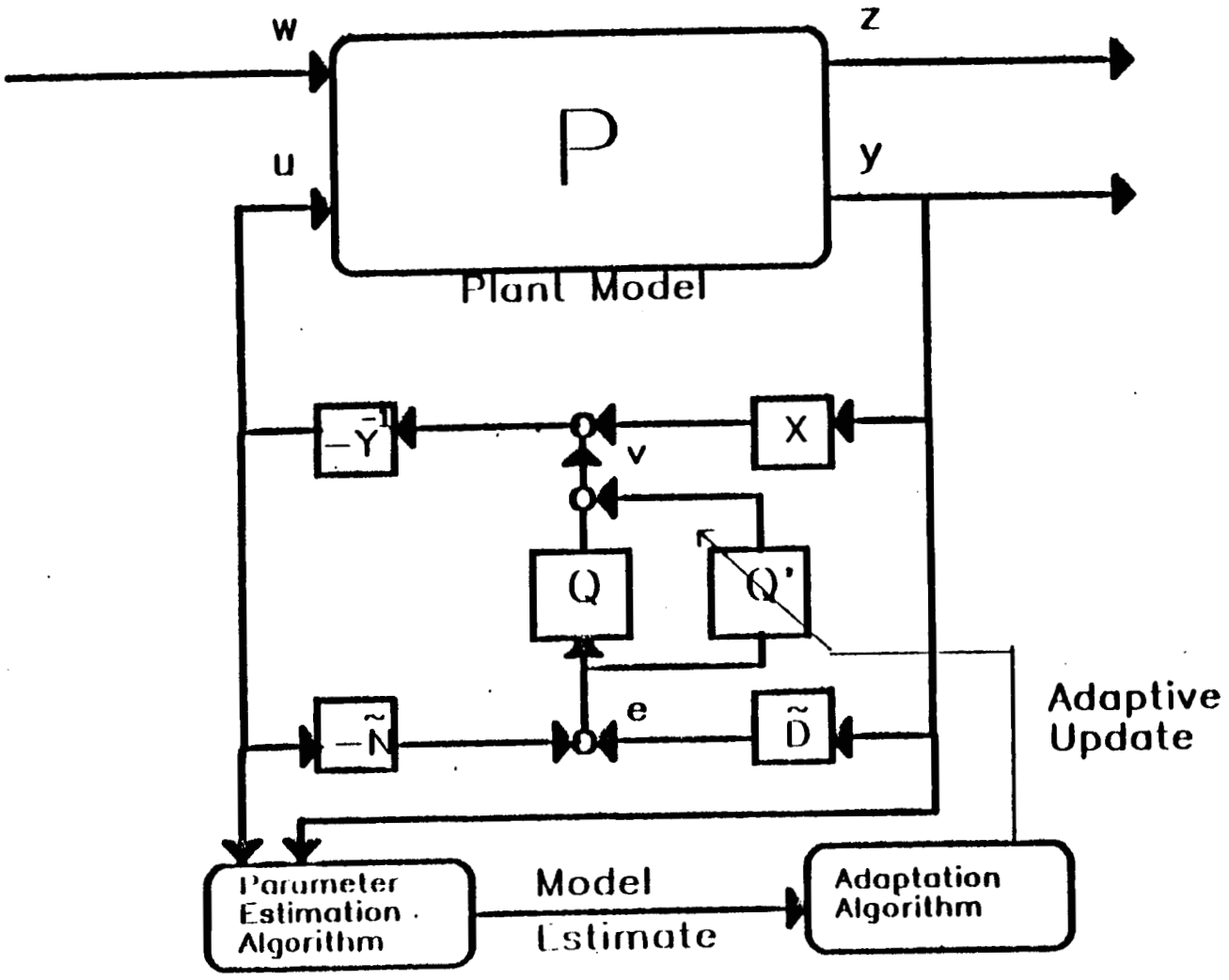

Figure 6.2-3

7.0 Conclusion

Control technology has been developed in this contract for the AOTV mission which minimizes the fuel used for atmospheric maneuvering. The control techniques developed can be used on a number of AOTV type vehicles. The control algorithms can be tailored to the guidance law and vehicle characteristics by adjusting only the control gains and break frequencies.

The control technique includes:

1) Adaptive trim design for c.g. control;
2) Semi-adaptive gain computer to minimize mission data loads;
3) Proportional or on-off thruster selection;
4) Control designs which minimize RCS fuel usage.

Initial control studies have also been conducted on advanced adaptive control concepts. The concepts considered include model reference adaptive, linear quadratic, Q-design, and self-tuning adaptive. Results indicate that the classical design is sufficient for known vehicle configurations and payloads. Increased performance can be achieved with advanced control techniques over a large range of missions and payloads.

The classical control techniques have been verified through detailed sensitivity studies using 6DOF simulation. The simulation studies show the following:

1) Small sensitivity (>20% tolerance) for all sensor effects,

$C_{l\beta}$, $C_{n\beta}$, Cy, and Cx aerodynamics, and mass properties (weight, inertia, X c.g. location);

2) Moderate sensitivity (10% to 20% tolerance) for Z c.g. location, atmosphere effects (winds, density), and Cx and $C_{m\alpha}$ aerodynamics;
3) High sensitivity (<10% tolerance) for entry state parameters (velocity, flight path angle, altitude, and inclination).

The critical vehicle parameter in controlling the reentry state is the vehicle lift/drag ratio. The AOTV L/D is required to have a value larger than .15 to handle a 3σ variation in the reentry state. Both vehicles analyzed, the Boeing Shaped Brake and the AFE have L/D larger than .15. (L/D Boeing Shaped Brake = .2, L/D AFE = .3)

8.0 RECOMMENDATIONS (FOLLOW-ON-STUDIES)

The importance of the control and guidance techniques to the performance and robustness of the AOTV mission was studied in the Control Technology AOTV contract. New, advanced technology proposed for follow-on studies would benefit the AOTV by lowering recurring costs through autonomy and increase flexibility to varying mission requirements through adaptability and automated tuning. The autonomous design would make the system insensitive to payload variation and fuel load. Lower costs would be achieved by eliminating software changes per mission and minimizing mission data loads. The high reliability, low maintenance is achieved by using fault-tolerant processors and sensors.

Our recommendations are to develop the technology for an autonomous three level modern control approach:

1) Integral linear quadratic control design (angle-of-attack, bank angle controller)
2) Mission data load automation using Q-design method (tuned controller through simple mission data load)
3) Adaptive fine-tuning based on parameter estimates generated in flight.

This technology could be applied directly to the AFE configuration and verified on 6DOF simulation. Other guidance laws developed for the AFE by NASA Marshall Flight Center and Draper Labs can also be included in the 6DOF simulation.

References

1) Carimele, C.J., and Gamble, J.D., "A Simplified Guidance Algorithm for Lifting Aeroassist Orbital Transfer Vehicles," AIAA-85-0348, January 1985.

2) Boyd, S., Balakrishnan, V., Barrat, C., Khraishi, N., Li, X., Meyer, D., Norman, S., "A New CAD Method and Associated Architectures for Linear Controllers", to appear in Transactions on Automatic Control, March 1988.

2) Vidyasagar, M., "Control System Synthesis: A Factorization Approach", MIT Press, Cambridge, 1985.

3) Moore, J., Tay, T. "The Class of All Stabilizing Controllers for Time-Varying Systems", to be published.

4) Tay, T., Moore, J., "Enhancement of Fixed Controllers Via Adaptive Disturbance Estimate Feedback", to appear, Proc IFAC Symposium, Aug. 1988.

APPENDIX

A.1 6DOF Simulation

Figure A.1-1 shows the hardware facilities used for the 6DOF simulation. The nonlinear equations of motion are hosted on the AD10. The autopilot and other slower processes are hosted on the Harris 1000. The AOTV simulation runs in real-time.

Figure A.1-2 is a block diagram of the entire 6DOF simulation. The dashed line indicates the separation of processes between the two computers. Each of the blocks in the diagram correspond to a FORTRAN subroutine in the simulation.

A.2 3DOf/6DOF Validation

The 3DOF and 6DOF simulations are similar in that they use the same guidance algorithm. While there are many obvious differences, a few very important ones are discussed here. First, 3DOF simulations neglect the effect of rotary inertia, an important quantity in the 6DOF simulation due to the rapid rotational commands from the guidance system. The 3DOF simulation uses a rate limiting scheme to approximate the rotational dynamics. We have found that a rate limit of 15 deg/sec best approximates the actual rotary dynamics for this vehicle. Second, the 3 DOF simulation uses a lift/drag aero model with constant coefficients while the 6DOF simulation derives the lift and drag

from the force and moment coefficients which are functions of angle of attack and sideslip angle. Third, the thrusters in the 6DOF simulation create additional translational loads on the system that are not present in the 3DOF simulation. Fourth, the integration step size in the 3DOF is one second while the step size in the 6DOF is .001 seconds. Lastly, the scaling in the AD10 computer used in the 6DOF simulation may have an effect on the results.

Time history comparisons for the 3DOF and 6DOF simulations are shown in Figures A.2-1 through A.2-7. The figures show a good match in the simulations, verifying correct dynamic models and implementation of the guidance algorithm. Figure A.2-7 is a plot of the bank commands. The difference in the two commands histories beginning at 160 seconds is due to the different calculated values of the inclination at that time.

Table A.2-8 shows the initial and final conditions for the nominal trajectory. The target window parameters are also included.

The 3DOF and 6DOF simulations both use the HYPAS guidance algorithm, which has two major modes of operation. During the entry phase the algorithm generates commands which attempt to maintain an equilibrium glide condition (lift = weight). During the exit phase the algorithm generates bank commands based on the desired radius of apogee and the predicted exit condition. The difference between the actual orbit plane and the desired orbit

plane is used to determine the sign of the bank command.

ENGINEERING TECHNOLOGY

Computer Resources Used in 6-DOF Simulation

Boeing Aerospace Company

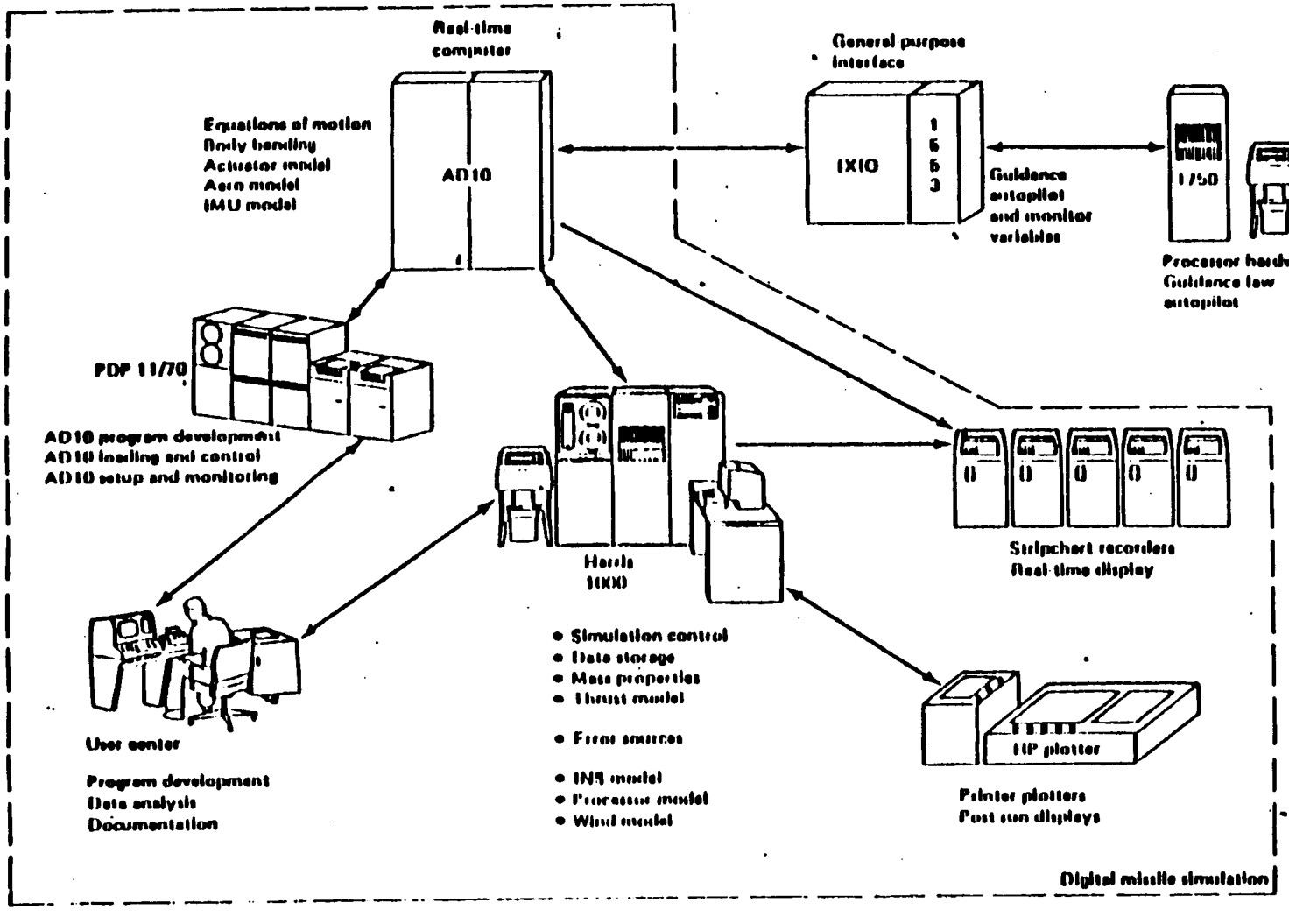

Figure A.1-1

Orbital Transfer and Reentry Control 6-DOF Simulation

ENGINEERING TECHNOLOGY

Boeing Aerospace Company

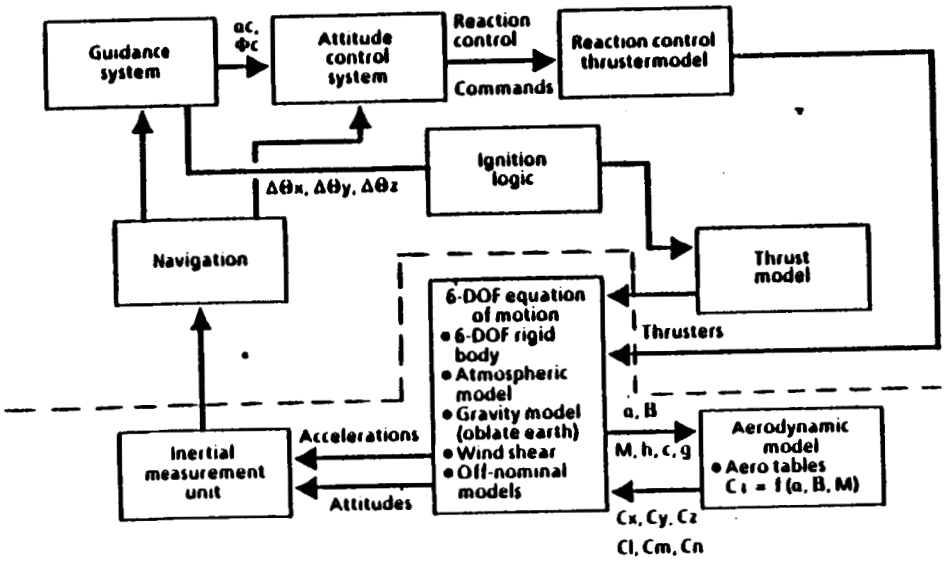

Figure A.1-2

111

ORIGINAL PAGE IS OF POOR QUALITY

HARRIS

AD10

444P1-007/New

ALTITUDE
OPEN LOOP COMPARISON

Boeing Aerospace Company

ENGINEERING
TECHNOLOGY

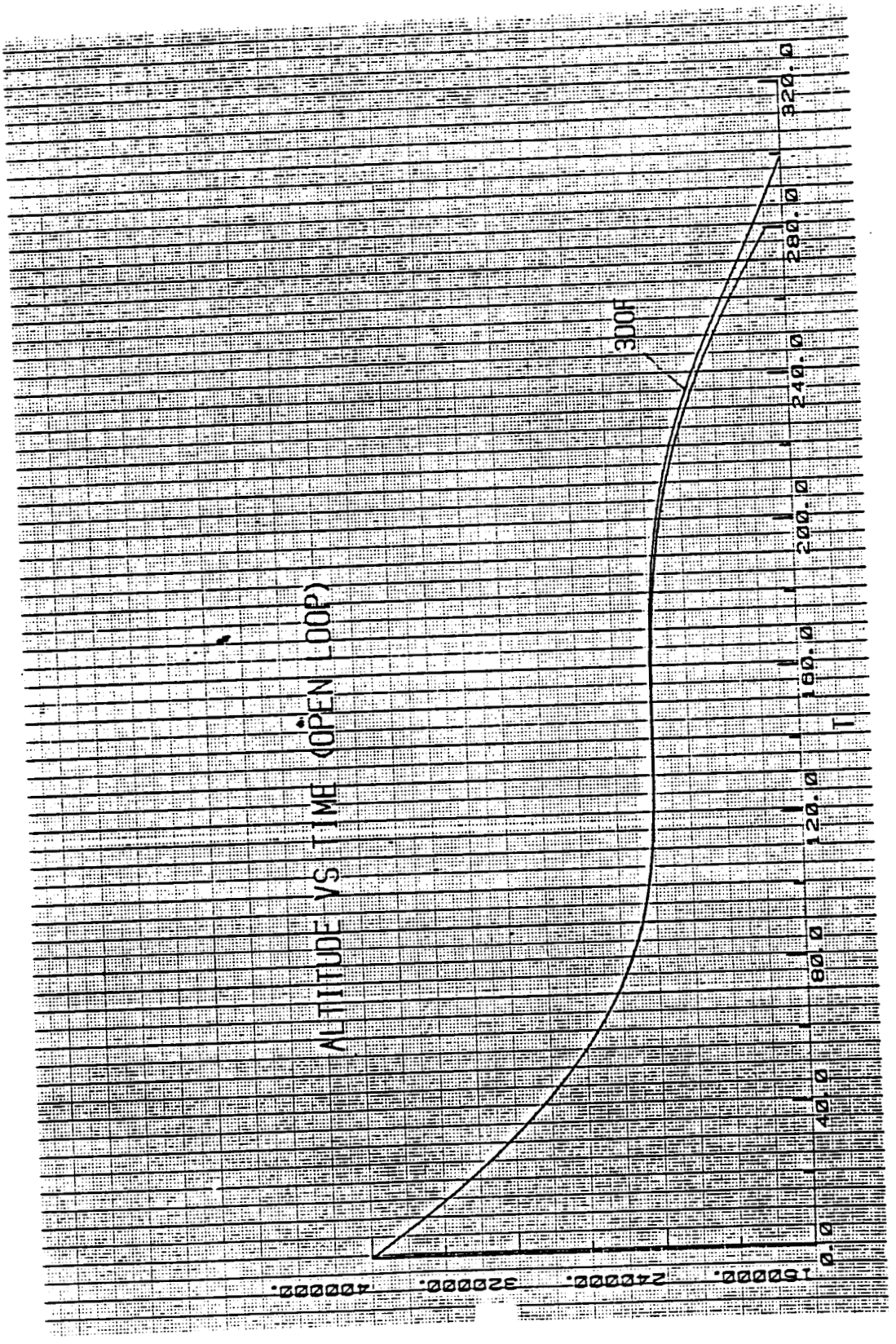

Figure A.2-1

VELOCITY
OPEN LOOP COMPARISON

Boeing Aerospace Company

ENGINEERING TECHNOLOGY

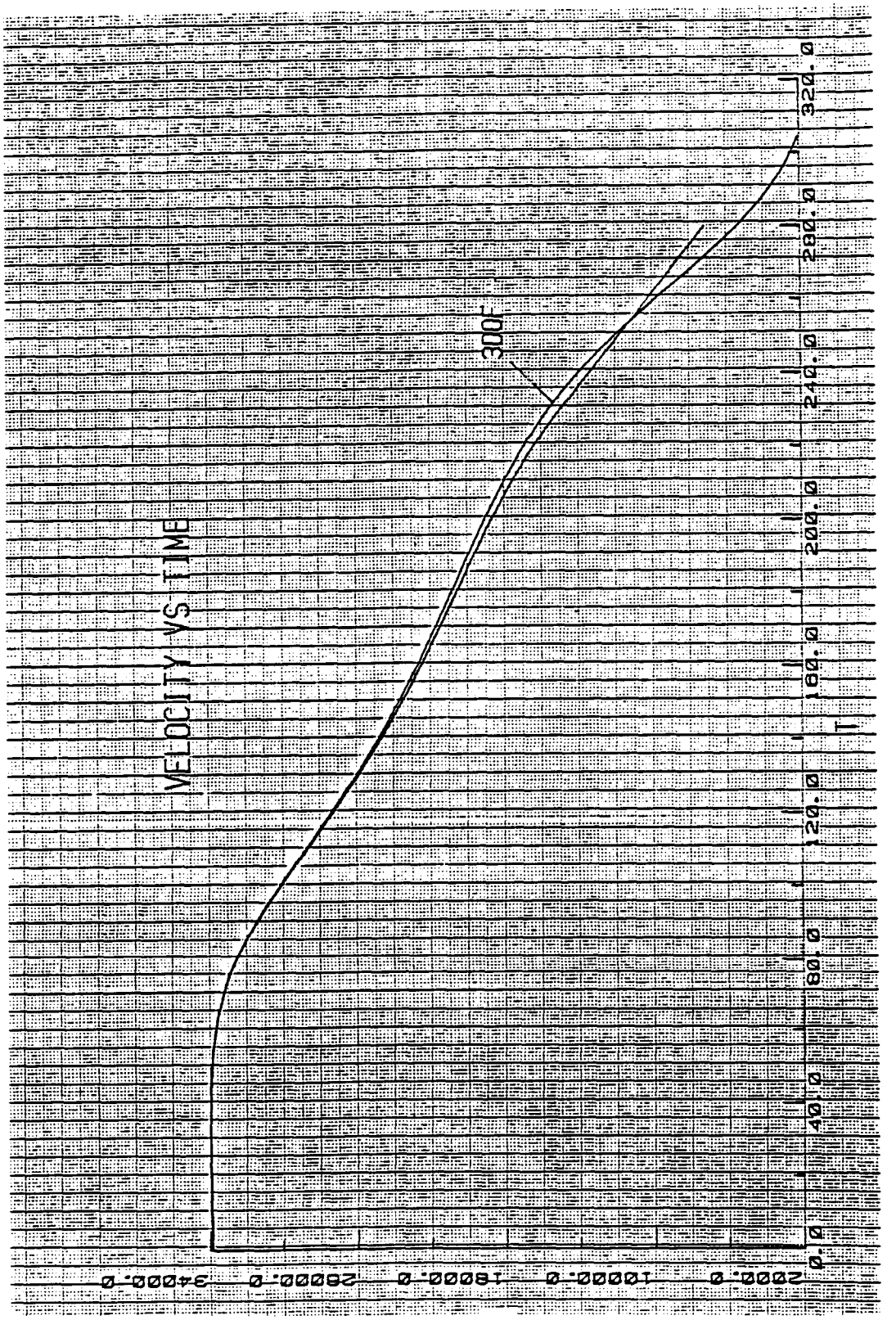

Figure A.2-2

ALTITUDE VS VELOCITY
6DOF VS 3DOF

ENGINEERING TECHNOLOGY

Boeing Aerospace Company

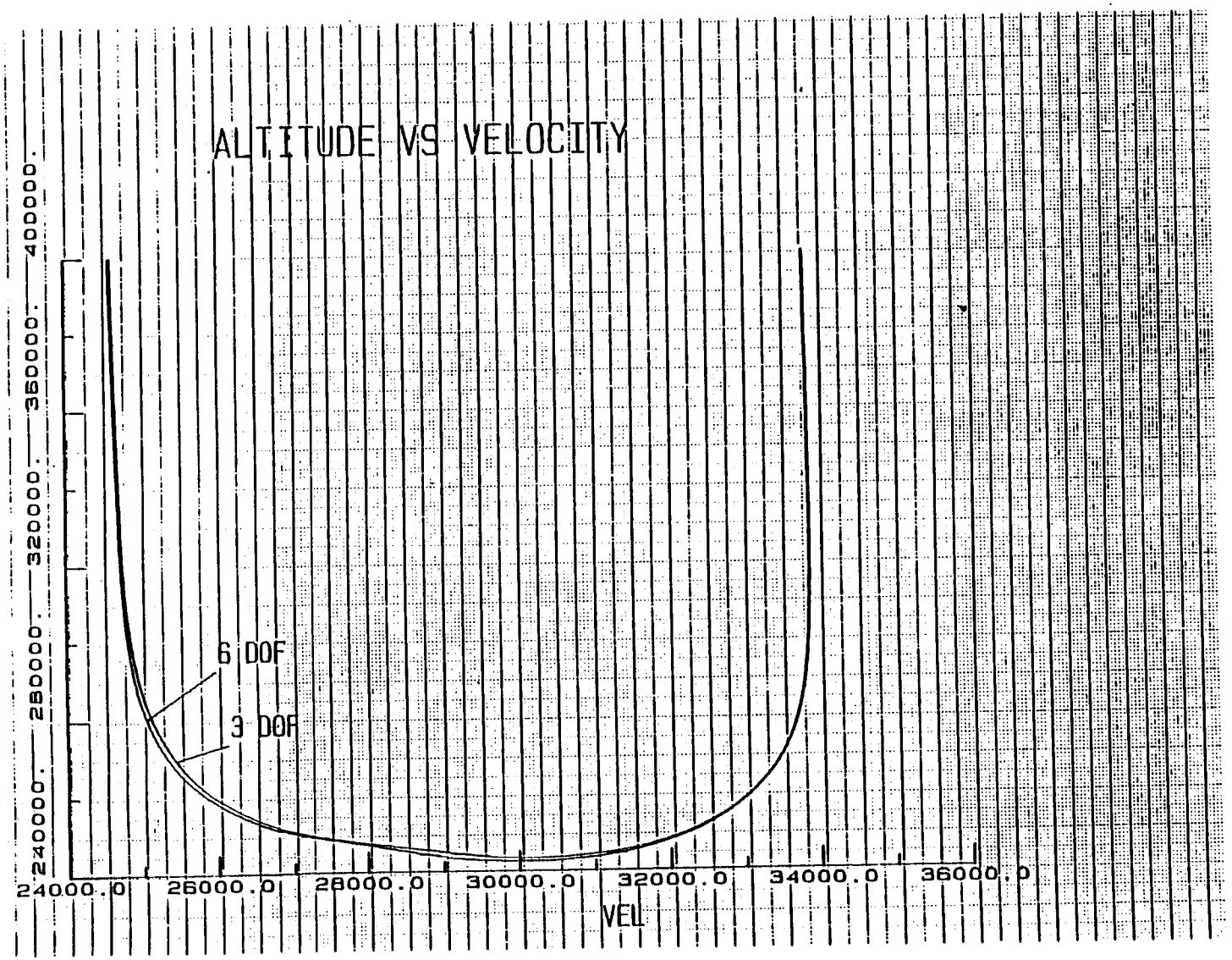

Figure A.2-3

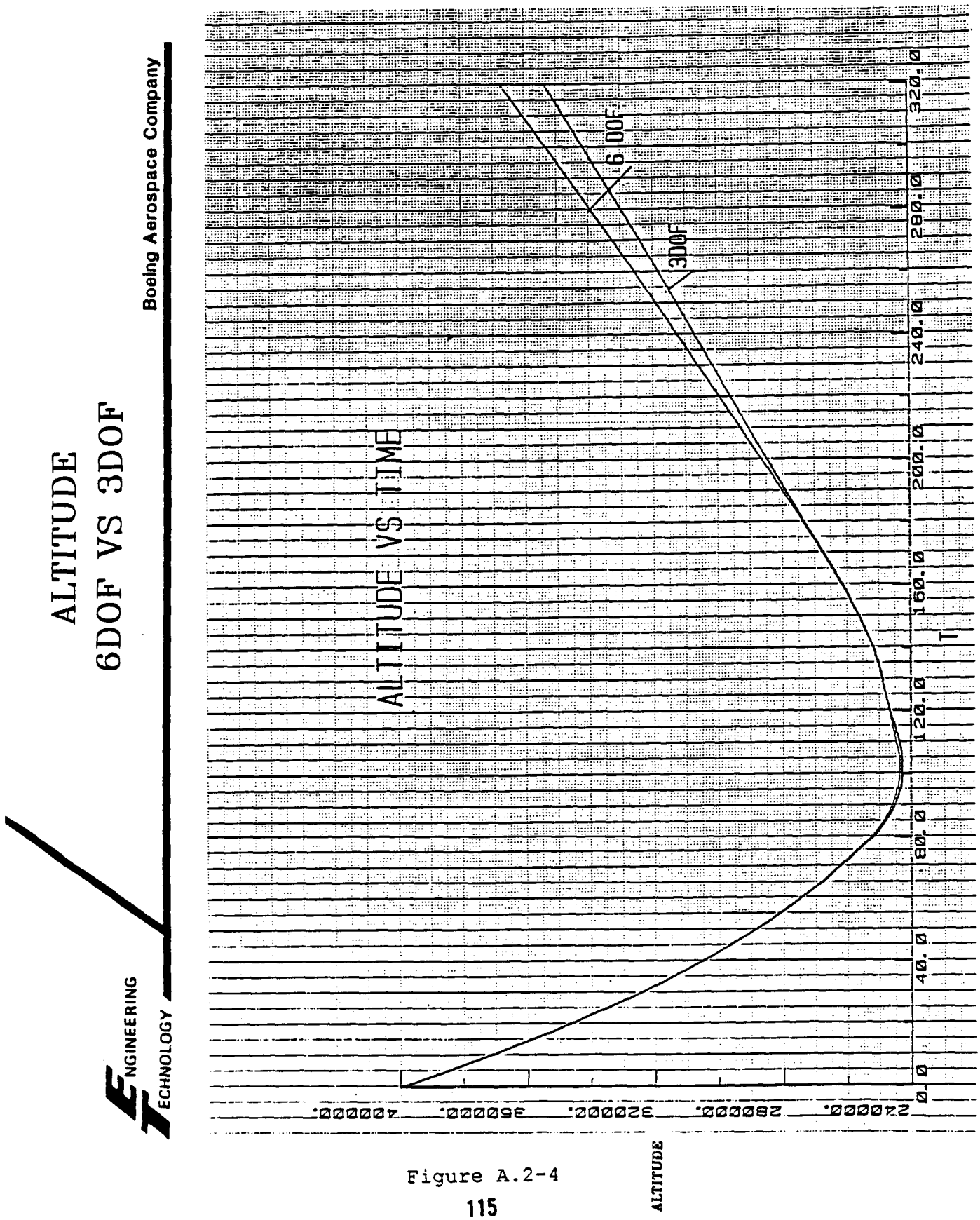

Figure A.2-4

DYNAMIC PRESSURE
6DOF VS 3DOF

ENGINEERING TECHNOLOGY

Boeing Aerospace Company

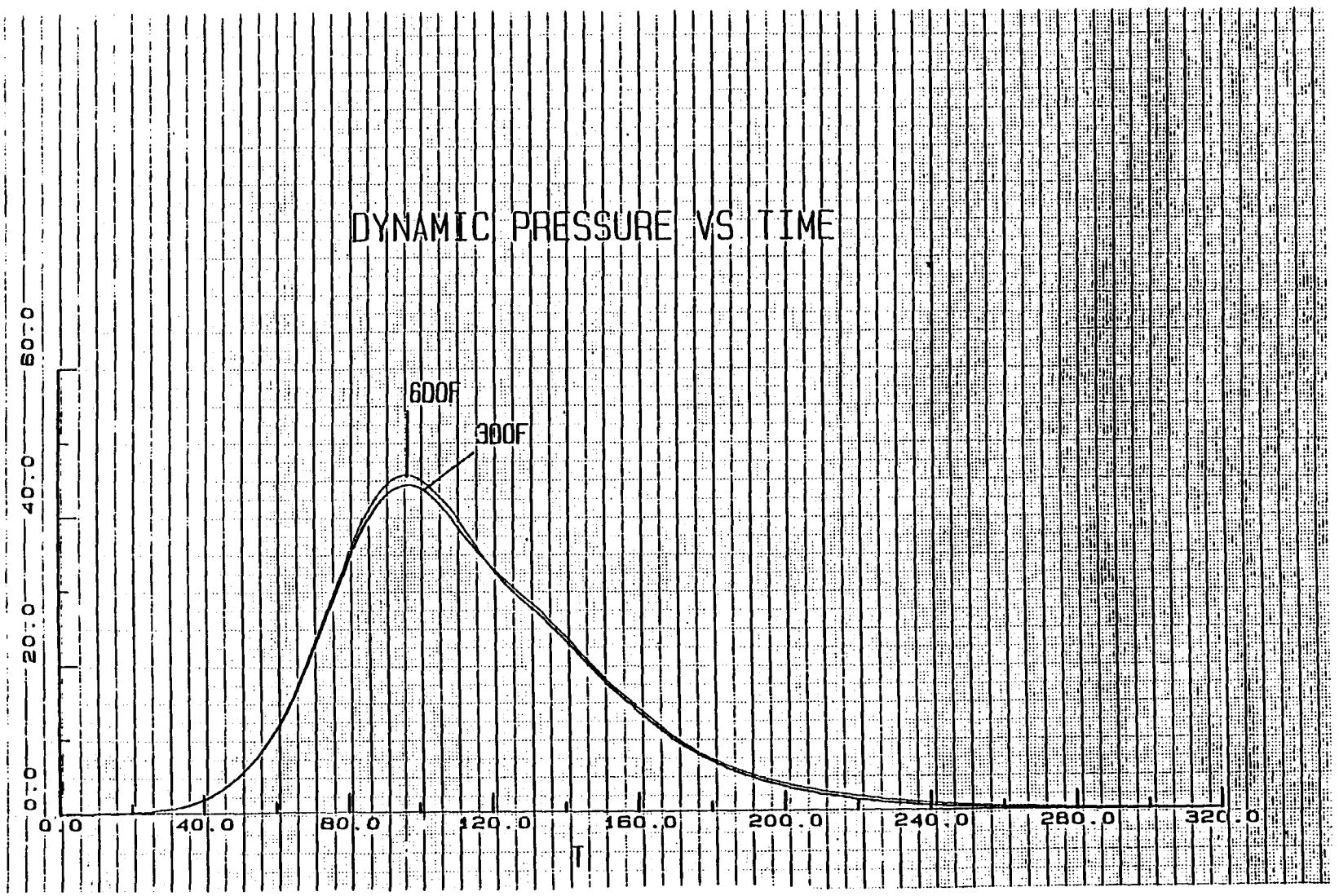

Figure A 2-5

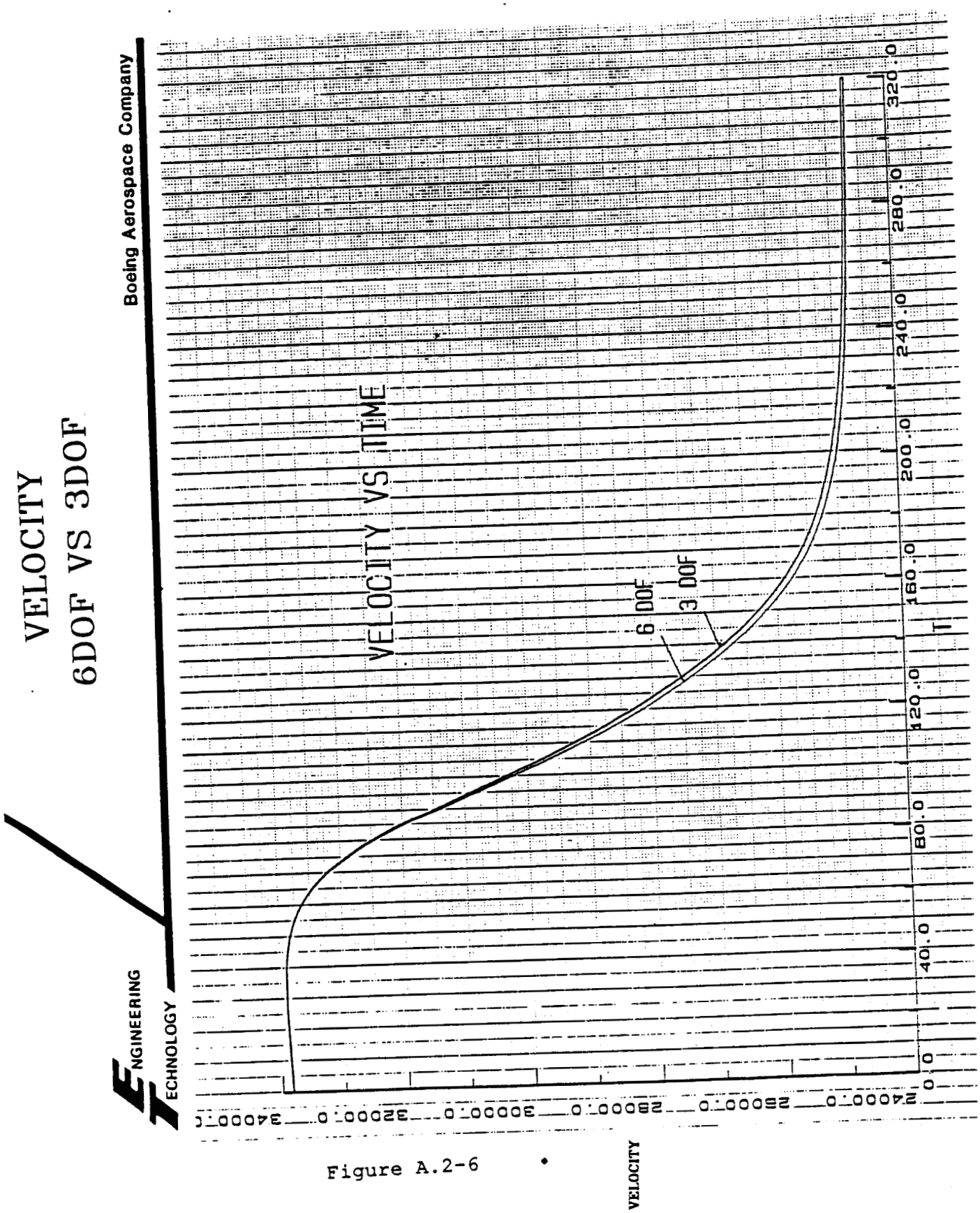

Figure A.2-6

BANK HISTORY COMPARISON

ENGINEERING TECHNOLOGY

Boeing Aerospace Company

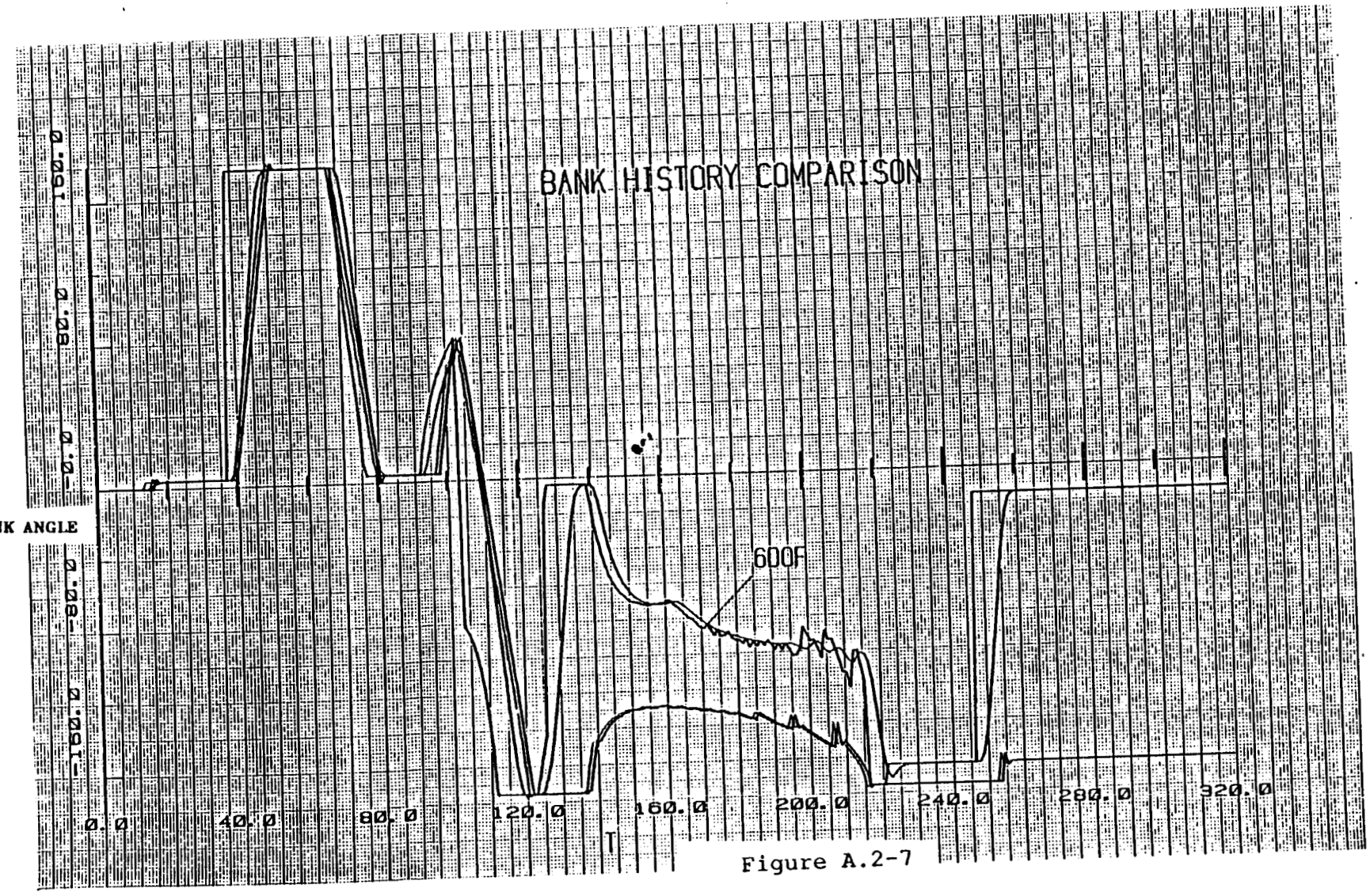

Figure A.2-7

Nominal Trajectory

Exit Condition (ECI)	Target	6 DOF	3 DOF
X (nm)	335.7	3338.4	3244.7
Y	959.1	953.2	1176.3
Z	520.7	514.2	637.4
$\dot{X}$ (ft/s)	-7601.1	-7293	-9328
$\dot{Y}$	21843	21854	21303
$\dot{Z}$	11860	11935	11573
ΔV (ft/s)	385.7	524.8	421.2
ΔV	385.7	437.0	406.0
ΔV_2	0	5.4	5.0
ΔV_3	0	82.4	10.2

Table A.2-8

```
C
C     ************************************************
C     ********            HYPAS                ********
C     ********            -------              ********
C     ********  HYBRID PREDICTIVE AEROBRAKING  ********
C     ********           SCHEME                ********
C     ********                                 ********
C     ********  JSC/ET GUIDANCE CONTROLLER     ********
C     ********       FOR LIFTING AOTV          ********
C     ********         SIMULATIONS             ********
C     ******** THREE DEGREE OF FREEDOM VERS.   ********
C     ************************************************
C
C     ************************************************
C     ******* MODIFIED FOR USE IN BAC GUIDANCE********
C     ******* SIMULATIONS                     ********
C     ************************************LBK 08/10/87
C
      SUBROUTINE GUID4
C
$ADD V:AOTVCM
C
C       IMPLICIT DOUBLE PRECISION (A-H. O-Z)
       DIMENSION UYD(3).UYDS(3)
       REAL M.KRHOD.NRR
C       DOUBLE PRECISION M.MU.K1.KRHOD
C       DOUBLE PRECISION NRR
C
CLBK 08/10/87
C
C*********************************************************************
C
C  SUBROUTINE INPUTS:
C       NAVIGATION STATE:
C          VR      = EARTH RELATIVE VELOCITY (FT/S)
C          BANK    = CURRENT VEHICLE BANK ANGLE (DEG)
C          ALFBIA  = CURRENT VEHICLE ANGLE OF ATTACK (DEG) (AERO)
C          DRAGA   = ACCLERATION DUE TO DRAG (FT/S^2)
C          FPACC   = ACCELERATION VECTOR IN FLIGHT PATH COORDINATES
C                    (FT/S^2)
C          XYZI    = ECI POSITION VECTOR (FT)
C          XYZID   = ECI VELOCITY VECTOR (FT/S)
C        DESIRED END CONDITIONS:
C          HEXIT   = DESIRED EXIT ALTITUDE (FT)
C          APOTG   = DESIRED EXIT APOGEE ALTITIUDE (NM)
C          DXYZI   = DESIRED EXIT ECI POSITION VECTOR (FT)
C          DXYZID  = DESIRED EXIT ECI VELOCITY VECTOR (FT)
C        PHYSICAL CONSTANTS:
C          MU      = GRAVITATIONAL CONSTANTS (FT^3/S^2)
C          RE      = EARTH RADIUS (FT)
C          FPNM    = FEET PER NAUTICAL MILE CONVERSION FACTOR
C          RADCON  = RADIANS PER DEGREE CONVERSION FACTOR
C        VEHICLE PARAMETERS:
C          CL      = COEFFICIENT OF LIFT
C          CD      = COEFFICIENT OF DRAG
C          WTZ     = VEHICLE WEIGHT (LBS)
C          S       = AERODYNAMIC REFERENCE AREA (FT^2)
C        ALGORITHM PARAMETERS:
C          GL      = GAIN FOR LIFT IN REFERENCE QBAR
C          GHDOT   = HDOT GAIN. EQ. GLIDE PHASE
C          GHDOTX  = HDOT GAIN. EXIT PHASE
C          GQ      = QBAR GAIN. EQ. GLIDE PHASE
C          GQX     = QBAR GAIN. EXIT PHASE
C          K1      = DENSITY FILTER GAIN
C          VTRIG   = EXIT PHASE TRIGGER VELOCITY (FT/S^2)
C          YBIAS   = CONSTANT COMPONENT OF INCLINATION DEADBAND
C          VSAT    = DIVIDER FOR VARIABLE COMPONENT OF INCL. DEADBAND(FT/S)
C          BNKOFF  = COSINE OF EQ. GLIDE BANK ANGLE LIMIT
C          BNKOFX= COSINE OF EXIT PHASE BANK ANGLE LIMIT
C          GNC17B  = CONSTRAINT FUNCTION GAIN
C          QSTART  = QBAR FOR GUIDANCE INITIALIZATION (LBS/FT^2)
C          AMXER   = INCLINATION DEADBAND BIAS
C          ZOFF    = INCLINATION DEADBAND EPSILON
           RHONOT  = ATMOSPHERIC DENSITY AT REFERENCE ALTITUDE (SL/FT^3)
           HNOT    = REFERENCE ALTITUDE FOR EXPONENTIAL DENSITY (FT)
C          HS      = SCALE HEIGHT FOR EXPONENTIAL DENSITY (FT)
C          RHOEX   = DENSITY AT EXIT PLANE (SL/FT^3)
C          GEXIT   = GRAVITATIONAL ACCLERATION AT EXIT PLANE (FT/S^2)
C          IGOX    = NUMBER OF TIME STEPS TO WAIT BEFORE CALCULATING
C                    REFERENCE ALTITUDE RATE
C
C          BANKCD  = COMMANDED BANK ANGLE (DEG)
                     COMMANDED TOTAL ANGLE OF ATTACK (DEG)
```

```
C      COMMON / HYPASCM / VR, BANK, ALFBIA, DRAGA, FPACC(3),
C     *                   XYZI(3), XYZID(3),
C     *                   BANKCD, ALPCD,
C     *                   HEXIT, APOTG, DXYZI(3), DXYZID(3),
C     *                   MU, RE, FPNM, RADCON,
C     *                   CL, CD, WT, S,
C     *                   GL, GHDOT, GHDOTX, GQ, GQX, K1, VTRIG,
C     *                   YBIAS, VSAT, BNKOFF, BNKOFX, GNC17B,
C     *                   QSTART, AMXER, ZOFF,
C     *                   RHONOT, HNOT, HS, RHOEX, GEXIT, IGOX
       EQUIVALENCE  (RX, XYZI(1)), (RY, XYZI(2)), (RZ, XYZI(3)),
      *             (XDOT, XYZID(1)), (YDOT, XYZID(2)), (ZDOT, XYZID(3))
CLBK 08/10/87
       DATA NPASS / 1 /
C
C EXAMPLE VALUES FOR SELECTED INPUTS
C
C   PHYSICAL CONSTANTS
C
       DATA RE       /20925741./,
      *     MU       /1.4076469D16/,
      *     FPNM     /6076.1154/,
      *     RADCON   /0.0174532/
C
C   VEHICLE PARAMETERS:
C
       DATA CL       /.29985/,
      *     CD       /1.44164/,
      *     WT       /22417./,
      *     S        /1256./
C
C   ALGORITHM PARAMETERS:
C
       DATA GL       /-0.75/,
      *     GHDOT    /0.20/,
      *     GHDOTX   /0.25/,
      *     GQ       /5.0/,
      *     GQX      /0.0/,
      *     K1       /0.2/,
      *     VTRIG    /28880./,
      *     YBIAS    /0.030/,
      *     VSAT     /26200./,
      *     BNKOFF   /0.997564/,
       DATA BNKOFX /0.965926/
      *     GNC17B   /3.6/,
      *     QSTART   /0.1/,
      *     AMXER    /0.8/,
      *     ZOFF     /.01/,
       DATA  IGOX     /2/
       DATA GEXIT    /31.0295/,
      *     RHOEX    /3.6164E-11/,
      *     HNOT     /300000./,
      *     RHONOT   /4.6235E-9/,
      *     HS       /17500./
C
CLBK 08/10/87
C
       IF(NPASS.GT.1)GO TO 2
C
C  INITILIZATIONS
C
       G = MU / (RE*RE)
       M=WTZ/G
       ICOUNT=0
       LATSW=0
       RLATSW=LATSW+1
       INHIBT=1
       CALL CROSS(DXYZID,DXYZI,UYD)
       CALL UNITV(UYD,UYD)
       NRR=0.
       HDREF=0.0
       IGO=1
       IEXIT=0
       KRHOD=1.0
       S2ROLL=1.0
       WEDGM=0.
       WEDGA=0.
       SLP=0.
       NPASS = 2
       RETURN
C
  2    CONTINUE
C  ************************************************
C  ************************************************
C  *********  GUIDANCE LOGIC  *********************
```

```
C  ***************************************************
      RV = SQRT ( RX*RX + RY*RY + RZ*RZ)
      V = SQRT(XDOT*XDOT + YDOT*YDOT + ZDOT*ZDOT)
      SGAM = DOT(XYZI,XYZID) / (RV * V)
      HDOT = V * SGAM
      VSQ =V/VSAT
      H = RV-RE
      GACT=MU/(RV*RV)
C
C ********** COMPUTE QBAR AS WOULD BE DERIVED ******************
C ********** FROM PREDICTED CD & ACCELEROMETERS ****************
C
C     DRAGA = -XACC*COS(ALPHAR)-ZACC*SIN(ALPHAR)
      QPRED = DRAGA*M/(CD*S)
C
C ********** COMPUTE RHO BASED ON DRAG *************************
C
      RHO = QPRED*2./VR**2.
      RHO62 = RHONOT * EXP(( HNOT - H ) / HS )
C
C ********** CALCULATE RHO/RHO62 AND FILTER TO CREATE **********
C *************** DENSITY MULTIPLIER = KRHOD *******************
C
      IF (V.LT.VTRIG) KRHOD=(1-K1)*KRHOD+K1*RHO/RHO62
C ************************************************************
C ***************** CONTROL EQUATIONS ************************
C ************************************************************
C
C ********** CHECK QBAR FOR GUIDANCE INITIATION ****************
C
      IF(H.GT.422000.)GO TO 100
      IF (QPRED .LT. QSTART) GO TO 100
      QSTART=0.
C
C ********** CALCULATE COS(PHI) FOR EQUILIBRIUM GLIDE **********
C ********** BANK ANGLE USED FOR VERT. LIFT MODULATION *********
C
      COPHI = (WTZ/(CL*QPRED*S)) * (1.0 - V**2 / (GACT * RV))
      COPHI1=COPHI
C
C     ******* QBAR REFERENCE EQUATION FOR ECUIL GL. *************
C
  10 QREF=M*GACT/(CL*S*GL)*(1.-V**2/(GACT*RV))
C
C ********** TEST FOR EXIT PHASE OR EQUIL. GLIDE ***************
C
      IF (V.GT.VTRIG) GO TO 15
C
C
C ***** CALCULATE REFERENCE ALTITUDE RATE FOR EXIT PHASE ********
C ************** EVERY IGOX INTEGRATION STEPS ******************
C
      ICOUNT = ICOUNT + 1
      IF(ICOUNT.NE.IGO)GO TO 15
      CALL HDOTC(M,H,KRHOD,GAMEXD)
C
C ***** SET GAINS FOR GUIDANCE CONTROL EQUATION IN EXIT PHASE ******
C
      ICOUNT=0
      IEXIT=1
      GQ = GQX
      GHDOT = GHDOTX
      IGO=IGOX
C
C ********** COMPUTE PLANAR WEDGE ANGLE ************************
C
  15 CONTINUE
      SLPS=SLP
      WEDGAS=WEDGA
      CALL CROSS(XYZID,XYZI,UYDS)
      CALL UNITV(UYDS,UYDS)
      UYDOT=ABS(DOT(UYD,UYDS))
      IF(UYDOT.GT.1.)UYDOT=1.
      WEDGA=ACOS(UYDOT)/RADCON
      SLP=WEDGA-WEDGAS
C
```

```
C
C ******** COMPUTE THE CONSTRAINT FUNCTION. Z ********************
C
      FEQ=GNC17B*(VSQ-1.)
      IF(FEQ.LT.YBIAS/2.)FEQ=YBIAS/2.
      Z=FEQ+WEDGM
      IF(Z.GT.AMXER+WEDGM)Z=AMXER+WEDGM
      IF(Z.LT.YBIAS)Z=YBIAS
      IF(SLP*SLPS.GT.Ø..OR.INHIBT.NE.1.OR.WEDGAS.GE.Z)GO TO 18
        INHIBT=2
        IF(FEQ.GT.YBIAS/2.)GO TO 17
        IF(WEDGAS.LT.WEDGM)WEDGM=WEDGAS
        GO TO 18
   17 CONTINUE
        WEDGM=WEDGAS
   18 CONTINUE
C
C ********* CHECK ROLL REVERSAL LOCK ********************
C
      IF(INHIBT.EQ.2.AND.ABS(WEDGA-Z).GT.ZOFF)INHIBT=3
C
C ********** SET ROLL REVERSAL COMMAND ON ***********************
C
      IF(WEDGA.LE.Z.OR.INHIBT.NE.3.OR.SLP.LE.Ø.)GO TO 2Ø
      S2ROLL=-S2ROLL
      NRR=NRR+1.
      LATSW=Ø
      RLATSW=LATSW+1
      IF(NRR.EQ.2.)LATSW=2
      IF(NRR.EQ.2.)RLATSW=LATSW+1
      INHIBT=1

    *** CALCULATE COMMANDED BANK ANGLE FOR EQUIL. GL. & EXIT *******
C
C ********** CALCULATE COMMANDED COS(PHI) ***********************
C
C     IF((IEXIT .EQ. 1) .AND. (QPRED .LT. .5)) GHDOT=.ØØØØ1
   2Ø COPHI=COPHI-GHDOT*(HDOT-HDREF)/QPRED+GQ*(QPRED-QREF)/QPRED
      COPHI2=COPHI
      IF((IEXIT.EQ.1).AND.(QPRED.LT. .5).AND.(IFIX.EQ.1))COPHI=1.Ø
C
C **** LIMIT BANK ANGLE TO 15-165 DEGREES BEFORE 3ØØK FT. *******
C
      IF(IEXIT.EQ.1.AND.H.GT.3ØØØØØ.)BNKOFF=BNKOFX
C     IF(COPHI .LT. -BNKOFF) COPHI=-BNKOFF
C     IF(COPHI .GT.  BNKOFF) COPHI= BNKOFF

      IF (COPHI.LT.-BNKOFF.AND.H.LE.3ØØØØØ.) COPHI=-BNKOFF
      IF (COPHI.GT. BNKOFF.AND.H.LE.3ØØØØØ.) COPHI= BNKOFF
      IF (COPHI.LT.-BNKOFF.AND.H.GT.3ØØØØØ.) COPHI=-BNKOFF
      IF (COPHI.GT. BNKOFF.AND.H.GT.3ØØØØØ.) COPHI= BNKOFF
C
C    PASS COMMANDED ANGLES BACK OUT  TO ENVIRONMENT
C
      BANKCD= S2ROLL*ACOS(COPHI)/RADCON
      ALPCD = ALFBIA
C
  1ØØ CONTINUE
      RETURN
      END
C
```

```
C
C  ***********************************************
C  SUBROUTINE HDOTC
C  ***********************************************

      SUBROUTINE HDOTC(M,H,KRHOD,GAMEXD)

C   ***********************************************
C  ******** EXIT PHASE REFERENCE ALTITUDE ********
C *********.    RATE PREDICTOR/CORRECTOR   ********
C ***********************************************
C
C        LOCAL VARIABLES
C       -----------------
C
C     APOTG = TARGET APOGEE ALTITUDE (NM)
C     DIFF = DIFFERENCE BETWEEN PREDICTED APOGEE AND TARGET APOGEE (NM)
C     GAMEX = PREDICTED EXIT FLIGHT PATH ANGLE (RAD)
C     GEXIT = GRAVITATIONAL ACCELERATION AT THE EXIT PLANE (FPSS)
C     HAPO = PREDICTED APOGEE ALTITUDE (NM)
C     HDDEX = PREDICTED ALTITUDE ACCELERATION AT EXIT (FPSS)
C     HNOT = REFERENCE ALTITUDE USED IN EXPONENTIAL DENSITY MODEL (FT)
C     HS = SCALE HEIGHT USED IN EXPONENTIAL DENSITY MODEL
C     QEX = PREDICTED DYNAMIC PRESSURE AT EXIT (PSF)
C     RE = EQUATORIAL RADIUS OF EARTH (FT)
C     REXIT = RADIUS AT EXIT PLANE (FT)
C     RHOEXIT = '62 STANDARD DENSITY AT EXIT PLANE (SL/FT3)
C     RHONOT = '62 STANDARD DENSITY AT REF. ALT. USED IN EXPON. MODEL (SL/FT3)
C     VEXIT = PREDICTED EXIT INERTIAL VELOCITY (FPS)
C     VEXITR = PREDICTED EXIT RELATIVE VELOCITY (FPS)
C
SADD V:AOTVCM
C
C
C      IMPLICIT DOUBLE PRECISION (A-H, O-Z)
      REAL M,KRHOD
C      DOUBLE PRECISION M,MU,KRHOD,K1
C
C     COMMON / HYPASCM / VR, BANK, ALFBIAS, DRAGA, FPACC(3),
     *                   XYZI(3), XYZID(3),
     *                   BANKCD, ALPCD,
     *                   HEXIT, APOTG, DXYZI(3), DXYZID(3),
     *                   MU, RE, FPNM, RADCON,
     *                   CL, CD, WT, S,
     *                   GL, GHDOT, GHDOTX, GQ, GQX, K1, VTRIG,
     *                   YBIAS, VSAT, BNKOFF, BNKOFX, GNC17B,
     *                   QSTART, AMXER, ZOFF, TSTEP, RRMAX,
     *                   RHONOT, HNOT, HS, RHOEX, GEXIT

      DELTA = 30.
      REXIT = HEXIT + RE
      I=0
      C = S*CD/2./M
C
C ******* MULTIPLY DENSITY BY DENSITY SCALE FACTOR   ********
C
      RHONOT=RHONOT*KRHOD
C
C ******* CALCULATE RHS OF PREDICTION EQUATION ************
C
      IF (HDREF.GT.200.) GO TO 20
      HDREF=200.
   20 RHS = C*RHONOT/HDREF*HS*(EXP((HNOT-HEXIT)/HS)-EXP((
     +HNOT-H)/HS))
      I=I+1
C
C *********** CALCULATE VEXIT RELATIVE ************************
C
      VEXITR = 1./(1./VR-RHS)
C
C *********** BIAS VEXIT RELATIVE TO VEXIT INERTIAL ***********
C
      VEXIT = VEXITR + (V-VR)

    ** ADD POTENTIAL/KINETIC ENERGY TRANSFER TO EXIT VELOCITIES ***
C
      V2 = ((GACT*H-GEXIT*HEXIT+(V**2.)/2.)*2.)**0.5
      DELV = V2-V
      VEXIT = VEXIT + DELV
      VEXITR = VEXITR + DELV
C
```

```
C              CALCULATE HDREF DIVERGENCE AT EXIT
C
      HDDEX=VEXIT**2./REXIT-GEXIT-(CL*.5*RHOEX*VEXITR**2.*S)/M
      IF (HDDEX.LT.0.) GO TO 42
      IF (H.GT.320000.) GO TO 40
      DELHD = SQRT(HDREF**2.+160000.*HDDEX) - HDREF
      GO TO 41
   40 DELHD = SQRT(HDREF**2.+2.*HDDEX*(400000.-H)) - HDREF
C
C ********** CALCULATE EXIT FLIGHT PATH ANGLE **********************
C
   41 IF((HDREF+DELHD).GT.VEXIT.OR.HDREF.LE.0.)GO TO 56
      GAMEX = ASIN((HDREF+DELHD)/VEXIT)
      GO TO 45
   42 GAMEX=ASIN(HDREF/VEXIT)
C
C ********** CALCULATE APOGEE ALTITUDE *****************************
C
   45 HAPO = (REXIT/(2.-REXIT*VEXIT**2./MU)*(1.+SQRT(1.-(REXIT*VEXIT*
     +COS(GAMEX))**2./MU*(2./REXIT-VEXIT**2./MU)))-RE)/FPNM
C
C
C ************ COMPARE PREDICTED AND DESIRED APOGEES ***************
C
      DIFF = HAPO - APOTG
      IF (ABS(DIFF).LT.0.5) GO TO 56
      IF (SIGN(1.D+00.DIFF).NE.SIGN(1.D+00.DIFFL)) DELTA = DELTA/2.
      DIFFL = DIFF
      IF (HAPO.GT.APOTG) HDREF=HDREF-DELTA
      IF (HAPO.LT.APOTG) HDREF=HDREF+DELTA
      GAMEXD = GAMEX / RADCON
      GO TO 20
C
   56 IF(HDREF.LT.0.)HDREF=0.
      RETURN
      END
      SUBROUTINE UNITV( A, B )
C
C     B = A / MAGNITUDE(A)
C
C      IMPLICIT DOUBLE PRECISION (A-H, O-Z)
      DIMENSION A(3), B(3)
      XMAG = SQRT( A(1)*A(1) + A(2)*A(2) + A(3)*A(3) )
      B(1) = A(1) / XMAG
      B(2) = A(2) / XMAG
      B(3) = A(3) / XMAG
      RETURN
      END
      SUBROUTINE CROSS( A, B, C )
C
C     C = A X B
C
C      IMPLICIT DOUBLE PRECISION (A-H, O-Z)
      DIMENSION A(3), B(3), C(3)
      C(1) = A(2) * B(3) - A(3) * B(2)
      C(2) = A(3) * B(1) - A(1) * B(3)
      C(3) = A(1) * B(2) - A(2) * B(1)
      RETURN
      END
      DOUBLE PRECISION FUNCTION DOT( A, B )
C
C     RETURNS DOT PRODUCT OF A AND B
C
C      IMPLICIT DOUBLE PRECISION (A-H, O-Z)
      DIMENSION A(3), B(3)
      DOT = A(1) * B(1) + A(2) * B(2) + A(3) * B(3)
      RETURN
      END
```

NASA

Report Documentation Page

1. Report No	2. Government Accession No.	3. Recipient's Catalog No.

4. Title and Subtitle
Aeroassisted Orbital Transfer Vehicle
Control Technology - Final Report

5. Report Date
August 1988

6. Performing Organization Code

7. Author(s)
W. W. Cimino
M. A. Langehough
I. A. Hirsch

8. Performing Organization Report No.

10. Work Unit No.

9. Performing Organization Name and Address
Control Technology Organization
Boeing Aerospace
P.O. Box 3999
Seattle, WA 98124-2499

11. Contract or Grant No.
NAS 8-37358

13. Type of Report and Period Covered
Final (June 87 - Aug. 88)

12. Sponsoring Agency Name and Address
Control Technology
National Aeronautics & Space Administration
George C. Marshall Space Flight Center
Marshall Space Flight Center, AL 35812

14. Sponsoring Agency Code

15. Supplementary Notes

16. Abstract

The focus of this control has been to develop the control technology required to identify the sophistication required for the Aeroassisted Orbital Transfer Vehicle (AOTV) control system. An angle of attack, bank angle command control technique has been developed which uses either on-off thruster or proportional thruster. An angle of attack adaptive controller was included to minimize the reactor control system (RCS) usage due to payload center of gravity uncertainties. The guidance and control techniques were verified using a detail six-degree-of-freedom (6DOF) simulation. Mission sensitivity was developed for uncertainties in the entry state, mass properties, atmosphere, aerodynamic, and sensor.

17. Key Words (Suggested by Author(s))	18. Distribution Statement
Control System On-Off Thruster Six-degree-of-freedom simulations Sensitivity Analysis Aero Braking Aeroassisted Orbital Transfer	

19. Security Classif. (of this report)	20. Security Classif. (of this page)	21. No. of pages	22. Price
UNCLASSIFIED	UNCLASSIFIED	126	

NASA FORM 1626 OCT 86